BLAST AND FRAGMENTS FROM SUPER-PRESSURE VESSEL RUPTURE

J. F. Pittman

Naval Surface Weapons Center
Silver Spring, Maryland

February 1976

NSWC/WOL/TR 75-87

NSWC TECHNICAL REPORT

WHITE OAK LABORATORY

BLAST AND FRAGMENTS FROM SUPERPRESSURE VESSEL RUPTURE

BY
J.F. Pittman

9 FEBRUARY 1976

NAVAL SURFACE WEAPONS CENTER
WHITE OAK LABORATORY
SILVER SPRING, MARYLAND 20910

NAVAL SURFACE WEAPONS CENTER
WHITE OAK, SILVER SPRING, MARYLAND 20910

UNCLASSIFIED

SECURITY CLASSIFICATION OF THIS PAGE (When Data Entered)

REPORT DOCUMENTATION PAGE		READ INSTRUCTIONS BEFORE COMPLETING FORM
1. REPORT NUMBER NSWC/WOL/TR 75-87	2. GOVT ACCESSION NO.	3. RECIPIENT'S CATALOG NUMBER
4. TITLE (and Subtitle) BLAST AND FRAGMENTS FROM SUPERPRESSURE VESSEL RUPTURE		5. TYPE OF REPORT & PERIOD COVERED FINAL 6. PERFORMING ORG. REPORT NUMBER
7. AUTHOR(s) J. F. Pittman		8. CONTRACT OR GRANT NUMBER(s)
9. PERFORMING ORGANIZATION NAME AND ADDRESS Naval Surface Weapons Center White Oak, Silver Spring, Maryland 20910 Code WR-15		10. PROGRAM ELEMENT, PROJECT, TASK AREA & WORK UNIT NUMBERS NSWC-1189/ERDA X0124 NSWC-1178/NASA X0124
11. CONTROLLING OFFICE NAME AND ADDRESS		12. REPORT DATE 9 February 1976 13. NUMBER OF PAGES 132
14. MONITORING AGENCY NAME & ADDRESS(if different from Controlling Office)		15. SECURITY CLASS. (of this report) UNCLASSIFIED 15a. DECLASSIFICATION/DOWNGRADING SCHEDULE

16. DISTRIBUTION STATEMENT (of this Report)

Approved for public release; distribution unlimited

17. DISTRIBUTION STATEMENT (of the abstract entered in Block 20, if different from Report)

18. SUPPLEMENTARY NOTES

19. KEY WORDS (Continue on reverse side if necessary and identify by block number)

PRESSURE VESSEL RUPTURE
BLAST
FRAGMENTS
HIGH PRESSURE ARGON

20. ABSTRACT (Continue on reverse side if necessary and identify by block number)

Seven spherical steel vessels, each with a volume of 1 ft^3, were pressurized with argon until they burst. Airblast and fragment parameters,were measured to aid in evaluating the hazards from high pressure vessel rupture. The vessels were designed to burst at either 15,000, 30,000, or 50,000 psi. Computer codes were developed to generalize and extend the experimental data.

For bursts where internal gas temperatures are between 300° and 400°K,

DD FORM 1 JAN 73 1473 EDITION OF 1 NOV 65 IS OBSOLETE
S/N 0102-014-6601

UNCLASSIFIED

SECURITY CLASSIFICATION OF THIS PAGE (When Data Entered)

20. (CONT'D)

increasing the vessel's burst pressure beyond 15,000 psi does not increase airblast output. As temperatures inside the vessel are increased above 400°K, higher pressure ruptures do increase airblast energy. As temperatures are increased further, the fill gas behaves ideally so that ideal gas assumptions can be used to set an upper limit to the energy output from high pressure vessel rupture. For a 15,000 psi rupture, ideal behavior is approached at temperatures above 1,300°K.

Each vessel separated at rupture into two hemispheres. These pieces were accelerated to velocities of about 300 ft/second; about half the calculated fragment velocities.

NSWC/WOL/TR 75-87 9 February 1976

BLAST AND FRAGMENTS FROM SUPERPRESSURE VESSEL RUPTURE

Vessels containing gases at pressures above 10,000 psi are becoming commonplace in industrial and research areas. Hazards resulting from their accidental rupture must be evaluated for their safe deployment. This report describes work done to extend the present data base to include very high pressure ruptures under various conditions.

The airblast portion of this task was performed for the Union Carbide Corporation, Nuclear Division, Y-12 Plant, under contract to the Energy Research and Development Administration of Oak Ridge, Tennessee. The NAVSURFWPNCEN Task number was NSWC-1189/ERDA X0124. The fragment portion of the study was performed for the Aerospace Safety Research and Data Institute, NASA Lewis Research Center under Task NSWC-1178/NASA X0124. The experimental work was carried out at the Naval Surface Weapons Center Dahlgren test facility. The mention of propietary items in this report implies neither critism nor endorsement of such products by NAVSURFWPNCEN.

Julius W. Enig

JULIUS W. ENIG
By direction

TABLE OF CONTENTS

ANNEXES

TABLE OF CONTENTS (CONT'D)

ANNEXES (CONT'D)

TABLES

ILLUSTRATIONS

TABLE OF CONTENTS (CONT'D)

ILLUSTRATIONS (CONT'D)

TABLE OF CONTENTS (CONT'D)

ILLUSTRATIONS (CONT'D)

TABLE OF CONTENTS (CONT'D)
ILLUSTRATIONS (CONT'D)

TABLE OF CONTENTS (CONT'D)

ILLUSTRATIONS (CONT'D)

CONVERSION TABLES

TO CONVERT	INTO	MULTIPLY BY
FEET	CENTIMETERS	30.48
FEET	METERS	0.3048
METERS	FEET	3.281
CENTIMETERS	FEET	3.281×10^{-2}
CUBIC FEET	CUBIC CMS.	28320
CUBIC FEET	CUBIC METERS	2.832×10^{-2}
CUBIC CMS.	CUBIC FEET	3.531×10^{-5}
CUBIC METERS	CUBIC FEET	35.31
POUNDS	GRAMS	453.59
POUNDS	KILOGRAMS	0.4536
GRAMS	POUNDS	2.205×10^{-3}
KILOGRAMS	POUNDS	2.205
TONS (SHORT)	POUNDS	2000
TONS (SHORT)	KILOGRAMS	907.185
$GRAMS/CM^3$	$POUNDS/IN^3$	3.613×10^{-2}
$GRAMS\ CM^3$	$POUNDS/FT^3$	62.43
$POUNDS/IN^3$	$GRAMS/CM^3$	27.68
$POUNDS/FT^3$	$GRAMS/CM^3$	1.602×10^{-2}
KG/M^3	$POUNDS/FT^3$	6.243×10^{-2}
$POUNDS/FT^3$	KG/M^3	16.02
PSI (POUNDS PER SQUARE INCH)	BARS	6.895×10^{-2}
BARS	PSI	14.504
PSI (POUNDS PER SQUARE INCH)	PASCALS (NEWTON/M^2)	6.897×10^3
PASCALS	PSI	1.45×10^{-4}
PSI	$DYNES/CM^2$	6.895×10^4
PSI - MSEC	BAR - MSEC	6.895×10^{-2}
$FT/LB^{1/3}$	$METERS/KG^{1/3}$	0.3967

1. INTRODUCTION

1.1 Background

Vessels containing gases at high pressures are used throughout industrial and research areas. Their users range from gasoline service stations to nuclear power plants to spacecraft. The potential hazards from accidental rupture must be considered in their design and siting. Hazards include blast waves and high energy fragments generated by vessel rupture.

Blast and fragment data from the pneumatic burst of high pressure vessels are not extensive. Empirical data include the low pressure work of reference (1) in which an Atlas missile was burst at a pressure of 49.7 psiA and the work of reference (2) which is based on the rupture of small glass spheres at pressures up to 400 psiA. The higher pressure work in reference (3) is based on the burst tests of full scale vessels at pressures ranging from 640 to 8145 psiA. Data from vessels burst above 8145 psiA are not available.

The investigation described in this report was designed to extend empirical data to higher pressures and to generalize the results through computer techniques.

1.2 Scope of the Investigation

Seven vessels were pressurized with argon until they burst. The area was instrumented to measure the blast and fragment parameters generated by vessel rupture. All vessels were T-1 steel spheres with an internal volume of 1 ft^3. Design burst pressures were 15,000, 30,000, and 50,000 psi.

Blast calculations were made in two ways. A one-dimensional calculation was used to calculate airblast parameters in a free-air situation. A two-dimensional hydrocode, TUTTI, was developed to give a better calculation of the blast field about vessels burst in real situations.

One vessel was burst inside a five-sided steel structure to obtain blast loading on containment walls in a real situation. The two dimensional hydrocode can be used to obtain blast loads on a confining structure's walls.

---

(1) Moskowitz, H."Blast Effects Resulting from Fragmentation of an Atlas Missile", AIAA Paper No. 65-195, AIAA/NASA Flight Testing Conference, Huntsville, Alabama, February 15-17, 1965
(2) Boyer, D. W. et al "Blast from a Pressurized Sphere", University of Toronto Institute of Aerophysics, Report No. 48, January 1958
(3) Pittman, J. "Blast and Fragment Hazards From Bursting High Pressure Tanks", Naval Ordnance Laboratory, Report No. NOLTR 72-102, May 17, 1972

2. EXPERIMENTAL OUTLINE

The experimental plan is given in detail in Annex A. It is summarized here to aid in understanding the investigation.

For the investigation, a pressure vessel was located a few inches above ground/firing pad level and was pressurized with argon until it burst. The vessel was instrumented to monitor internal gas pressure and temperature and circumferential expansion. The area around the vessel was instrumented to measure the airblast generated by the rupturing vessel. A system of breakwires was assembled about the vessel to measure vessel-wall fragment velocities. A semi-circular arena made from pressed board panels was set up to recover vessel wall fragments.

The expermental layout is shown in Figures 2.1 and 2.2. A drawing of a 50,000-psi vessel is shown in Figure 2.3. Details of all pressure vessels are given in Table 2.1.

3. AIRBLAST RESULTS

Airblast generation by high pressure vessel rupture is controlled by a number of factors. These include the geometry of vessel breakup, the volume of the vessel, the type of gas in the vessel, and the temperature and pressure in the vessel at failure. In this experiment, the test vessel internal volume was 1 ft^3 for all tests. The internal gas temperature at rupture was between 300 and 374°K, a spread not expected to affect airblast generation. A monotomic fill gas, argon, was used. Thus the only variables in the experiment were: the controlled one, vessel pressure at rupture, and the uncontrolled one, the geometry of vessel breakup.

3.1 Effects of Rupture Geometry

All the vessels used in this test program burst into two pieces. Both the 15,000 and 30,000-psi vessels burst into two hemispheres. The 50,000-psi vessels separated into two pieces, one slightly larger than the other as discussed in Annex B where vessel rupture histories have been reconstructed. From these reconstructions, we determine the direction of maximum gas motion, or jetting. Asymmetries in the blast field about the bursting vessel correlated with the direction of the jetting.

The estimated direction of jetting for each shot is plotted in Figure 3.1. This estimates the jet direction in the horizontal plane only. Estimates of jetting in the vertical direction will be discussed for specific cases.

Airblast overpressure data from all unconfined tests are plotted in Figures C.5, C.9, and C.13 in Annex C. Curves fitted by eye to these data are shown in Figures 3.2, 3.3, and 3.4. These figures show the overpressure/ground range relationship for gage lines 1 and 2 for each test. A single gage was deployed on a third line after shot 1. Data recorded at this position were suspect for shots 3 and 4 in that it generally read half the expected overpressure. The entire gage/electronics were changed after shot 4; after this overpressures were recorded that support the conclusions drawn here.

Curves from Figures 3.2, 3.3, and 3.4 have been replotted in Figures 3.5, 3.6, and 3.7; this time they are grouped according to their angular relationship to the estimated jet direction. Figure 3.5, shows overpressure/ground range curves measured along lines ranging from 13° to 33° from the estimated direction of maximum argon motion. At ground ranges greater than 20 feet, (overpressures less than 5 psi), the vessel burst pressure has little effect on airblast overpressures.

Even at closer ranges and higher overpressures, differences in overpressure in Figure 3.5 may have been due to geometry rather than burst pressure. For instance, the 15,000-psi vessel's bottom half served as a shield for the closer gage positions (see Figure B-5). For the 22°, 50,000-psi curve,the vessel burst so as to direct the blast upward. The 33°, 50,000-psi vessel's blast was directed downward (see Figure B-12 and the paragraph below).

The angles between the gage lines and the argon jets were greater for the data displayed in Figure 3.6. The anomaliy where the 68°, 50,000-psi curve shows higher pressures than the 57°, 50,000-psi curve may be due to the fact that the first opening for one tank occurred along a line described by the tanks center and a point on its surface that was nearly vertical to the ground in one case (57°) and horizontal in the other (68°). Thus for the 68° case, close in gages were shielded giving low pressure close in; but the jet was broader horizontally, tending to generate higher pressures further out. The 57° jet was broad in the vertical direction. The family of curves in Figure 3.6 indicate lower overpressures for a given distance than is shown in Figure 3.5. They are however, higher than those for even larger angles shown in Figure 3.7.

The overpressure/ground range relations plotted in Figure 3.7 show a greater angular distance from the jet than is shown in Figures 3.5 and 3.6; and therefore, lower pressures were measured along these lines than those in Figures 3.5 and 3.6. The greater angular dispersion of the data in this figure also make for wider dispersion of the curves.

From the above, the factor controlling the magnitude of the airblast overpressure from the high pressure vessels ruptured in this investigation was the jetting direction of the high pressure gases. For fill gas temperatures in the range of 300°K, increasing rupture pressure does not significantly increase the airblast pressure for rupture pressures above 15,000 psi.

3.2 Effects of Temperature and Pressure

The airblast energy transferred to the surrounding medium from vessel rupture depends on the internal temperature and pressure of the gas at burst. Fill gas temperatures were generally about 330°K, although for test 7, they climbed to 374°K. At these low temperatures, vessel pressure at rupture did not significantly affect airblast, i.e., airblast pressures from the 50,000-psi ruptures were not measurably higher than those from the 15,000-psi ruptures. The reason for this is that there is very little difference in the expansion energy of argon at these pressures. Consider the expansion data in Table 3.1 below based on a real argon equation of state from reference (4). The data are for a 1 ft^3 volume of argon

(4) Din, F. "Thermodynamic Functions of Gases, Volume 2: Air, Acetylene, Ethylene, Propane, and Argon", Butterworths, London, 1956

at 290°K. The expansion energy, i.e.the work done against the atmosphere, is taken as the difference in internal energy after isentropic expansion to a pressure of 1 atmosphere.

TABLE 3.1 ENERGY IN ARGON PRESSURE VESSELS

Vessel Pressure in psi	Density in gm/cc	Internal Energy drop on expansion cal/gm	Total Energy for 1 Ft^3 Volume cal	TNT Equivalent* in pounds for 1 Ft^3
15,000	0.99	13.48	3.81×10^5	0.82
30,000	1.24	12.45	4.38×10^5	0.95
50,000	1.39	11.81	4.64×10^5	1.00

* Based on heat of detonation of 1018 cal/gram

There is little difference in the expansion energies at these pressure levels. The shell of a 50,000-psi vessel is about 4 times as massive as that of a 15,000-psi vessel and therefore absorbs relatively more kinetic energy than does the lighter vessel. This should decrease the differences even further.

The remarks on energy equivalence in the remainder of this discussion do not imply that tank rupture airblast is identical to blast generated by equivalent TNT charges. The TNT equivalence given in Table 3.1 is used as an energy unit. As may be seen in Section 3.5, neither the overpressure versus distance nor the impulse versus distance curves for tank rupture are identical to those from TNT. While the energy available from vessel rupture does not increase above that for an ideal gas, shock wave parameters are still a strong function of gas temperature. Figure E.6 shows the dependence of the initial air shock pressure on temperature for real and ideal argon for several rupture pressures.

Consider now the case where the vessel's internal gas temperature is very high. As temperature is increased (somewhere above 1350°K for 15,000-psi pressure) argon behavior approaches that of an ideal gas. Since for an ideal gas, the expansion energy is independent of temperature and molecular weight, the ideal gas internal energy represents an upper limit to the blast energy available from an argon vessel rupture.

This upper limit is shown in Figure 3.8. Note that for 1 ft^3 of argon burst at 15,000 psi and 1273°K, the TNT energy equivalent approaches 2 pounds. Further fill gas temperature increases will not increase this energy beyond 2.15 lbs TNT. Argon approaches an ideal monotomic gas asymptotically with temperature increase. The reason for this is that at constant pressure, a temperature increase is accompanied by a density decrease. At low densities, the intermolecular forces that cause non-ideality become unimportant. At pressures above 15,000-psi, temperatures greater than 1300°K are required for argon to approach ideal behavior. Isentropes generated from the data in reference (5) are shown in Figure 3.9. From these, argon must be near 2100°K at 50,000-psi to approach ideal behavior.

(5) Brahinsky, H.S. and Neel, C.A., "Tables of Equilibrium Thermodynamic Properties of Argon Vol. III Constant Entropy". Arnold Engineering and Development Co., No. AEDC-TR 69-19, Vol. III AD684532, March 1969.

The upper limits for other gases are shown in Figure 3.10. The upper energy bound for a diatomic gas at 15,000 psi is about 3.25 lbs TNT equivalent versus about 2.15 lbs equivalent for argon.

The free air overpressures calculated via WUNDY, a one-dimensional hydrocode and plotted in Figure 3.11 illustrate the dependence of airblast pressure on argon temperature.

3.3 Effects of Volume

Of all the factors that determine airblast from pressure vessel rupture, the effect of change in vessel size may be easiest to handle. Cube root scaling, as used to compare airblast parameters in explosives studies, seems applicable here.

Cube root scaling is most applicable to spherical or point source explosions in free air. Change the charge shape, put a case around the charge, or fire the charge near a boundary and the use of cube root scaling must be qualified.

Insufficient vessel-burst data exists to verify the use of cube root scaling. Certainly, one expects it to apply to spherical tanks burst under the conditions where the only variable is the vessel volume. Thus distances, times, and shockwave impulses that characterize the airblast from vessels of different sizes are related by the ratio of the cube root of their volume.

There are more uncertainties for vessels not spherical in shape. The most likely vessel shape will be cylindrical. Conventional explosive cylinders generate an airblast field near the charge that reflects the charge dimensions and the detonation scheme (reference 6). However in the case of a cylindrical charge, asymmetries in the blast front disappear by the time the blast wave has propagated to the point where the airblast overpressures are about 5 psi. From then on, the front expands spherically.

Perturbations due to the detonation scheme of a conventional explosion never appear on the tank rupture blast front. These are replaced by perturbations caused by the vessel failure scheme. The high initial shock velocities that allow the shock front from a conventional explosion to approach spherical symmetry at late times may not exist in the vessel rupture situation. Therefore, the blast front from vessel rupture may never overcome its initial asymmetries. In spite of these problems, no better method exists to relate the blast from different sized vessels than one using cube root scaling. As the vessel rupture approaches an ideal spherical explosion, cube root scaling will obtain.

3.4 Effects of a Confining Structure

Most working high pressure vessels will be housed in some kind of structure built to contain or modify the blast and fragment patterns should accidental rupture occur. Estimates of damage to personnel and nearby structures must take into account the effect of this confining structure on damaging airblast pressures.

(6) Wisotski, J. and Snyer, H. "Characteristics of Blast Waves Obtained from Cylindrical High Explosive Charges". Denver Research Institute, DRI#2286, Nov 1965

The confining structure test described in Annexes A and C show some of the effects resulting from the presence of a five-sided enclosure about a bursting high pressure vessel. Curves fitted to the measured data from Figure C.17 are shown as solid lines in Figure 3.12.

For the confined test on which the solid-line curves in Figure 3.12 are based, the vessel burst at a point that directed the major gas motion against a sidewall of the structure.

If the vessel had burst in a manner so as to direct the argon jet out through the open wall of the structure, then airblast overpressures would have been even higher. The dashed line in Figure 3.12 was obtained from the average of the curves in Figure 3.5. This curve probably represents the maximum airblast overpressures in front of the structure.

The dotted curve in Figure 3.12 represents the average of the curves shown in Figure 3.6. This curve gives pressures along lines up to 71° from the argon jet. Even for these conditions, airblast overpressures at some distance from the bursting vessel are higher than would have been predicted for a confined burst. Thus, under certain burst conditions the five-sided confining structure does not reduce airblast overpressure.

Pressure on the interior walls will also depend on burst geometry and internal gas temperature. The 2-dimensional Hydrocode, TUTTI, will calculate the entire pressure load on the walls as a function of time for all burst conditions.

3.5 Comparison of Data

Measured airblast overpressures are compared with calculated data in Figure 3.13. The upper bound of the shaded area was arrived at by taking the average of the data from Figure 3.5; the lower bound is the average of the data from Figure 3.7.

The data from the one-dimensional calculation, WUNDY, was modified to fit the burst geometry of these experiments. Specifically, data above 40 psi are from Figure E.11. Data below 20 psi was obtained from Figure 3.11. In this case, the WUNDY Curve for all burst pressures with an argon temperature of 290°K (17°C) was used. The one-dimensional calculations are for a free air burst. To account for the presence of the ground, the energy output was doubled. Therefore, distances were multiplied by $(2)^{1/3}$ or 1.26. The TNT curve was obtained from Figure C.1 using the equivalent weight data from reference 7.

Airblast overpressures at a ground range of 1.0, Figure 3.13, range from 10 psi for the lower bound of the measured data to about 1,000 psi for the TNT data. The curves converge at lower overpressure levels. The upper bound of the measured data

(7) Swisdak, M., "Explosion Effects and Properties: Part 1 - Explosion Effects in Air", Naval Surface Weapons Center Report NSWC/WOL/TR 75-116

from the TUTTI claculation, and the TNT data coincide at overpressures below about 5.0 psi. Thus either the TUTTI results or the TNT curve represent an upper bound to the airblast overpressures generated by vessels ruptured in this investigation.

4. FRAGMENT DATA

Detailed fragment data are given in Annex D. All vessels burst into two pieces. Of these 14 pieces, 10 were recovered. Weights of the recovered sections ranged from 51.1 pounds to 271 pounds. The recovered sections were those that hit the arena walls and were stopped or those that hit the ground or firing pad and traveled only a short distance. The positions where the pieces of the vessels were found are shown in Figure D.1.

The fragment velocity system did not function satisfactorily. Either the pieces of the vessel failed to hit a screen; or when they did, the electronic counters did not function. Fortunately, a piece of the vessel hit the firing pad on all the unconfined tests except shot 5. This produced a distinctive signal on the time resolved pressure gage recordings. The points where the vessel segments hit the firing pad and the original position of the vessel were used to determine the distance the fragment traveled. Early fragment velocities were determined from this information. For the test where the vessel half did not hit the firing pad, shot 5, (see Table D.1) one section hit velocity screens.

The mean velocity measured for the approximately 50-pound portion of the 15,000-psi vessels was 320 feet/second. The minimum velocity measured was 310 feet/second and the maximum was 330 feet/second.

For the 30,000-psi vessel, the mean velocity measured was 353 feet/second for the 147 pound segment of shot 3 and 274 feet/second for the 108-pound segment of shot 7. The average of all fragment velocities measured on shots 3 and 7 is 326 feet/second with the highest value measure 373 feet/second and the minimum velocity measured 250 feet/second. The wide velocity differences are between the two shots rather than between individual measurements on a single shot.

For the 50,000-psi vessels, the average velocity measured for the 258 pound portion of the vessel used on shot 4 was 215 feet/second. The only velocity screen measurements were made on shot 5. The heavier portion of the vessel, 271 pounds, traveled 17.5 feet at an average velocity of 273 feet/second. The lighter portion, 142 pounds traveled a distance of 6.8 feet in the opposite direction at an average velocity of 278/feet/second. Average velocity for all 50,000-psi Vessel fragments was 235 feet/second.

Case velocities from the one-dimensional code calculation are shown in Figure 4.1 for the 15,000-psi vessel. Note that measured velocities are less than half the calculated value. A method for calculating case velocity from reference 3 gives similar results, i.e., higher than measured values by a factor of 2. No explanation for this discrepancy is readily available. A sophisticated technique for fragment velocity calculation is given in reference 8. However it was not applied to these experiments.

8. Baker, W. et. al. "Assembly and Analysis of Fragmentation Data for Liquid Propellant Vessels," NASA CR 134538 Prepared for NASA Lewis Research Center, Aerospace Safety Research and Data Institute by Southwest Research Institute, San Antonia, Texas, Jan 1974

5. SUMMARY

Several factors control the airblast field from the pneumatic burst of high pressure vessels. Those related to the vessel and its contents include the type, temperature, volume, and pressure of the gas in the vessel and the geometry of rupture.

For a vessel filled with a monotomic gas and burst at a temperature below about 330°K, increasing burst pressure from 15,000 to 50,000 psi does not measurably increase blast energy. However, at elevated fill gas temperatures, rupture energy is increased. The upper limit is reached when internal temperatures are high enough to cause the fill gas to approach ideal gas behavior. These temperatures are about 1300°K for 15,000 psi and about 2100°K for 50,000 psi. Further increases in fill gas temperatures will not significantly increase expansion energy. Thus the ideal gas assumption sets an upper bound to the expansion energy from high pressure vessel rupture. However, the way in which this expansion energy increase influences airblast overpressures is non-linear. Airblast overpressure-distance curves must be computed for each burst temperature/pressure regime.

Blast output from spherical high pressure vessels of different volumes burst at the same temperature and pressure can be related by dividing distances and times by the cube root of the volume. Airblast from cylindrical vessels may be handled similarly by considering them to be an equivalent volume sphere if the length to diameter ratio of the cylinder is not much greater than 2/1. It is believed that this procedure is relatively accurate; however, the degree of certainty cannot be determined given the paucity of available data.

The blast field from pressure vessel rupture is strongly influenced by burst geometry. The vessels used in this investigation burst into two pieces creating strong argon motion along a line defined by the vessels center and the point on the shell where first rupture occurs. Airblast overpressures at gages along the line of the jet show overpressures a factor of 4 or more greater than pressures along a line in the opposite direction from the jet.

Two methods were used to calculate the airblast from bursting high pressure vessels. A two-dimensional hydrocode, TUTTI, was used to calculate airblast overpressures near the vessel and in non-ideal situations, i.e., in the presence of obstructions. A one-dimensional hydrocode, WUNDY, may be used to arrive at airblast overpressures in uncomplicated situations or at distances greater than 5 or 6 vessel radii from the burst. TUTTI tends to give airblast overpressures in the high range of the measurements -- an acceptable situation where the data is to be used to establish safety criteria. WUNDY tends to give pressures in the middle range of the measured data.

The wall fragments observed in this test program weighed from 50 pounds for the 15,000 psi vessel to 271 pounds for the 50,000 psi vessels. These were accelerated to velocities up to 350 feet/second. For many situations, fragments are a greater threat than is the blast generated by high pressure vessel rupture.

ACKNOWLEDGEMENTS

The author is indebted to many people for their help in completing this investigation. Within the Naval Surface Weapons Center, J. Petes and J. Proctor were consultants. D. Lehto did the theoretical work and was helpful in the interpretation and analysis of the data. J. Powell was project engineer for the Dahlgren Laboratory.

H. Pohto, K. Valentine, R. Greene, and J. Kois of the Union Carbide Corporation, Nuclear Division, Y-12 Plant acted as technical advisors and consultants.

The NSWC/WOL field personnel were C. Kelly, P. Peckham, and F. Bampfield.

TABLE 2.1 TANK DATA

BURST PRESSURE (PSI)	INTERNAL RADIUS (INCHES)	SHELL THICKNESS (INCHES)	EXTERNAL RADIUS (INCHES)	TANK WEIGHT (POUNDS)	WEIGHT OF ARGON AT BURST PRESSURE (POUNDS)	NUMBER OF STANDARD FT^3 REQUIRED TO PRESSURIZE VESSEL TO RATED PRESSURE**
15,000	7.50	0.48	7.98	102	62.2	560
30,000	7.50	0.99	8.49	300	77.5	700
50,000	7.50	1.73*	9.23	413	86.6	780

*THIS VESSEL WAS UNDERCUT TO A MINIMUM THICKNESS OF 1.45" (SEE FIGURE 2.3)

** AT 17°C

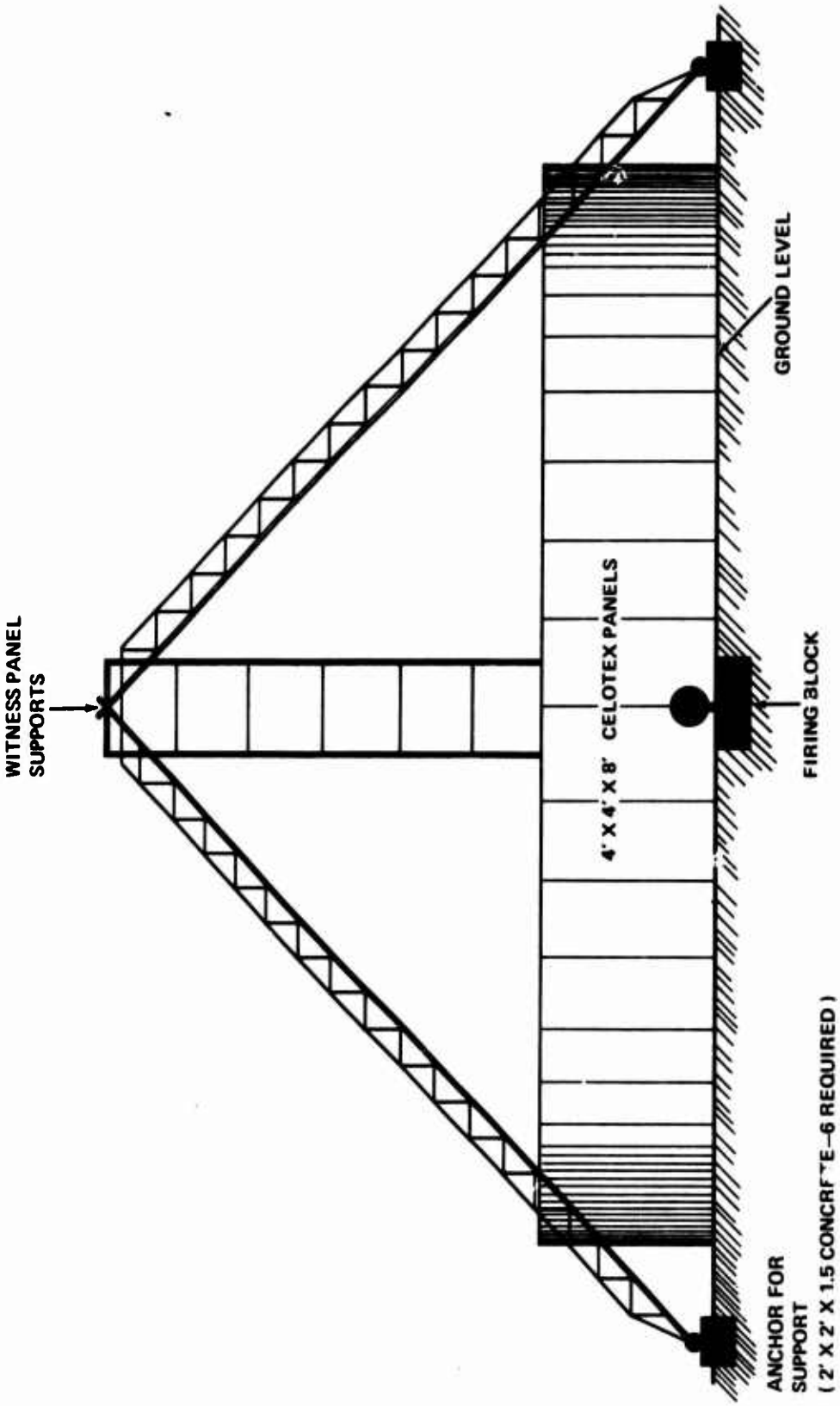

FIG. 2.1 FIRING SITE INSTALLATION; ELEVATION VIEW.

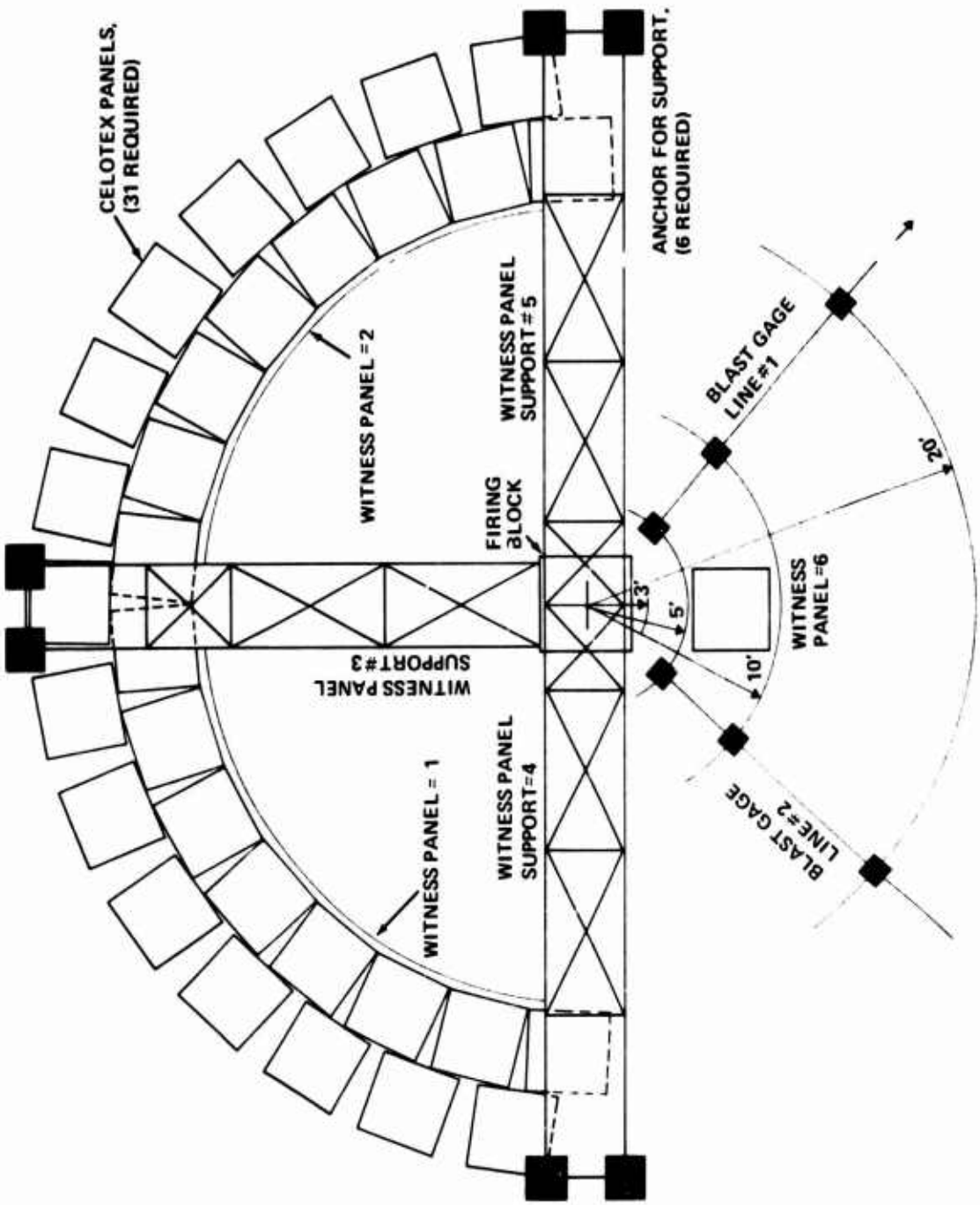

FIG. 2.2 FIRING SITE INSTALLATION; PLAN VIEW

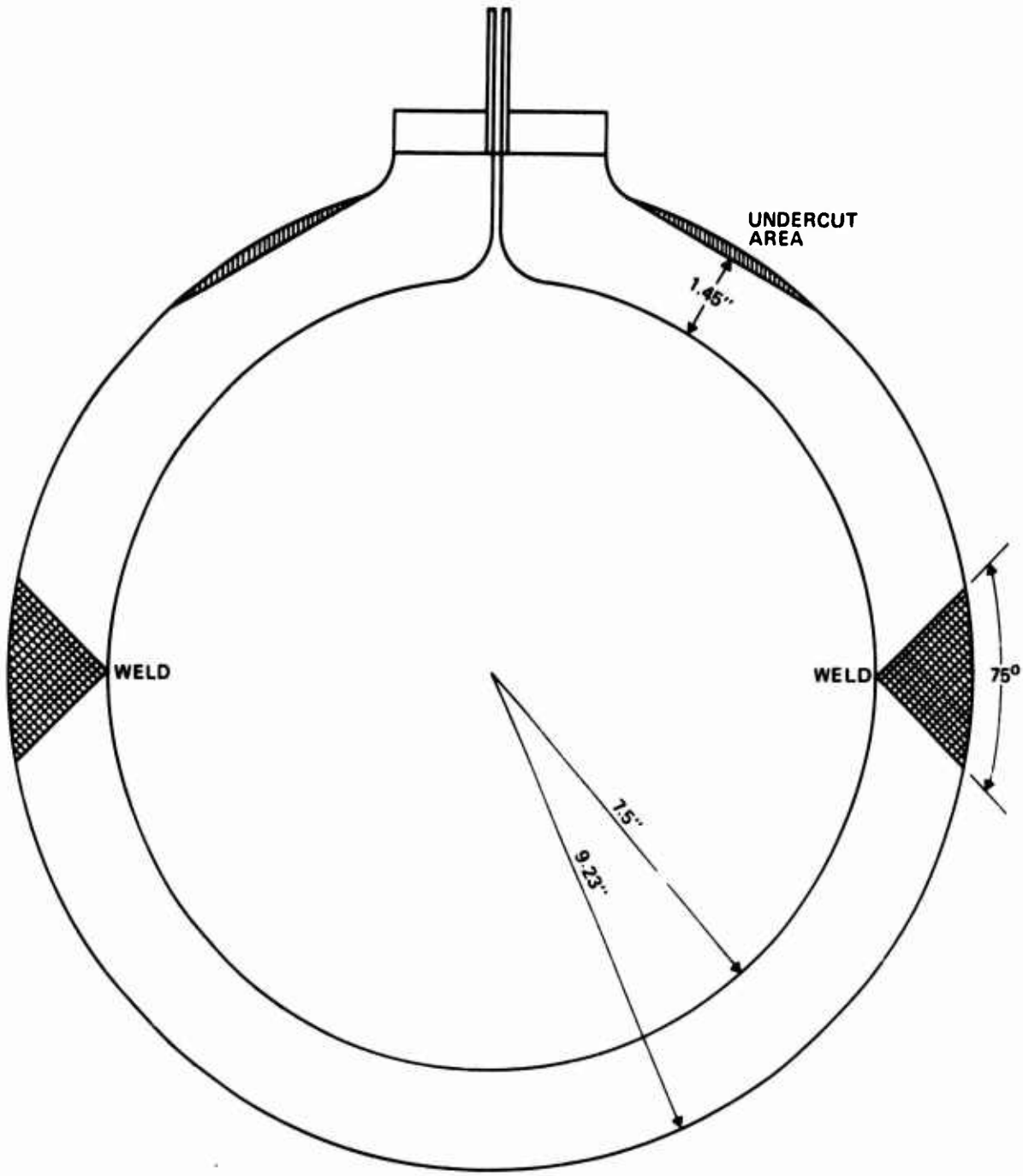

FIG. 2.3 50,000-PSI TEST VESSEL

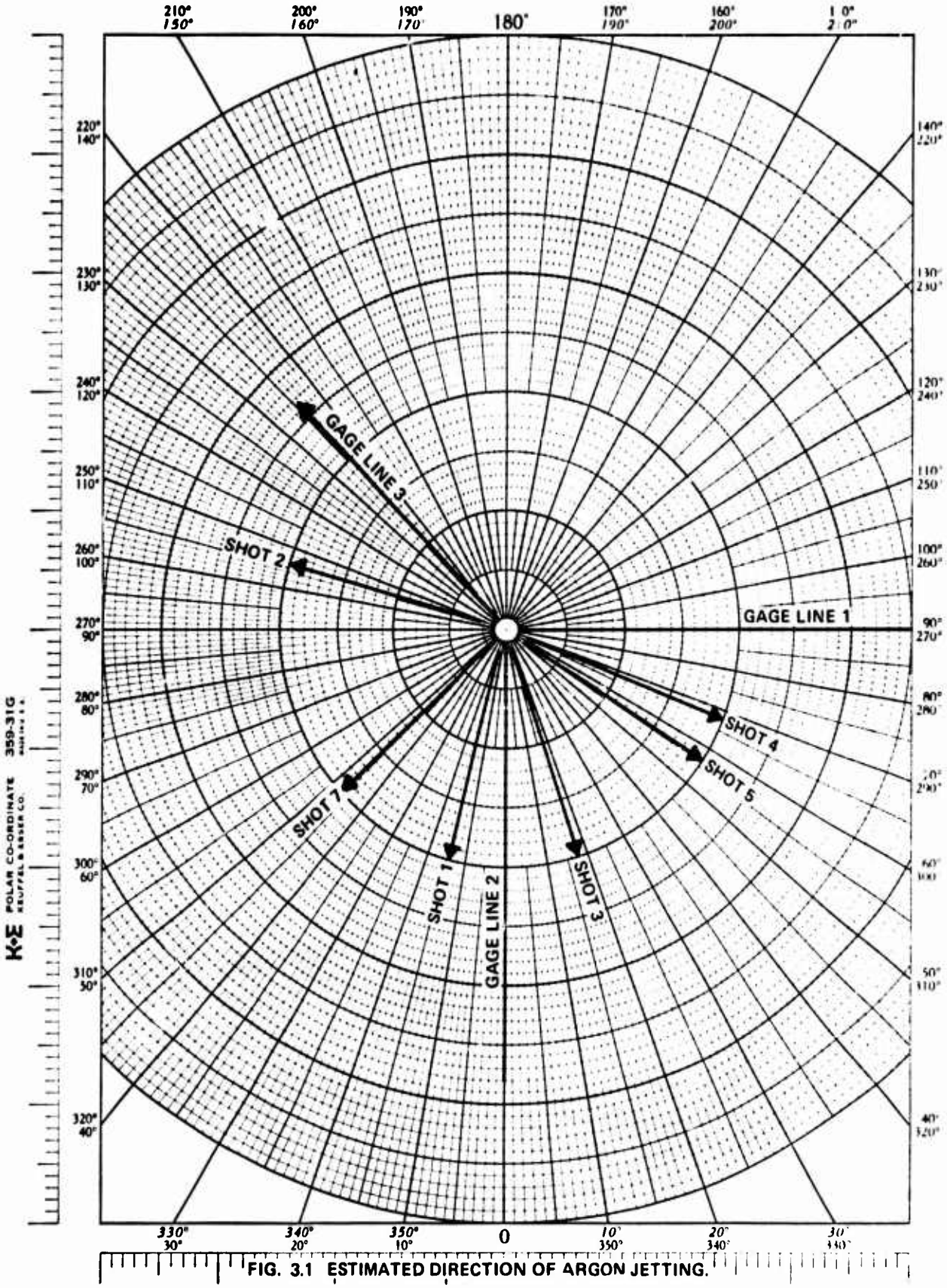

FIG. 3.1 ESTIMATED DIRECTION OF ARGON JETTING.

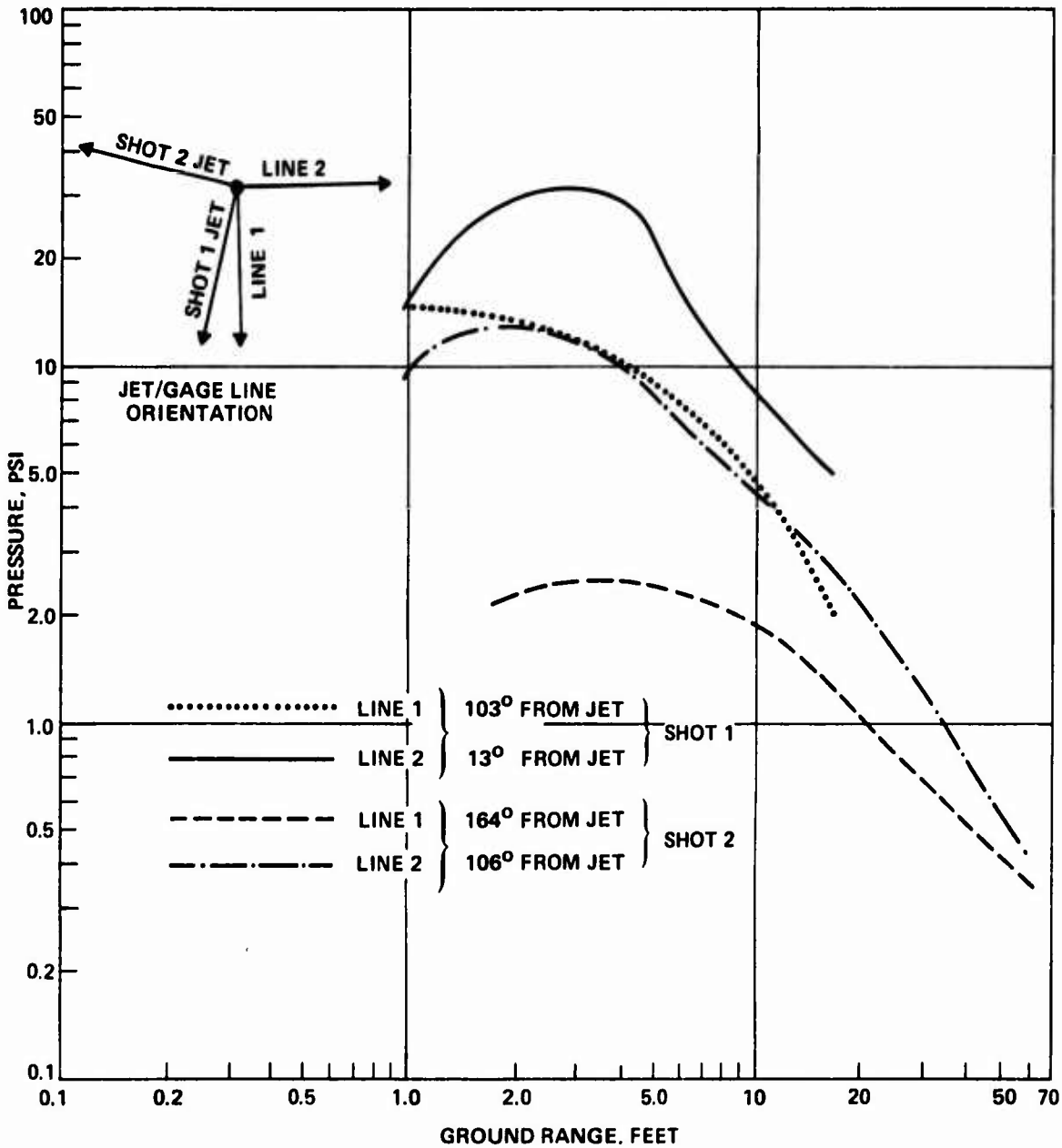

FIG. 3.2 AIRBLAST OVERPRESSURE FROM 15,000 - PSI VESSEL RUPTURE.

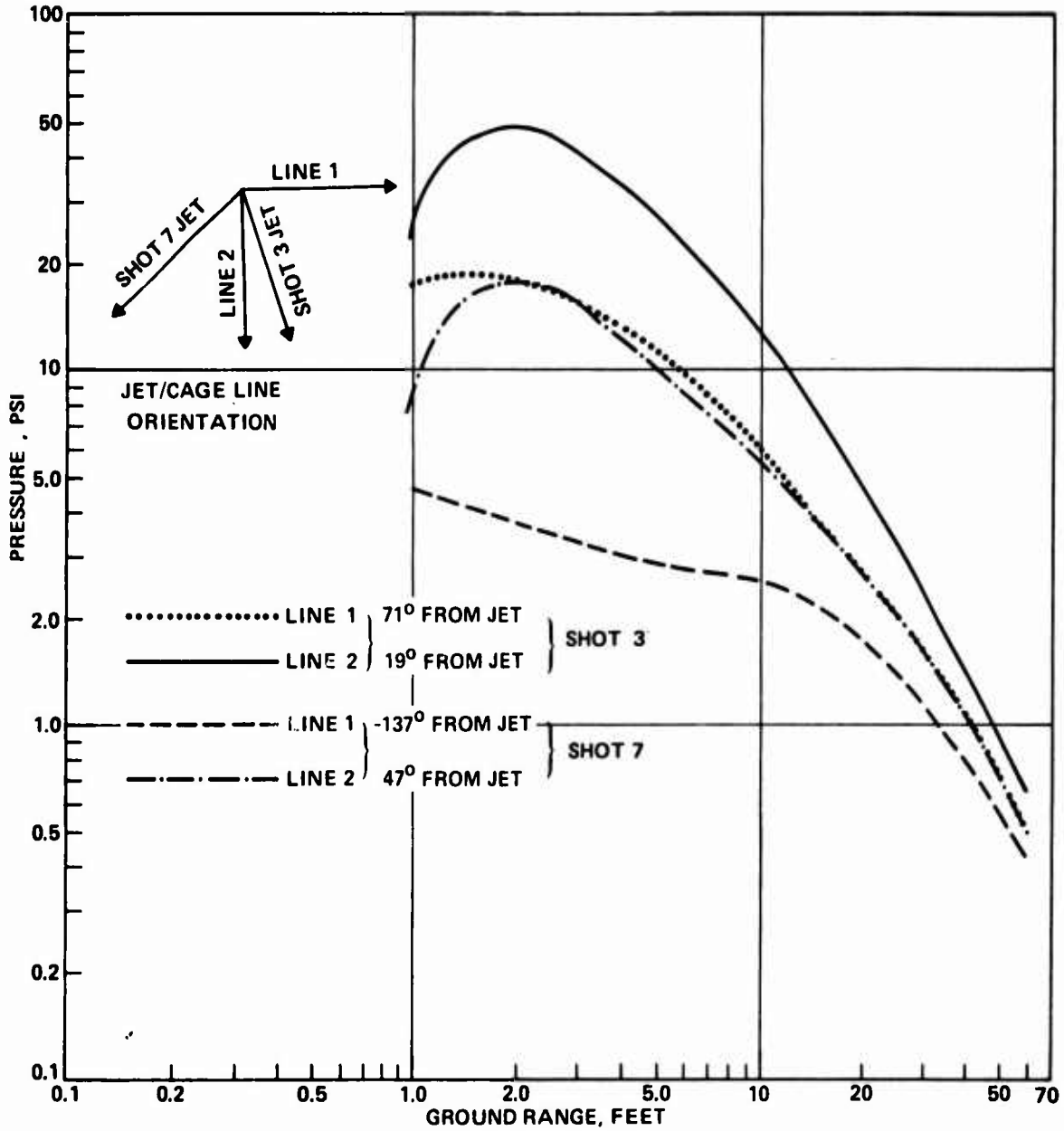

FIG. 3.3 AIRBLAST OVERPRESSURE FROM 30,000 - PSI VESSEL RUPTURE

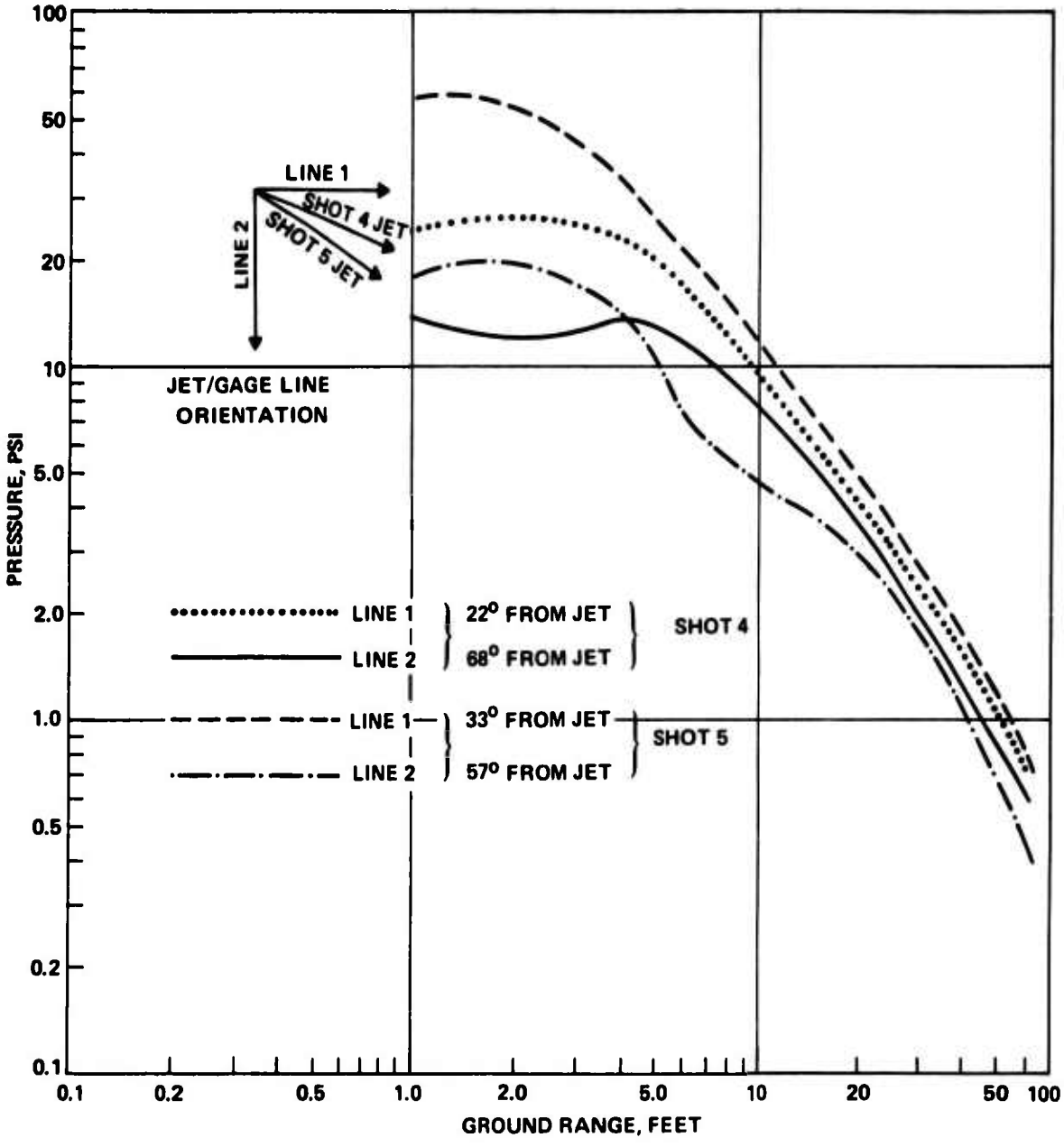

FIG. 3.4 AIRBLAST OVERPRESSURE FROM 50,000 - PSI VESSEL RUPTURE

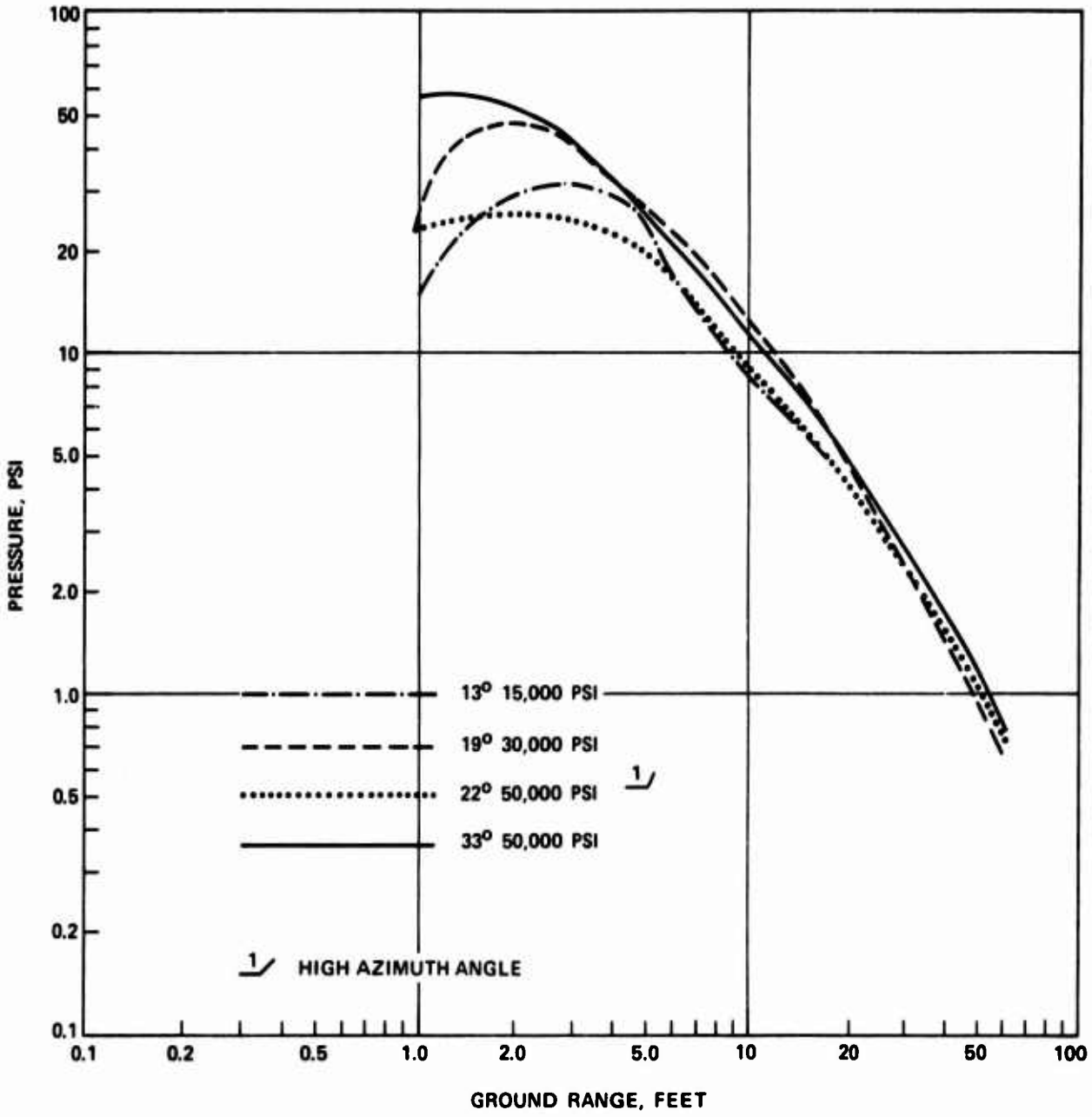

FIG. 3.5 OVERPRESSURE ALONG GAGE LINES ORIENTED WITHIN 33° OF THE ARGON JET

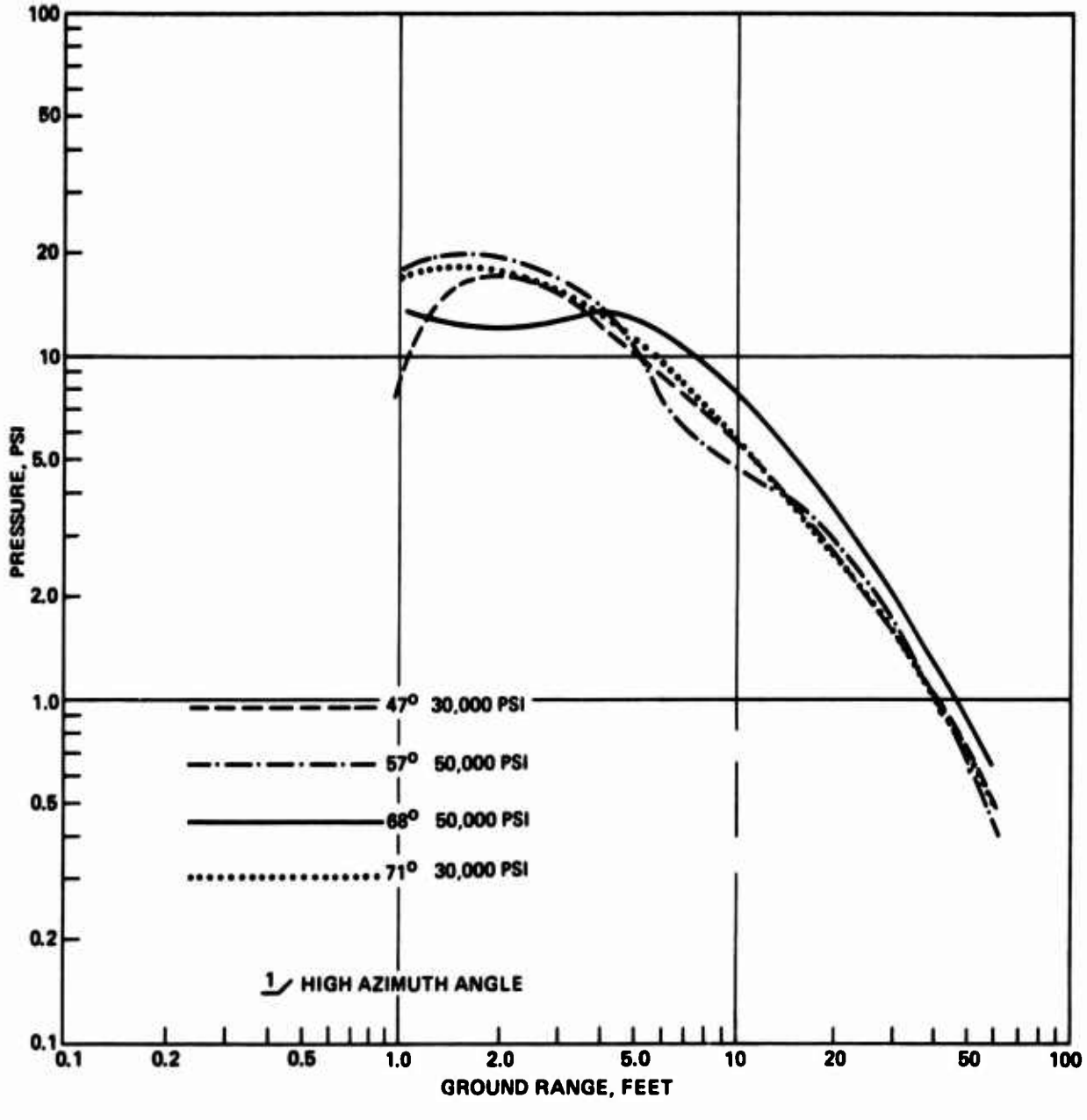

FIG. 3.6 OVERPRESSURE ALONG GAGE LINES ORIENTED WITHIN 47° to 71° OF THE ARGON JET.

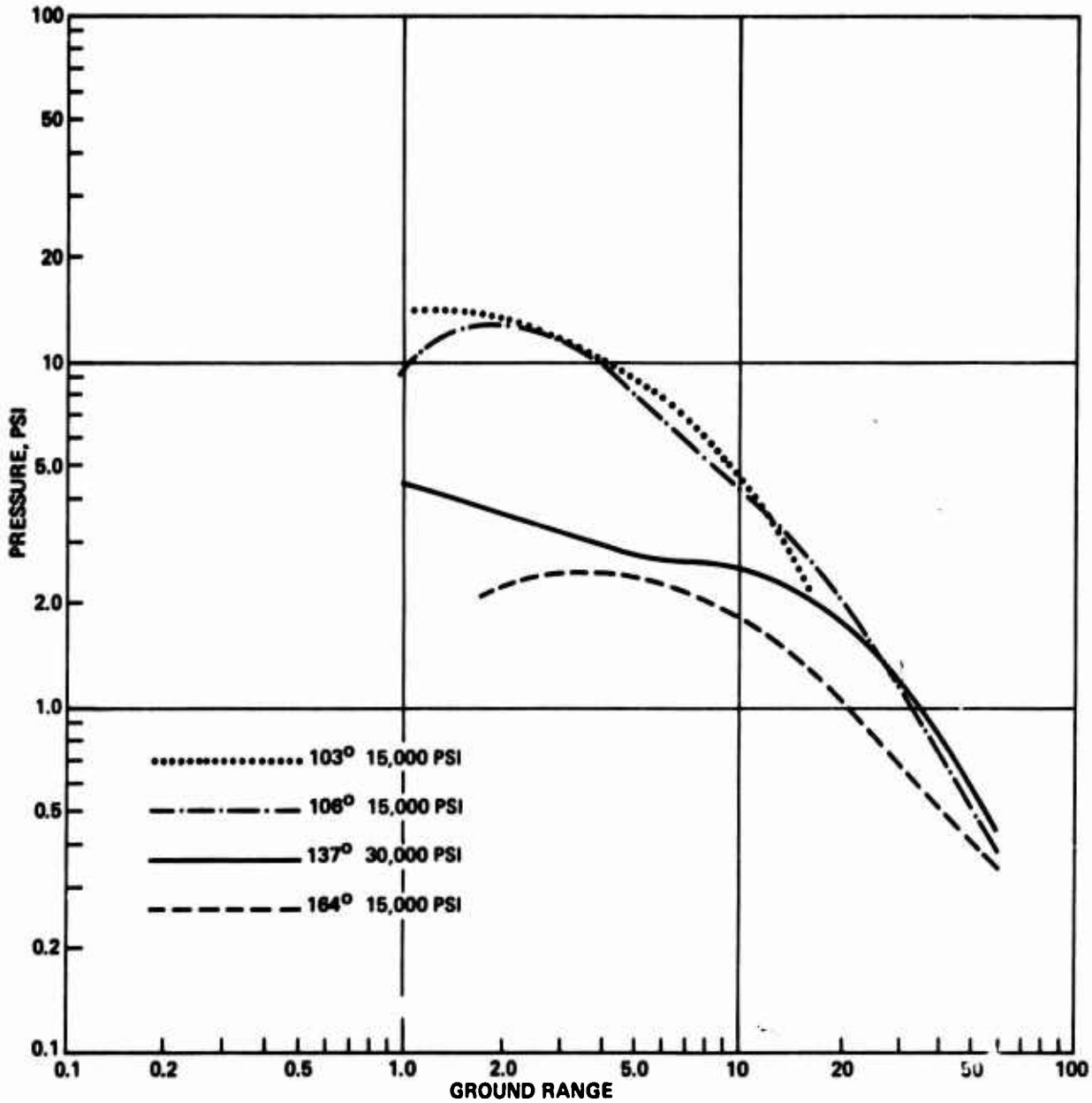

FIG. 3.7 OVERPRESSURE ALONG GAGE LINES ORIENTED WITHIN 103° TO 164° OF THE ARGON JET.

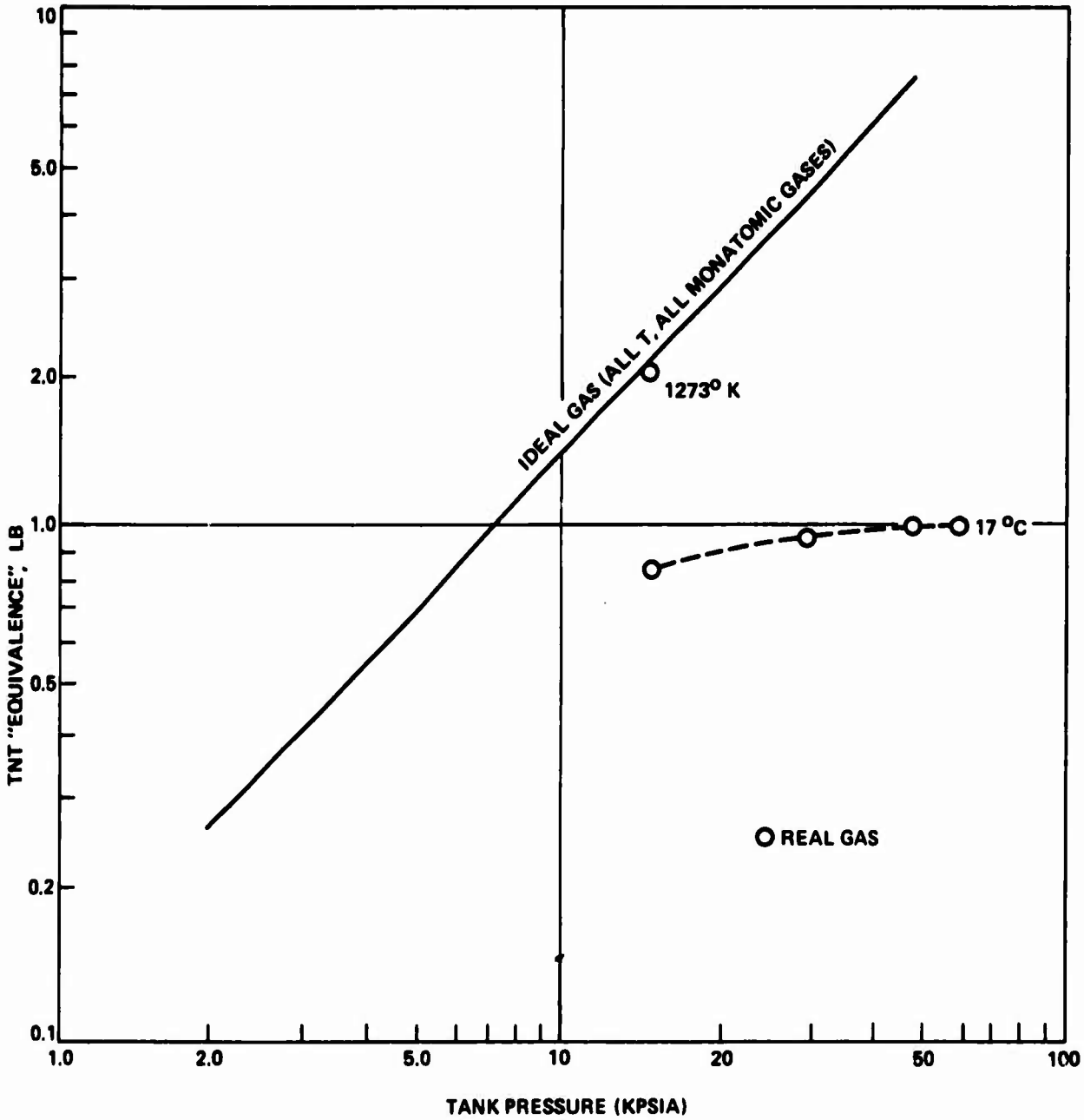

FIG. 3.8 TNT ENERGY EQUIVALENCE OF 1 FT^3 PRESSURIZED ARGON TANKS

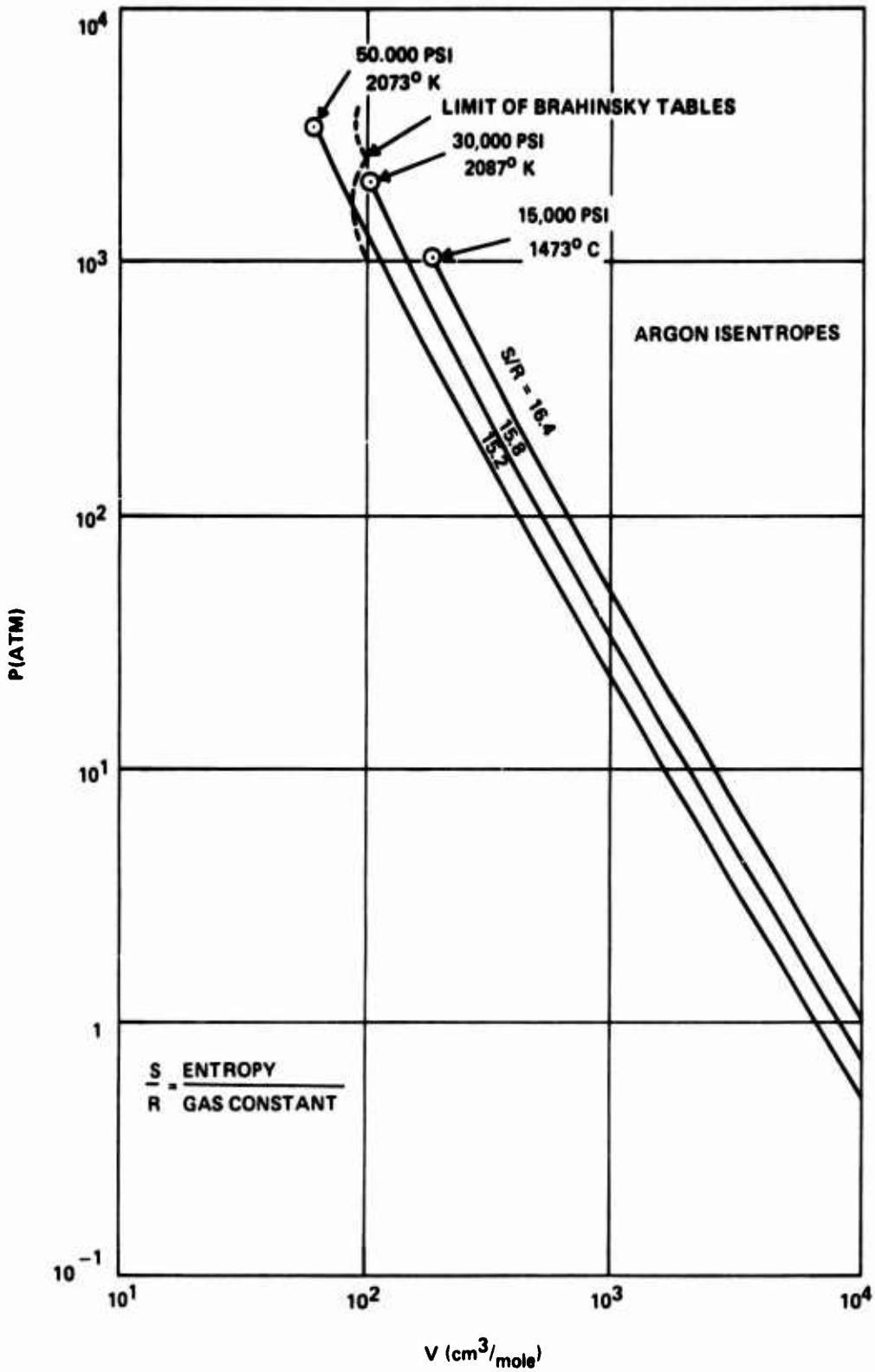

FIG. 3.9 ISENTROPES FOR HIGH TEMPERATURE ARGON

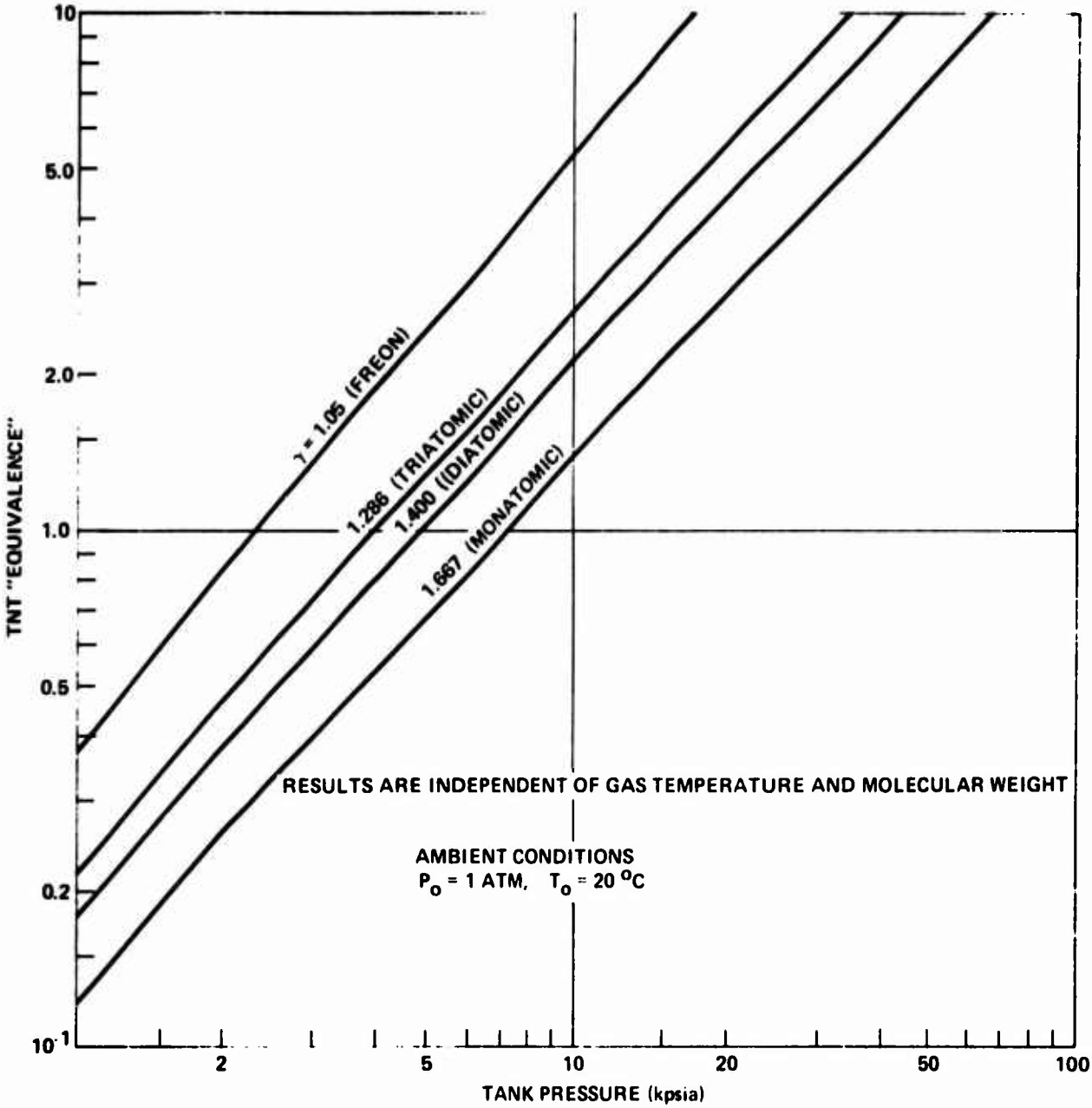

FIG. 3.10 TNT EQUIVALENCE OF 1.0 FT^3 PRESSURIZED TANKS FILLED WITH IDEAL GAS.

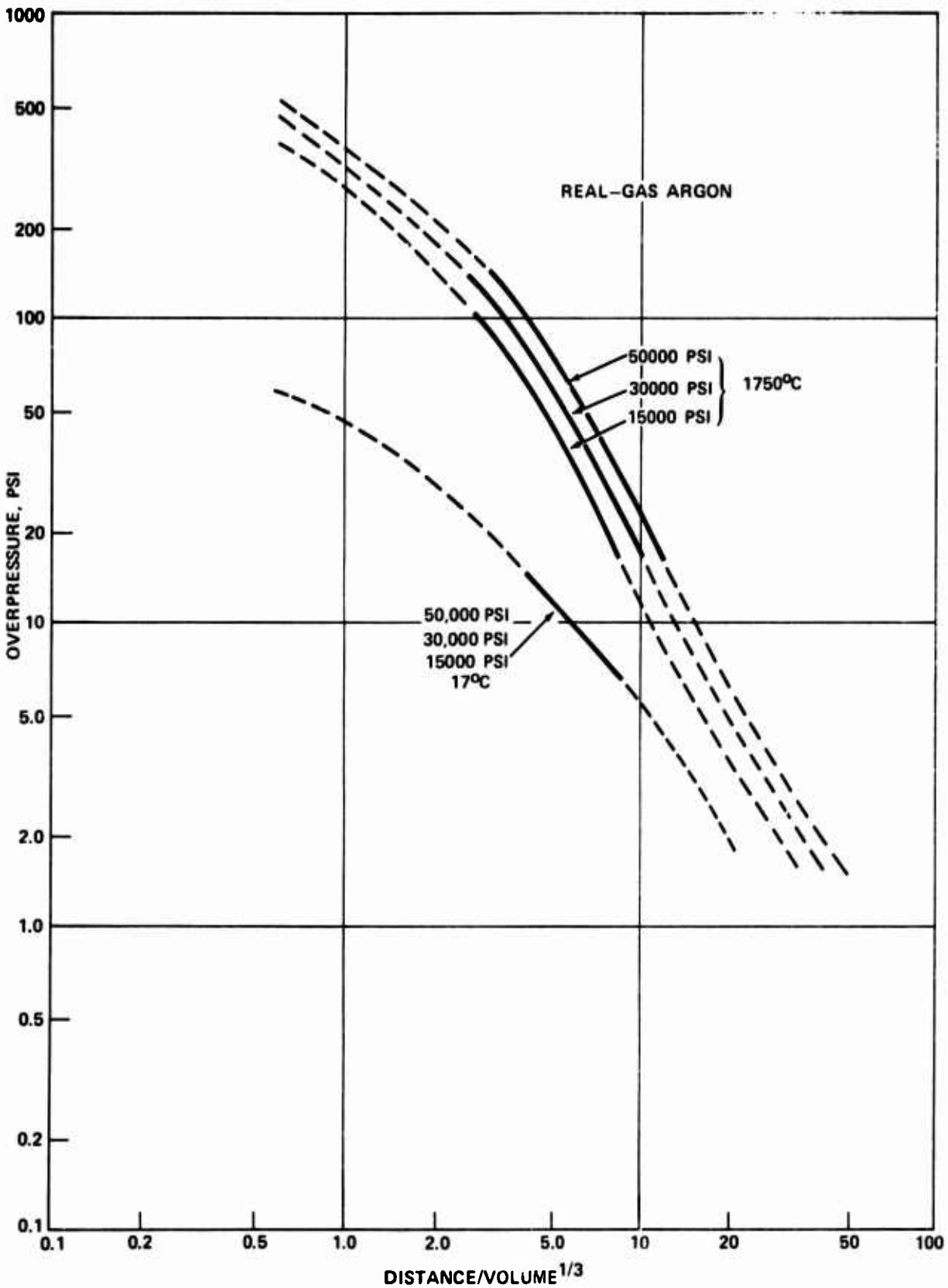

FIG. 3.11 PEAK FREE-AIR SHOCK OVERPRESSURE VS DISTANCE FOR ARGON TANKS

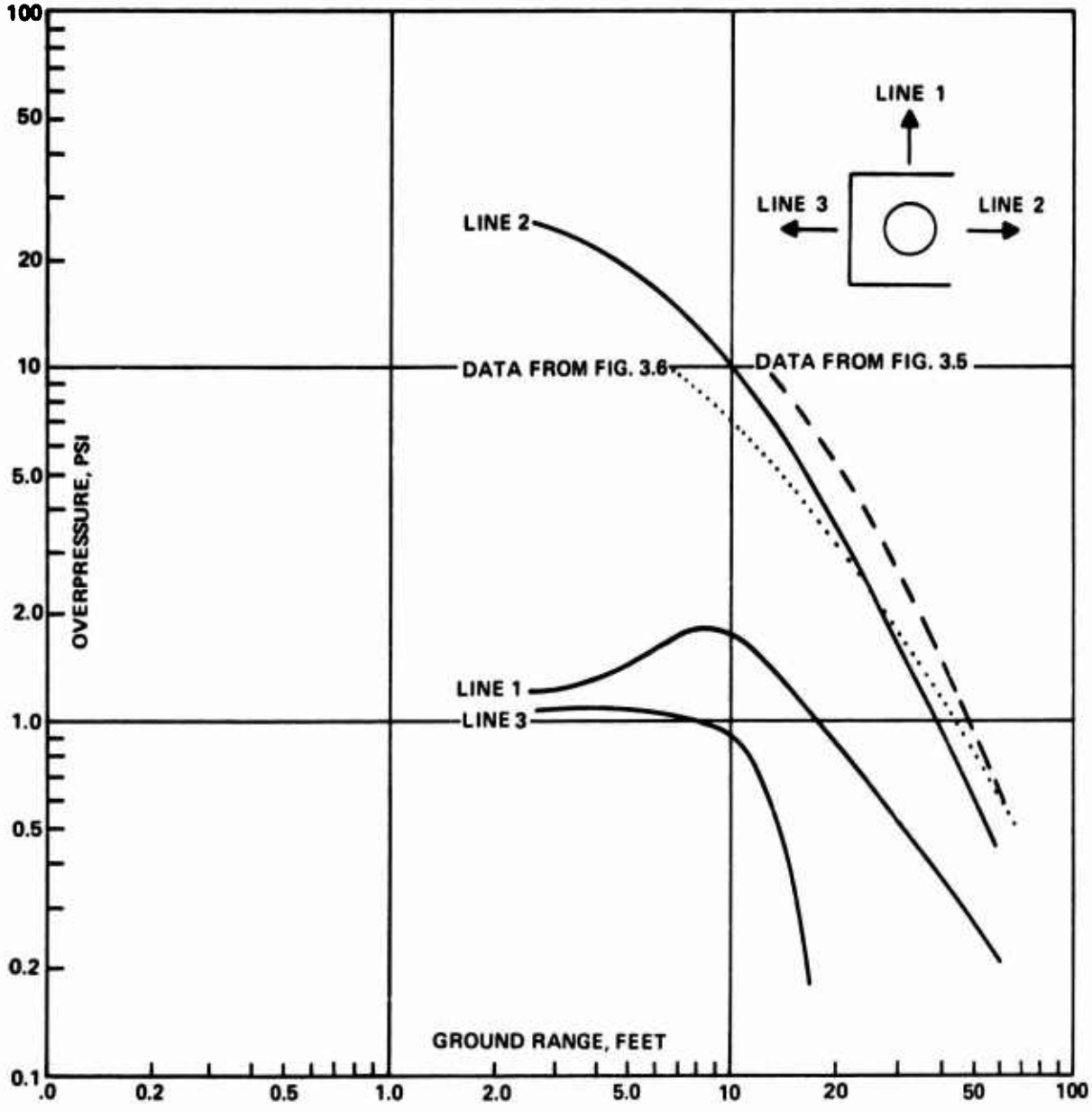

FIG. 3.12 COMPARISON OF AIRBLAST OVERPRESSURES FROM CONFINED TEST WITH FREE FIELD DATA

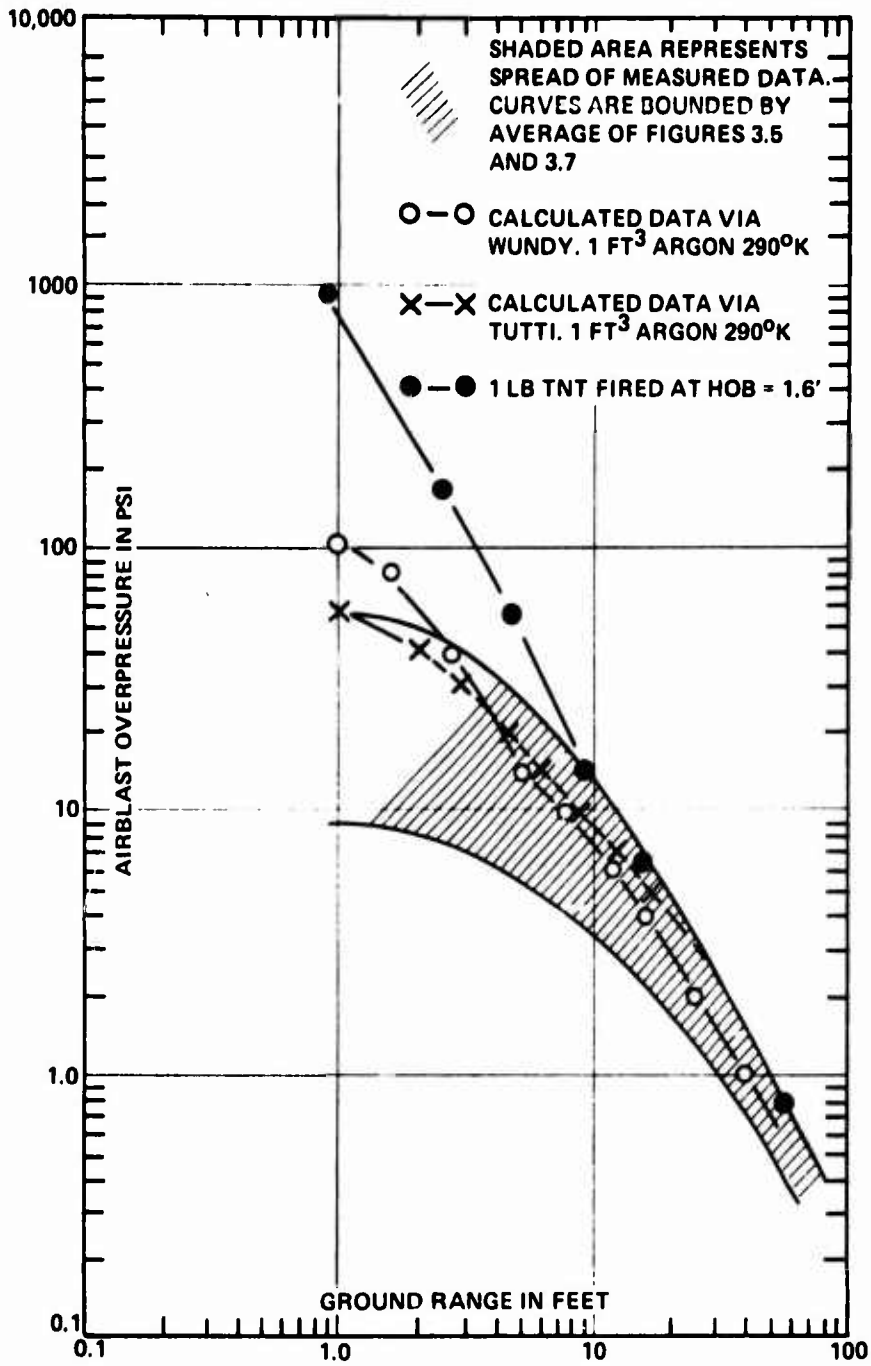

FIG. 3.13 COMPARISON OF DATA

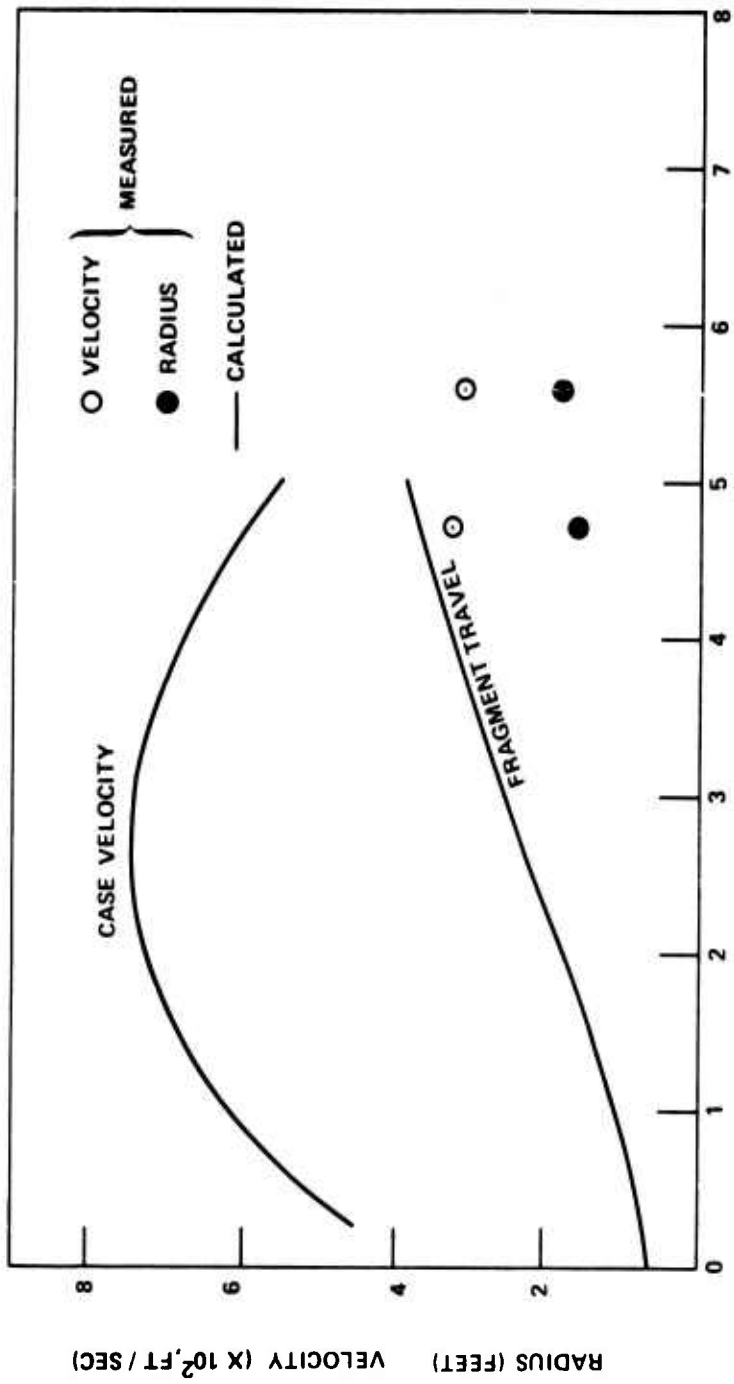

FIG. 4.1 CALCULATED AND MEASURED VELOCITIES FOR 15,000 - PSI FRAGMENTS.

ANNEX A EXPERIMENTAL PLAN

A.1 Pressure Vessels

All test vessels were spherical containers with an internal radius of 7.5 inches and a volume of one cubic foot. They were made from preformed hemispheres of T-1 steel welded together. A section of high pressure tubing welded into the vessel's boss provided a gas inlet. This arrangement is shown in Figure 2.3. Three of the vessels were designed to burst at 15,000 psi, two were designed to burst at 30,000 psi, and the remaining two were designed to burst at 50,000 psi.

The yield strength of T-1 steel is 137 Kpsi, the ultimate strength is 151 Kpsi. Measured yield and ultimate strengths of the equatorial weld material were 114 Kpsi and 121 Kpsi respectively. Other vessel data pertinent to this investigation are given in Table 2.1.

The argon fill gas weight in Table 2.1 is given for a 1 ft^3 volume. It is based on the compression data for argon given in Section 2.2 of this report. A standard cubic foot (SCF) of argon as used here is given as 0.111 pounds of argon at 290°K and 14.4 psiA, (reference A.1).

A.1.1 Pressure Vessel Expansion

Pressure vessel expansion was recorded as a function of pressure from beginning of pressurization to burst. Measurements were made along two mutually perpendicular circumferences as shown in Figure A.1. The system consisted of cords wrapped around the vessel and attached to linear potentiometers, An increase in vessel circumference moved the slide on the potentiometer producing a resistance increase proportional to the increase in circumference. Potentiometer outputs were recorded on chart recorders.

A.2 Pressurization System

The multi-stage pressurization system, shown schematically in Figure A.2, was manufactured by the Haskel Engineering and Supply Company of Burbank, California*. The argon was supplied from bottles at a pressure of between 1,000 and 2,350 psig. This pressure was increased to 35,000 psig by the model 14 ATS-315C gas booster. The model 15939-2 intensifier increased the pressure from 35,000 psig to a maximum of 60,000 psig. The intensifier piston was driven by a model GS-100-C hydraulic pump. Both the booster and the hydraulic pump were driven by an air compressor supplying 200 SCF/minute at 100 psig.

Pumping rate of the system is a function of the air drive pressure, the argon supply pressure, and the outlet pressure. Pressurization times for the vessels depended on pumping rate and the pressure in the vessel. Compression data for argon is shown in Figure A.3 (reference A.1). Average pumping rates were about 9 SCF/minute for the 15,000-psi vessels, 5 SCF/minute for the 30,000-psi vessels,

(A.1) Din, F. "Thermodynamic Functions of Gases, Volume 2: Air, Acetylene, Ethylene, Propane, and Argon "Butterworths, London, 1956.
*Mention of a manufacturer's products by name constitutes neither criticism nor endorsement by the Naval Surface Weapons Center.

and 4.9 SCF/minute for the 50,000-psi vessels.

Internal vessel pressures were measured with a transducer near the inlet of the test vessel. As shown in Figure A.2 the gage was fed through a 20 foot section of high pressure tubing connected into the main line 280 feet from the pump and 20 feet from the test vessel. The static error band for the transducer was $\pm$0.4% full scale based on a terminal straight line. Thermal effects gave a zero voltage shift of 0.05% of full scale per °C. The gage output was recorded in real time on a chart recorder.

A thermocouple extending into the test vessel continuously monitored the argon temperature in the vessel. The output of the thermocouple was recorded on a strip chart recorder. System circuitry and a typical calibration curve for a chromel/alumel device are shown in Figure A.4.

A.3 Airblast Instrumentation

A.3.1 Blast Gages and Layout

Airblast generated by vessel rupture was measured along two lines for the six unconfined tests as shown in Figure A.5. The seven gages used on each line were deployed in the following manner. The first two gages, 1-1 and 2-1 from Figure A.5, were flush mounted in the concrete firing pad at a ground range of 1 foot. These gages were either Kulite Semiconductor Product's model HSK-375 or Susquehanna Instrument's model ST-4. The second two gages were located at mid vessel height and 1 foot from the vessel's perimeter. These were Model ST-7 gages made by the Susquehanna Instrument Company. The third two gages, positions 1-3 and 2-3, also mounted in the firing pad, were at a ground range of 2.5 feet. These gages were models LC-70 or LC-71 gages made by Celesco Industries. Positions 1-4 and 2-4, 1-5 and 2-5, and 1-6 and 2-6 were located in individual 2 x 2 feet concrete pads at ground ranges of 5, 10, and 16.5 feet respectively. The gages used in these positions were also model LC-70's or LC-71's. Positions 1-7 and 2-7 were at a ground range of 60 feet. These gages, model LC-33's made by Celsco Industries, were mounted 1 foot above the ground. Another LC-33 gage, position 3-1 in Figure A.5, was mounted 1 foot above the ground and at a ground range of 13.2 feet.

Figure A.6 shows the gage layout for the confined test. Changes from the unconfined test layout were: the closest gage positions were removed, an additional gage line was installed, and six face-on gages were installed flush with the walls of the confining structure. These gages were supported by mounts outside the structure, as shown in Figure A.7. A potting compound isolated the gage mounts from the structure walls to prevent unwanted acceleration being imparted to the gages by the wall motion. (Figure A.8).

One ST-4 and one LC-70 gage was used in each wall. A thin sheet of pyrolytic graphite was glued to the face of each LC-70 gage to insulate the gage against the low temperature of the expanding argon.

A.3.2 Blast Instrumentation

Gage signals were fed to charge amplifiers located at the gages. Signals from the charge amplifiers were fed through coaxial cables to the recording equipment located in an instrument trailer some 500 feet from ground zero.

The recording system consisted of 12 oscilloscope channels and 14 magnetic tape channels. The oscilloscopes, tape recorder, and the auxiliary equipment used for time bases, synchronization, and power were housed in a special instrumentation trailer. This and similar systems have been used at the Center over the past several years. They are described in reference A.2.

Two of the tape recorder's channels were used to record time code information and playback signals. Thus 12 tape channels and 12 oscilloscope channels were available for blast recording. Since 15 gages were used for the unconfined tests, 9 gages were recorded on both tape and oscilloscopes. For the confined test, 21 gages were used so that only three channels were recorded on both systems.

A.4 Confining Structure

One 15,000 psi vessel was burst inside a 5-sided,cubical steel structure, Figures A.7 and A.8. The open side of the vessel was perpendicular to the ground. The test vessel was centrally located in the structure.

The structure's internal volume was determined by roughly scaling it to the volume of an autoclave facility in operation at the Oak Ridge Y-12 Plant. The autoclave facility's volume is about 14,700 ft^3. The autoclave external volume is about 500 ft^3 giving a volume ratio of 29. The test vessel's volume is 1.2 ft^3. Thus the confining structure's volume of 35 ft^3 roughly scaled the Y-12 Plant Facility.

A.5 Fragment Recovery and Velocity System

A.5.1 Fragment Recovery

The fragment recovery and velocity system design was based on the possibility that the test vessels might rupture in a brittle manner, i.e., break up into several fragments.

A semi-circular arena was constructed to recover a sample of the vessel fragments. The arena was made from Celotex bundles placed as shown in Figure 2.2. Each bundle was made from 84 sheets, each 4' x 8' x 0.5" to form a bundle 4' x 8' x 42". These bundles were deployed as shown in Figure 2.2 to form the arena.

A.5.2 Fragment Velocity System

All fragment velocity measurements were made using arrival time techniques. The instrumentation consisted of seven electronic counters. All counters were started by a zero time signal. This signal was generated by the interruption of an electrical current in a break wire wrapped around the vessel's outer surface. The counters were stopped by "velocity screens" placed at various positions about the vessel. These screens consisted of a continuous wire, wrapped about a frame-work. The wire carried a current that was interrupted, when severed by a fragment, to supply a stop signal. Signal shapers were used between the break wires and the counters to insure uniform signals to the counter inputs.

A.2 Tussing, R., "A Four Channel Oscilloscope Recording System", Naval Ordnance Laboratory, NOLTR 65-21, 18 May 1965

Screen locations are shown in Figures 2.1 and 2.2. Screen sizes varied according to their location as may be seen. The entire arena wall was divided up into screens 1 and 2. Screens 3, 4, and 5 were located on a teepee arrangement above the vessel. Screen 6 was located behind the vessel and Screen 7 was located around the test vessel. Because the vessel failed to fragment in a brittle manner, the screen arrangement was varied for the seven tests.

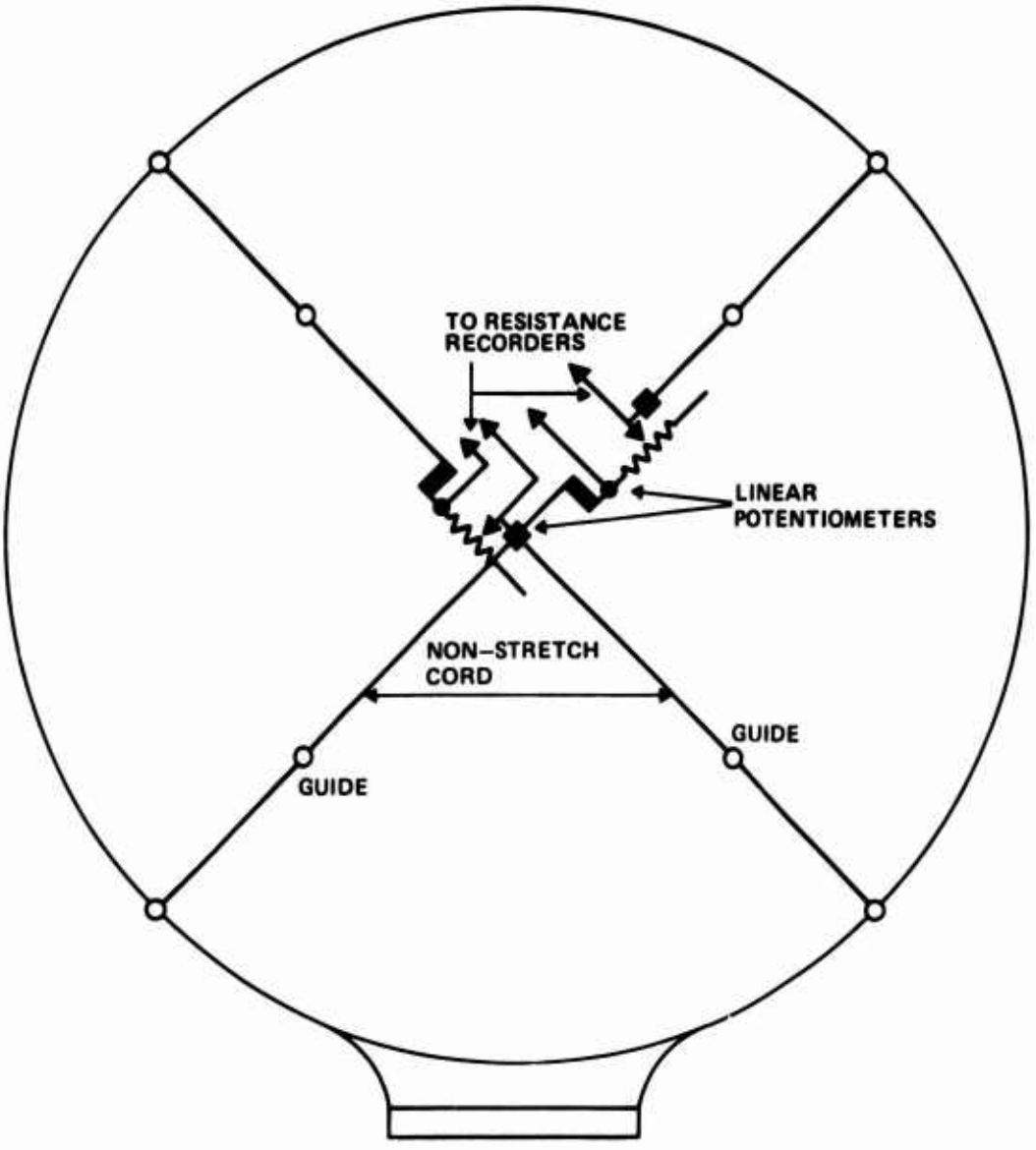

FIG. A.1 VESSEL EXPANSION SENSORS

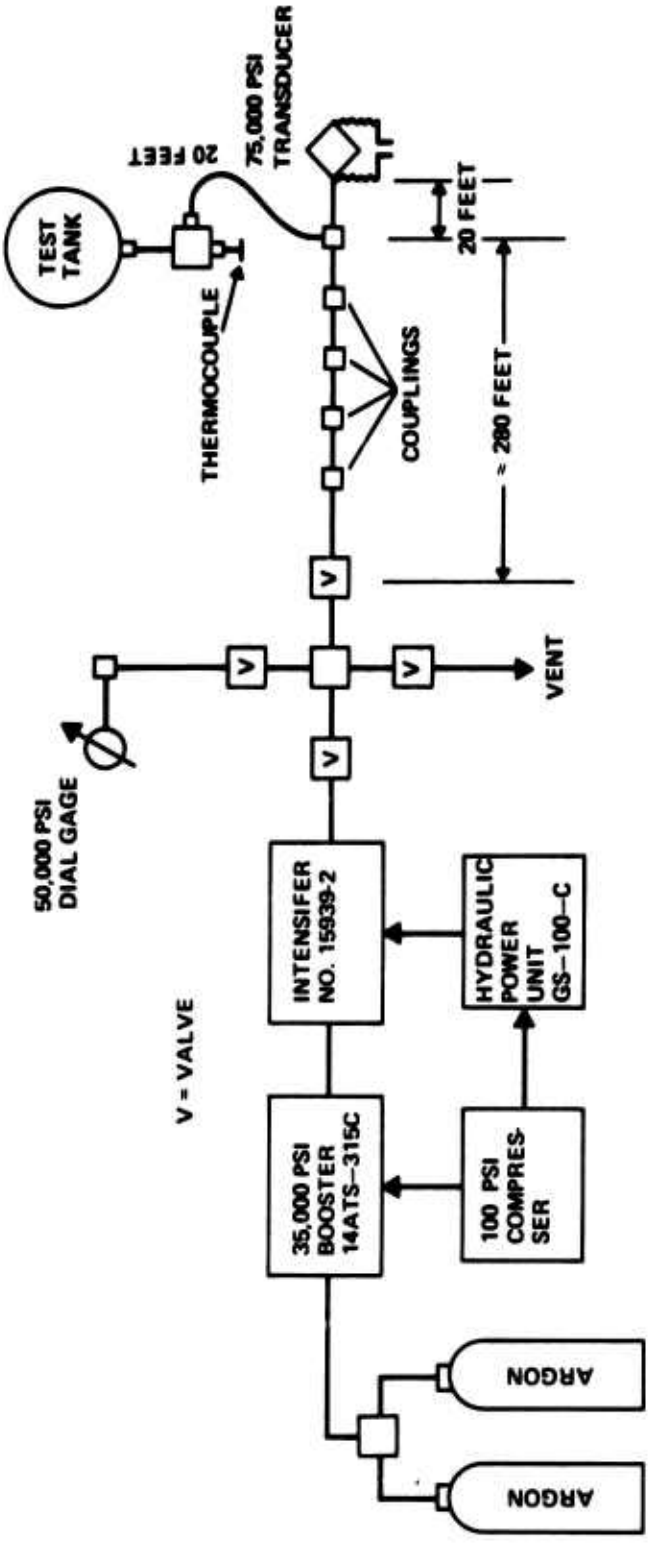

FIG. A.2 HIGH PRESSURE SYSTEM

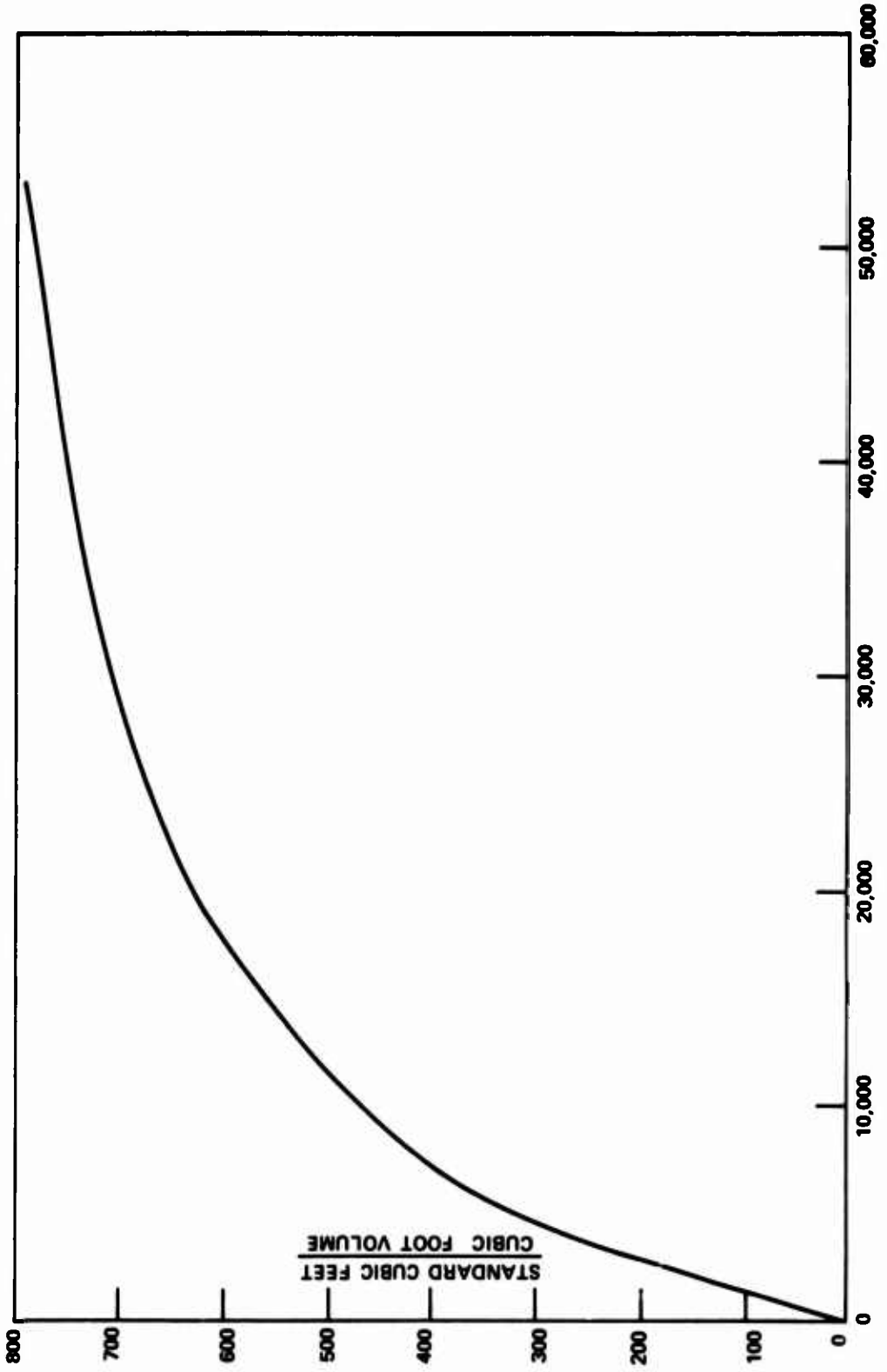

FIG. A.3 ARGON COMPRESSION DATA; 17°C

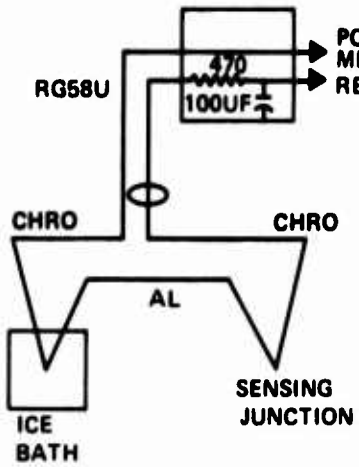

CAL FOR CIYI RECORDER

4.77 MV = 48.2 DIV = 0.98 $^{MV}/_{DIV}$

TEMP^{o} C	DIV	MV.	$MV/^{o}C$
0	0	0	
19.4	8.0	0.784	0.404
22.2	8.5	0.833	0.375
37.0	14.2	1.39	0.374
54.0	20.0	1.96	0.0362
92.2	37.5	3.67	0.0398

FOR 68^{o} F = 20^{o} C, VOLTAGE MEASURED ON POTENTIOMETER WAS 0.76 MV = 0.038 $^{MV}/^{o}C$

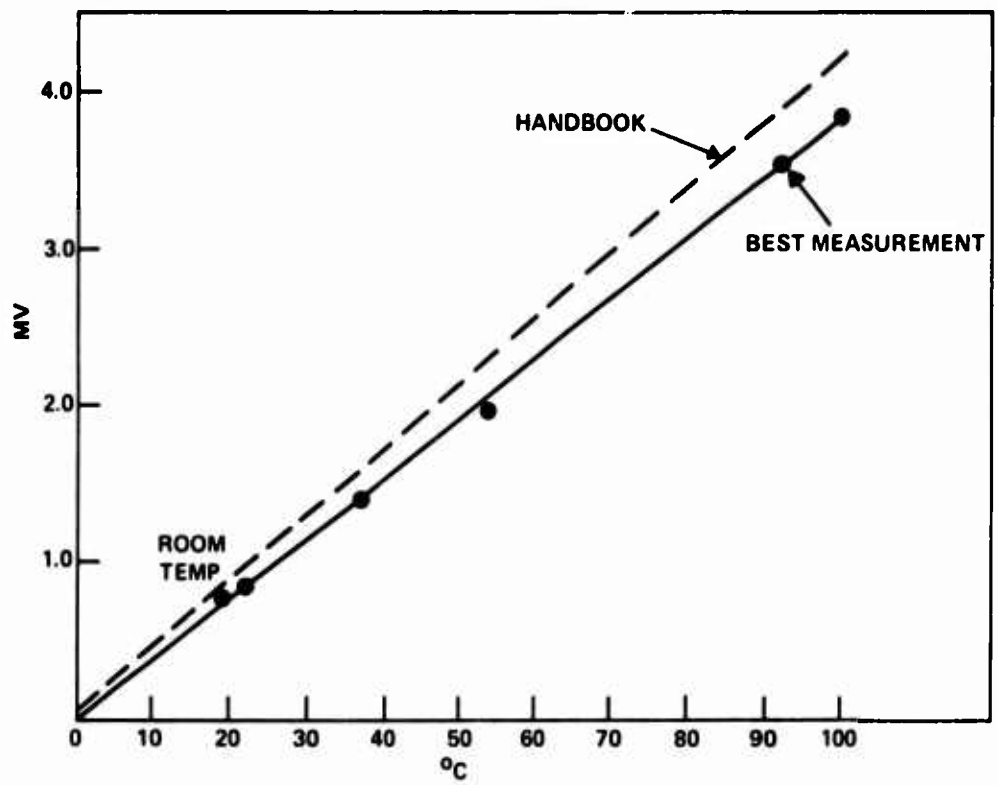

FIG. A.4 CHROMEL – ALUMEL TC CALIBRATION

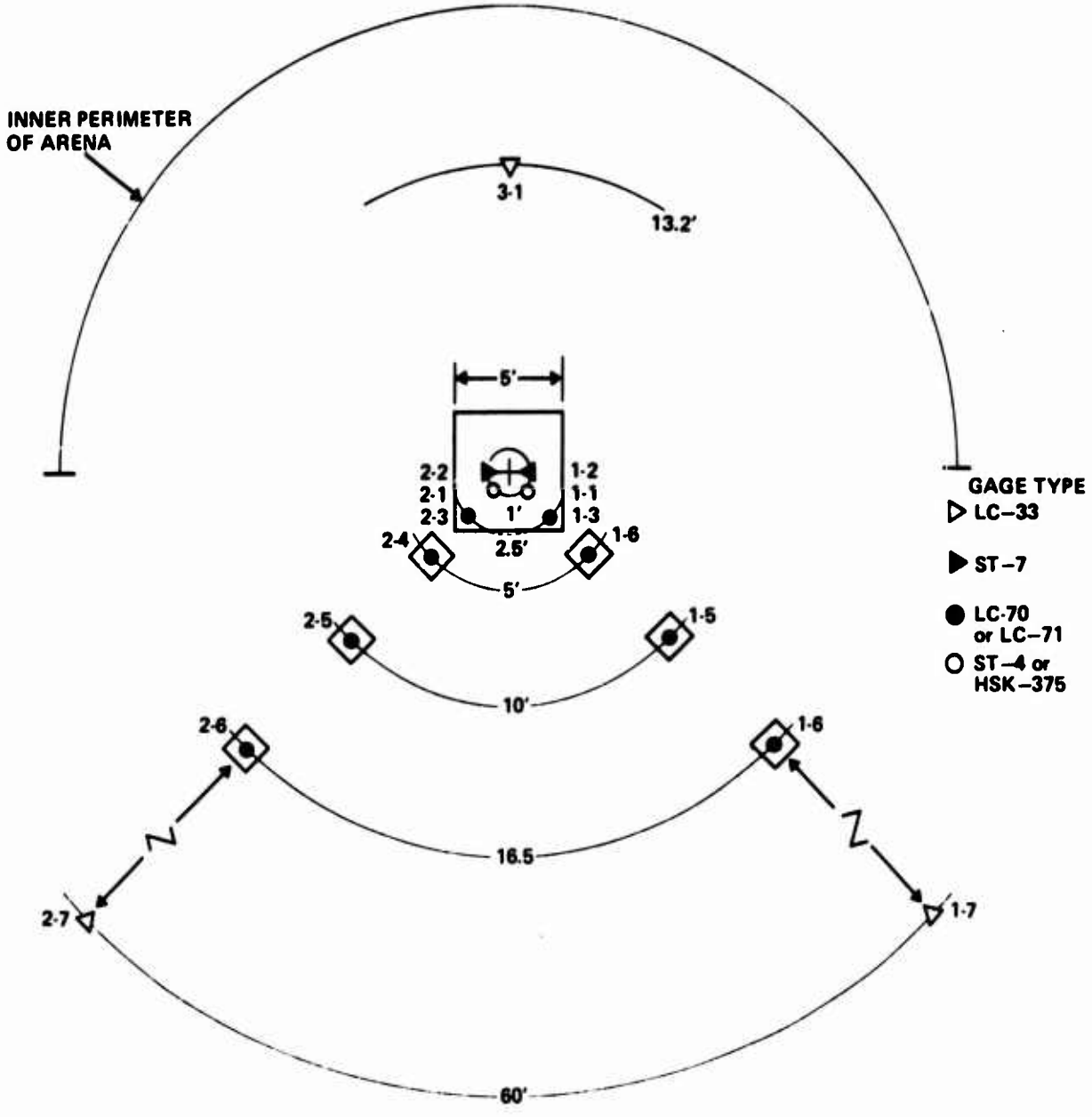

FIG. A.5 FIELD LAYOUT FOR UNCONFINED TESTS

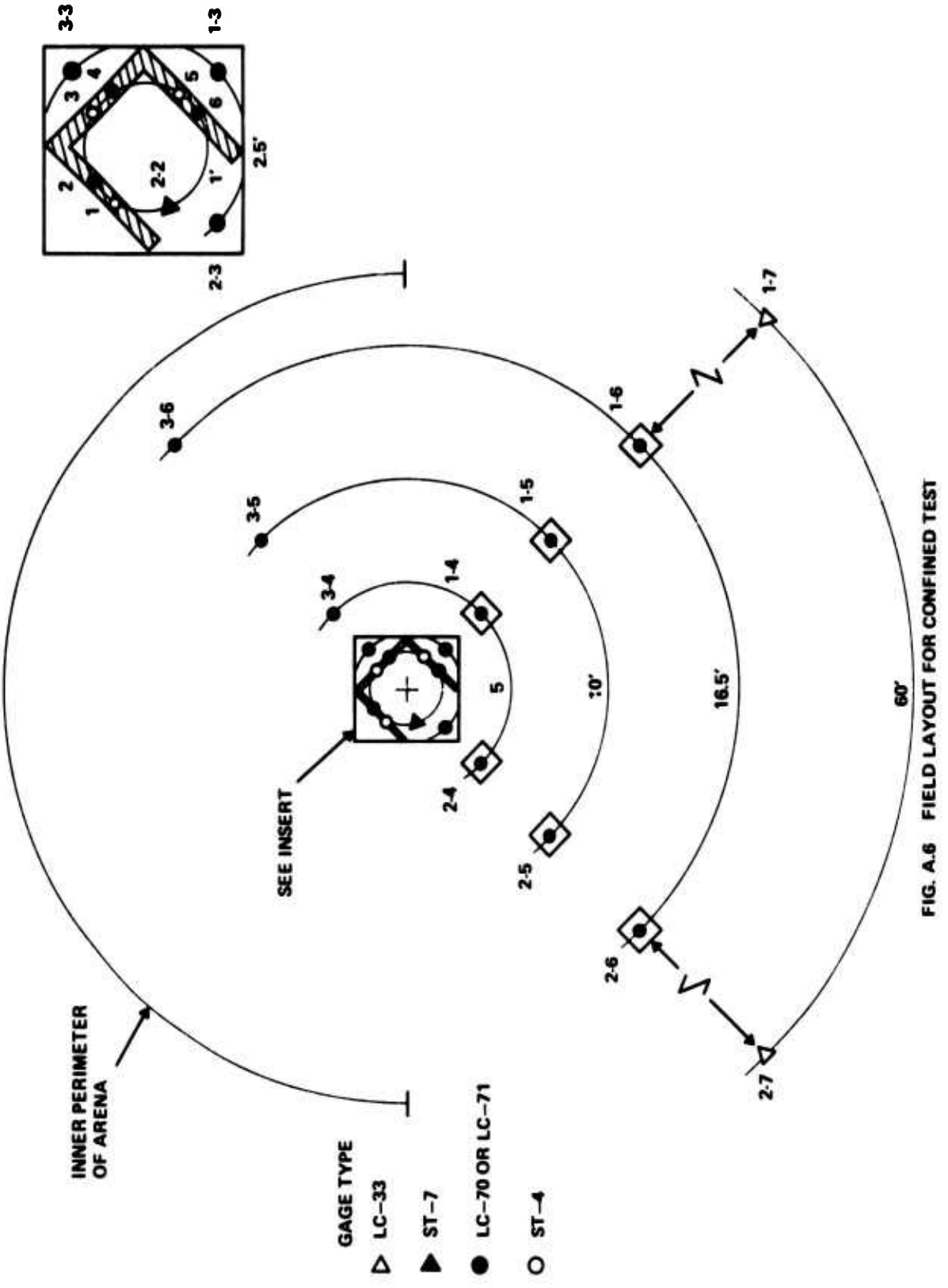

FIG. A.6 FIELD LAYOUT FOR CONFINED TEST

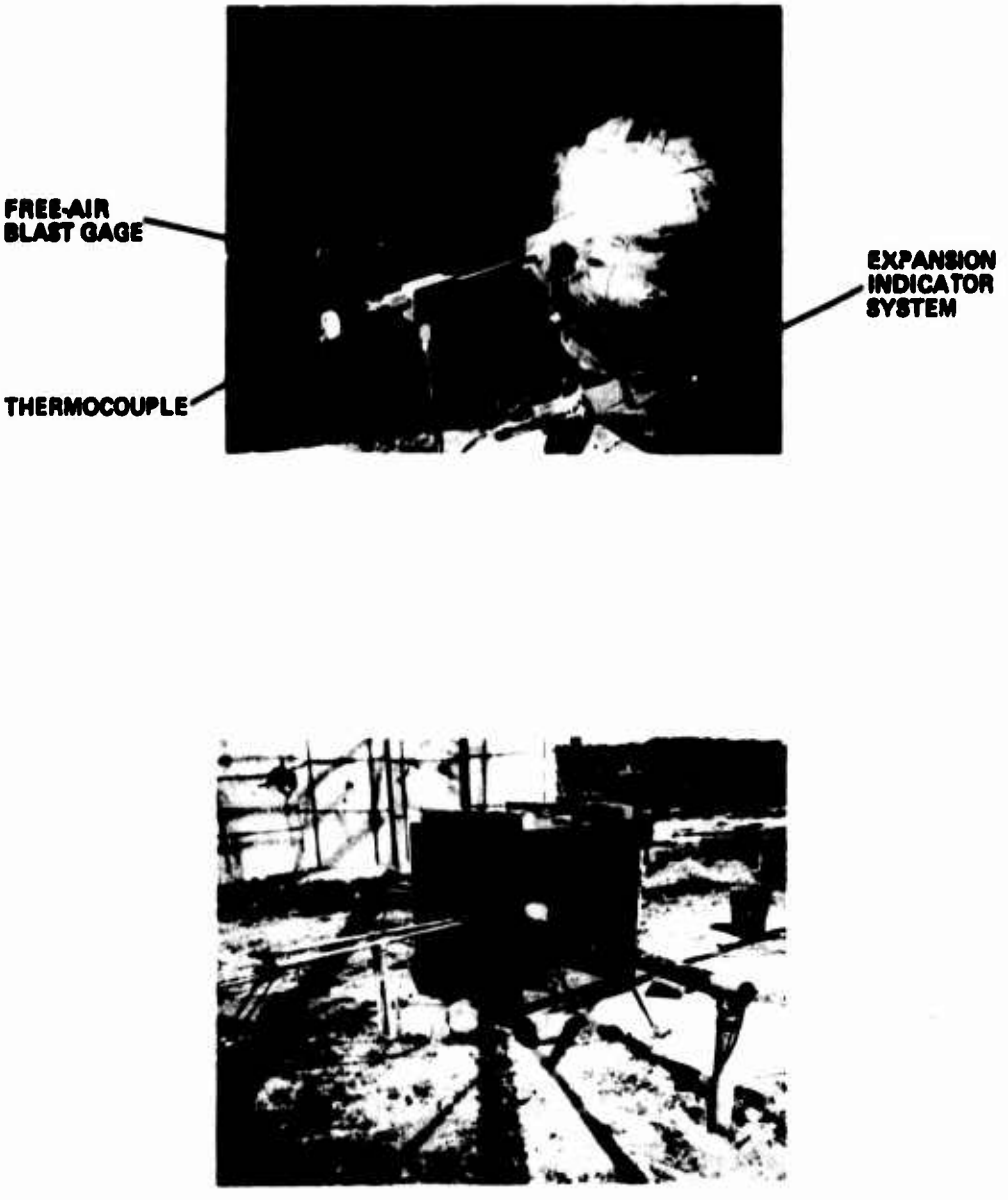

FIG. A.7 FIVE-SIDED STRUCTURE AND VESSEL

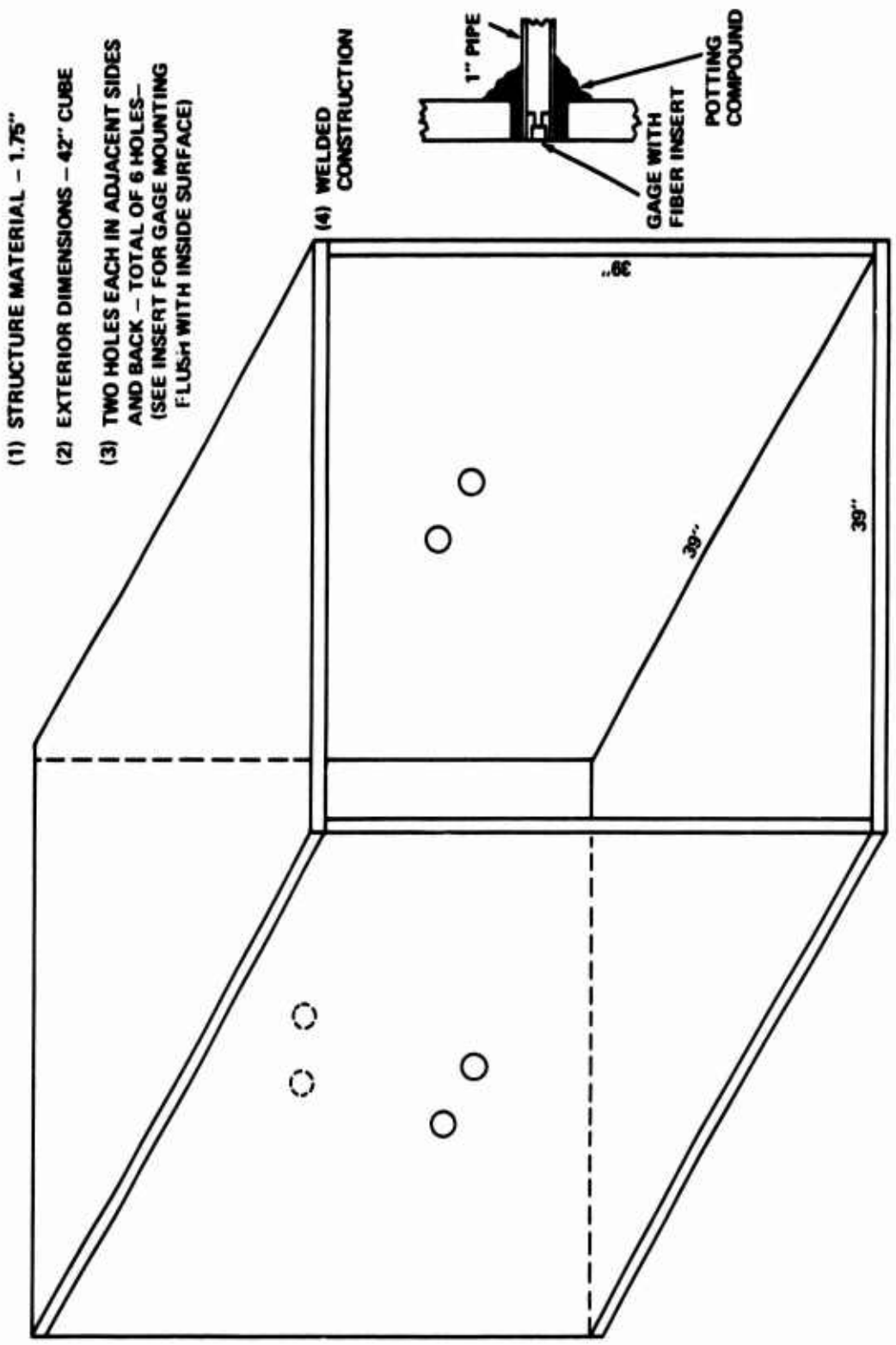

FIG. A.8 FIVE-SIDED STRUCTURE

ANNEX B VESSEL RUPTURE HISTORIES

This Section is included to display the internal vessel pressure and temperature, and the vessel expansion history recorded during pressurization. Figure B.1 shows a 15,000-psi vessel on the stand ready for test. In this case the equational vessel weld plane is parallel with the ground/firing pad. Since the rupture geometry greatly affected the airblast field, a description of each vessel rupture is given.

B.1 Rupture Histories of 15,000-psi Vessels

Internal vessel pressures and temperatures are shown for the three 15,000-psi bursts in Figures B.2, B.3, and B.4. No preburst vessel expansion was indicated on any 15,000-psi vessel.

Only actual pumping times are plotted in the Figures. In some cases, argon was bled into the test vessel directly from the supply bottles. This bleed-time was not included in the pressurization times given for any vessel. A total pumping time of 45 minutes was required to pressurize the shot-1 vessel from 2150 psi to burst at 14,950 psi as shown in Figure B.2.

The pump was halted several times during pressurization to perform various tasks such as changing argon supply bottles, clearing the firing area, or adjusting instrumentation. These halts are marked by discontinuous changes in the pressurization or temperature curves. After a pause, the resumption of pumping was accompanied by a sharp temperature increase. Note those in Figure B.2 at 0, 12, and 25 minutes. Beyond 30 minutes, the system was slowly approaching equilibrium temperature. Net temperature rise for shot 1, Figure B.2 was 35°C.

Figure B.3 shows the pressurization rate and internal gas temperature for shot 2. The pumping began when the internal vessel pressure was 500 psi and continued until the rupture occurred at 14,750 psi after some 76 minutes pumping time. The pumping rate was very slow up to 5,000 psi . Therefore, the internal gas temperature decayed following the initial jump at the resumption of pumping after a pause. The ambient temperature remained constant during the pumping phase; the internal argon temperature increased from 5 to 27.5°C.

Figure B.4 shows the pressurization rate and internal gas temperature for shot 6, the confined vessel test. This vessel ruptured at 14,400 psi after 73 minutes pumping. Internal gas temperature rose from 21°C ambient to 65°C, a net increase of 44°C.

Figure B.5 shows the estimated rupture geometry for the shot-1 vessel. Prior to rupture, the vessel was set up as shown in Figure B.1, in this case with the equatorial weld plane parallel with the earth/firing pad surface. At rupture, the vessel opened like a clam shell with the first opening occuring along the equatorial weld at a point intersected by the arrow showing the shot-1 jet direction. After opening, the reaction forced the bottom half downward and away from the jet direction. It then hit the pad and ricocheted upward over the arena walls and landed some 665 feet from ground zero. Based on the trajectory of the bottom half, the shot-1 vessel's top half rocketed off at an elevation angle of 54° in the same

direction as the bottom half. (See Figure D.1).

A similar scenario seems to fit the rupture geometry of the shot-2 vessel. It too burst at the equator but with rupture beginning at a point in the direction of the estimated argon jet for shot-2 shown in Figure B.5. The bottom half was forced downward, striking the firing pad and ricocheting upward and outward. The bottom half was found 552 feet from ground zero. Based on the trajectory of the bottom half, the top half's trajectory was estimated to have an elevation angle of 64° and to be directly away from the estimated shot-2 argon jet (Figures B.5 and D.1); the top half was not found.

The remaining 15,000-psi vessel was burst in the confining structure. In this case, the equatorial weld plane was perpendicular to the earth/firing pad surface. The bottom half (the half containing the boss and gas inlet tube) faced toward the opening of the confining structure as shown in Figure A.7.

This vessel also ruptured at the equatorial weld. The top half of the vessel struck the rear wall of the confining structure. The impact mark was centered 3" below and 7" to the left of the rear wall's center. The bottom or outward facing half of the vessel struck the ground along a trajectory that was the mirrow image of the top half's path.

This opening pattern directed an argon jet toward a point on the right wall (facing the opening and looking in) of the structure. The resultant forces turned the structure 34° clockwise and moved it back some two feet. (Figure B.6).

B.2 Rupture Histories of 30,000-psi Vessels

Rupture histories recorded for the 30,000-psi vessels are shown in Figure B.7 and B.8. The shot-3 vessel burst at 34,400 psi after 98 minutes pumping time (Figure B.7). Pumping began with the vessel at 2300 psi. The internal vessel temperature rose from 14°C ambient to 23°C within 2 minutes after pumping began. It then began a decrease for the next 16 minutes because of the slow pressurization rate. At this point, fresh gas supply bottles increased the pumping rate and the rate of temperature rise. The temperature eventually rose to 43°C followed by a decrease during the last four minutes of pumping. This decrease was caused by a decrease in pressurization rate as vessel pressure approached 35,000 psi, the limit of the pressurization system's first stage.

An increase of the vessel's circumference was measured as the pressure increased from 30,000 psi to burst. This increase amounted to 0.10 inches on one gage and 0.065 inches on the other.

Figure B.8 shows the pressurization history for the shot-7 vessel. This vessel's walls were machined down by 0.12 inches in an effort to induce a failure mode not connected with the equatorial weld. After 115 minutes pumping time, the vessel ruptured at 31,800 psi . Because of air compressor problems, the pumping system's intensifier was needed to complete pressurization from 30,000 psi to rupture. This accounts for the sawtooth appearance of the pressure and temperature curves above 30,000 psi . The intensifier was manually cycled at a rate of about 0.5 cycles/minute.

The internal gas temperature reached a maximum of 91°C before cooling as the pressurization rate fell with the use of the intensifier. Ambient temperature also increased during pressurization so that the maximum net temperature rise was 72°C.

The circumferential expansion was 0.43" and 0.45" as measured by gages 1 and 2 respectively.

The shot 3 vessel was burst with the equatorial weld parallel with the earth/firing pad surface. The vessel ruptured along the equatorial weld. At rupture, the bottom half of the vessel was driven almost straight down, ricocheted off the firing pad, went up in the air and struck the arena wall on its way down. The top half of the vessel was never found. Geometry of rupture and argon jetting is shown in Figure B.9.

The shot-7 vessel was oriented with the equatorial weld perpendicular to the earth/firing pad surface. The bottom or boss/inlet half of the vessel pointed away from the arena along a line bisecting the angle between gage lines 1 and 2.

The shot-7 vessel also burst at the equatorial weld even though the vessel's shell had been thinned by 0.12 inches. (The weld area was not cut down). Both the top and bottom halves were found; the top half after striking the arena wall and remaining in the arena, the bottom half after plowing a furrow in the dirt and landing 180 feet from ground zero. Shot-7 rupture geometry is shown in Figure B.9.

B.3 Rupture Histories of 50,000-psi Vessels

The parameters measured during pressurization of the 50,000-psi vessels are shown in Figure B.10 for shot 4 and Figure B.11 for shot 5. Both vessels ruptured at 50,400 psi after about 150 minutes of pumping. The sawtooth shape of the pressure and temperature readouts in Figures B.10 and B.11 begin at pressures above 30,000 psi when it became necessary to use the manually cycled intensifier. The cycling rate is roughly 0.5 cycles/minute.

The temperature drop between cycles is seen to be greater for the shot-5 vessel in Figure B.11 than for the shot-4 vessel in Figure B.10. The net temperature rise was 36°C for shot 4 and 44°C for shot 5.

A circumferential expansion of 0.70 inches was recorded on gage 1 for shot 4 (Figure B.10). The other gage did not register on this vessel. Gage 2 recorded an expansion of 0.35" on shot 5. Gage 1 did not register for this event.

Both 50,000-psi vessels were placed on the firing stand with the equatorial weld perpendicular to the earth/firing pad surface. The bottom half of the vessel pointed away from the arena wall and along a line bisecting the angle between gage lines 1 and 2.

Both vessels were undercut so they were thinner in the area around the boss. (See Figure 2.3). In both cases, failure started in this area and proceeded in a plane roughly perpendicular to the equatorial weld. Thus the vessel burst into two pieces of unequal size as may be seen in Figure D.1.

In the case of shot 4, the rupture plane was nearly parallel to the ground/firing pad surface with about a 10° tilt to the right looking from the bottom or boss half. The larger portion traveled downward and struck the firing pad. It then ricocheted, striking the arena wall and remained within the arena. (Figure B.12). The upper portion (the smaller of the two) was not found.

The shot-5 vessel's rupture plane was nearly vertical, i.e., the plane tilted about 16° from the vertical in a counterclockwise direction when viewed from the boss end of the vessel. The smaller portion traveled upward and struck the right arena wall 6 feet above the ground. The larger portion struck the ground 3.25 feet from ground zero. From there, it bounced into the left arena wall near the ground.

The estimated directions of the argon jets, based on the motions of the fragments are shown in Figure B.12.

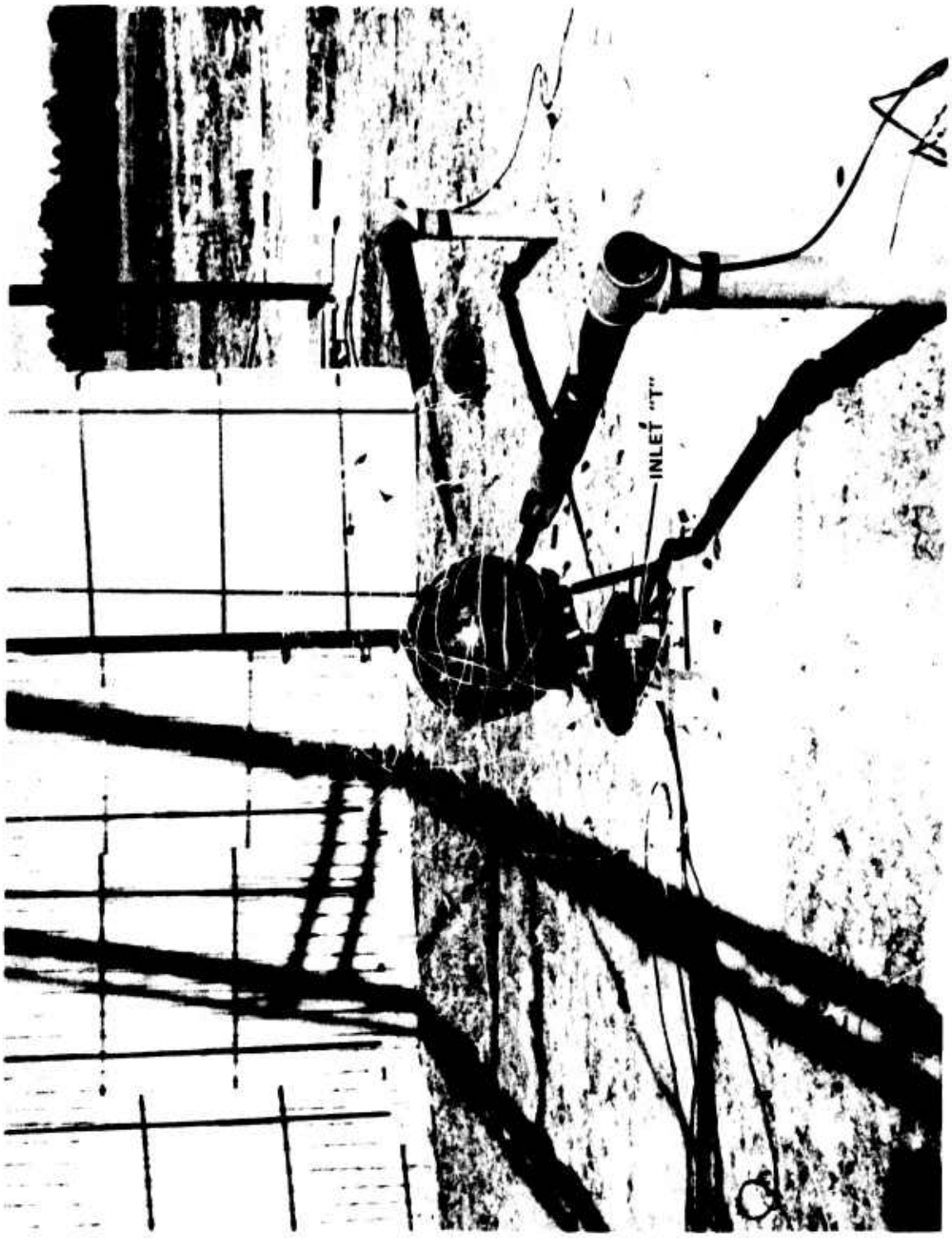

FIG. B.1 15,000-PSI VESSEL ON STAND READY FOR TEST

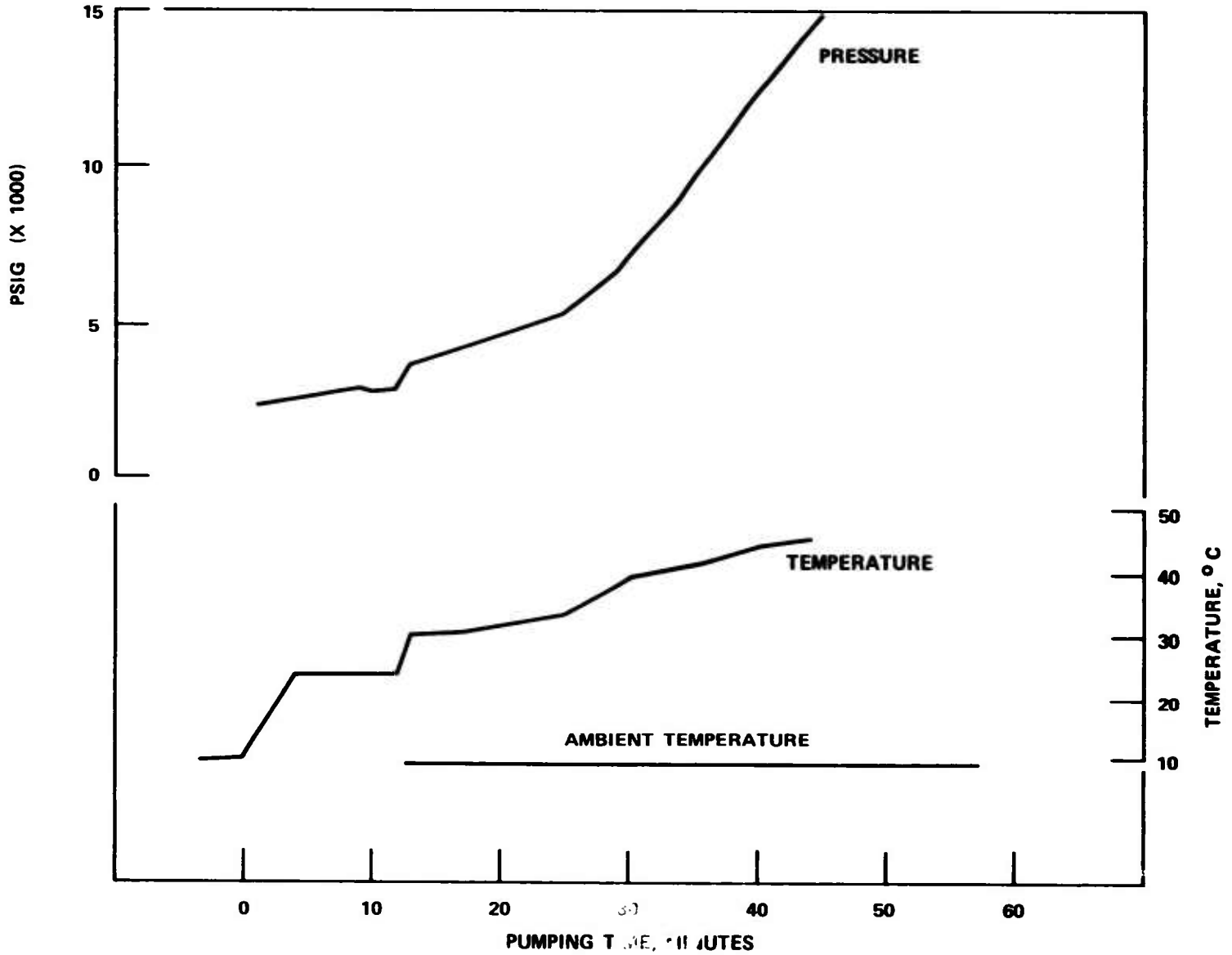

FIG. B.2 MEASURED VESSEL PARAMETERS; SHOT 1.

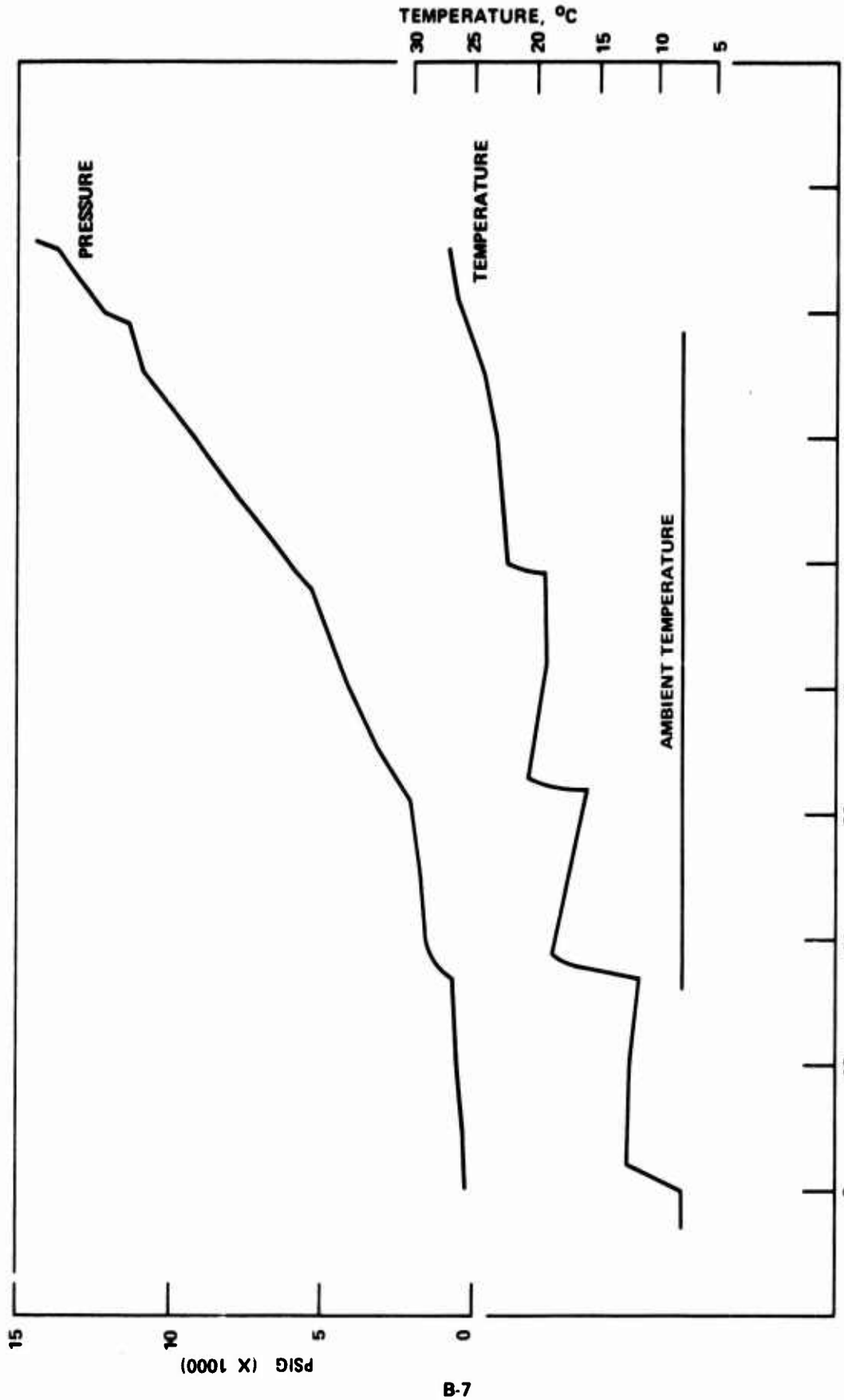

FIG. B.3 MEASURED VESSEL PARAMETERS; SHOT 2.

FIG. B.4 MEARSURED VESSEL PARAMETERS; SHOT 6

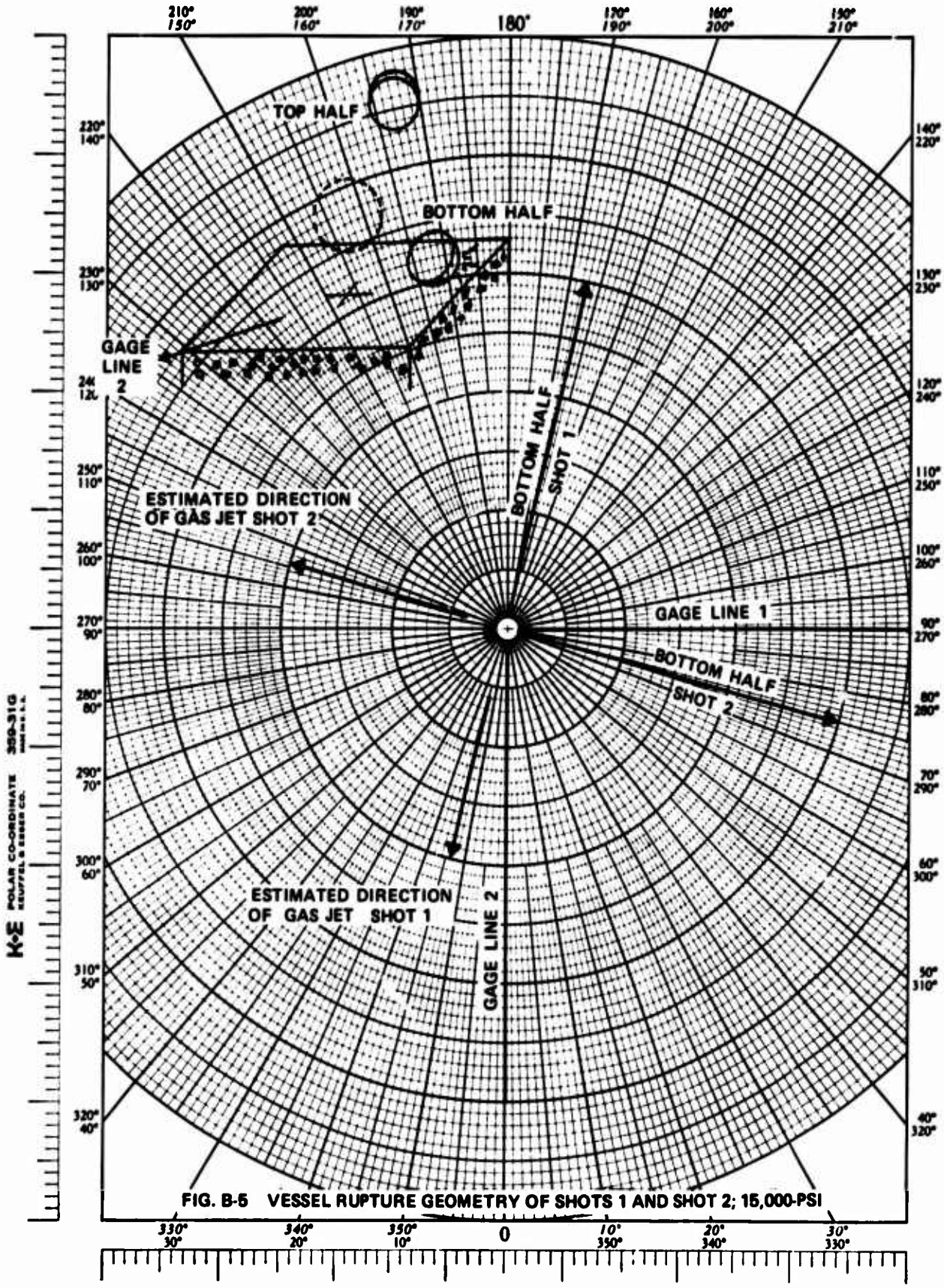

FIG. B-5 VESSEL RUPTURE GEOMETRY OF SHOTS 1 AND SHOT 2; 15,000-PSI

$\theta = 34^{\circ}$
$\beta = 56^{\circ}$

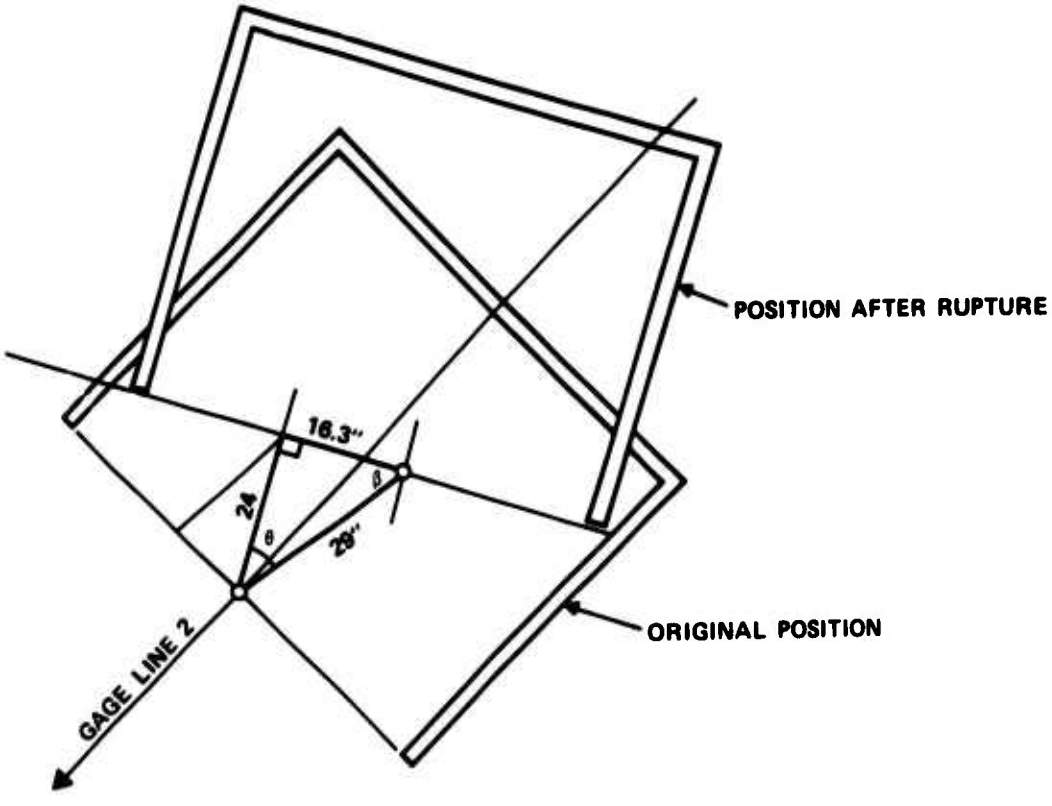

FIGURE B.6 MOTION OF CONFINING STRUCTURE

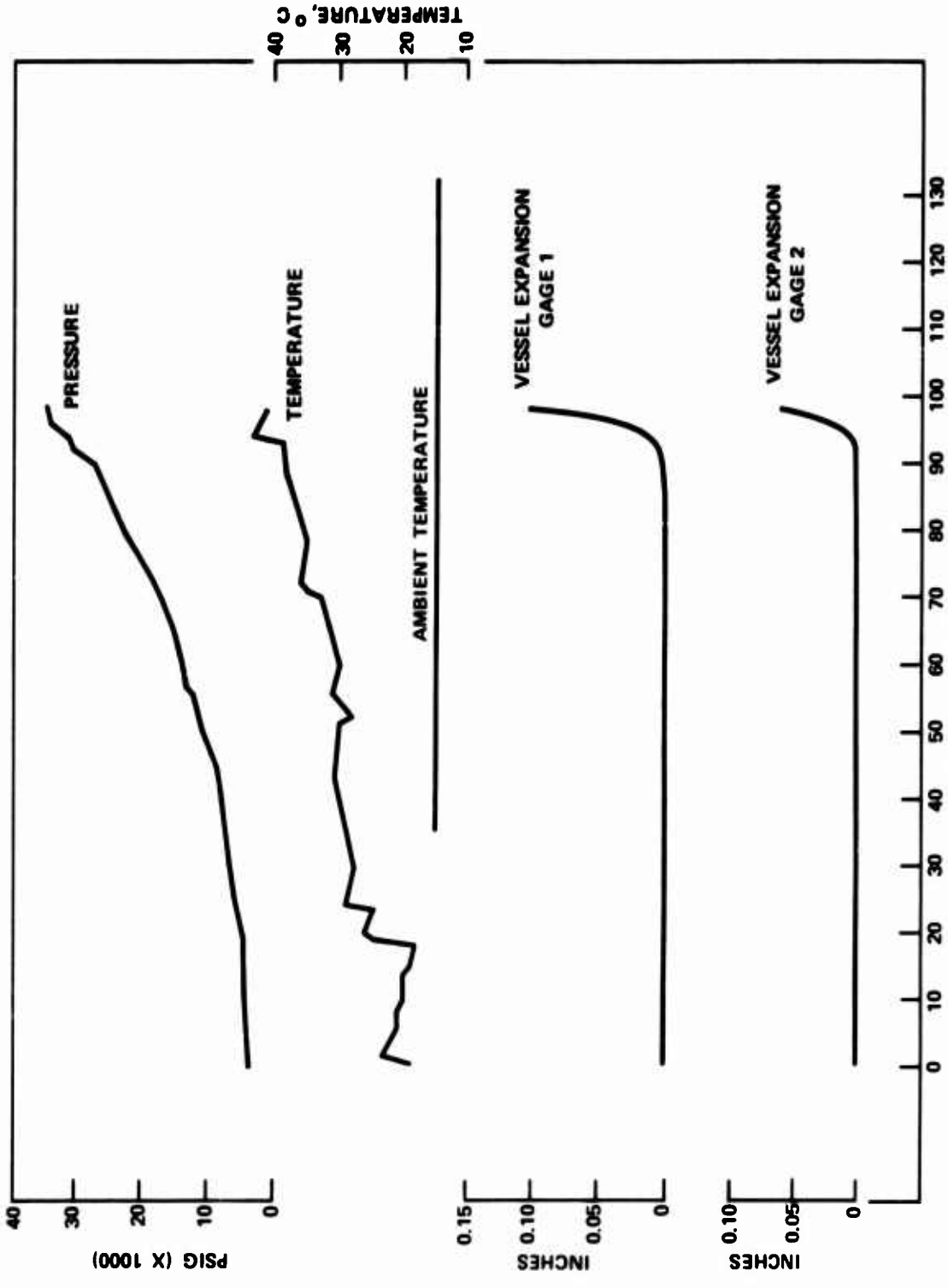

FIG. B.7 MEASURED VESSEL PARAMETERS; SHOT 3

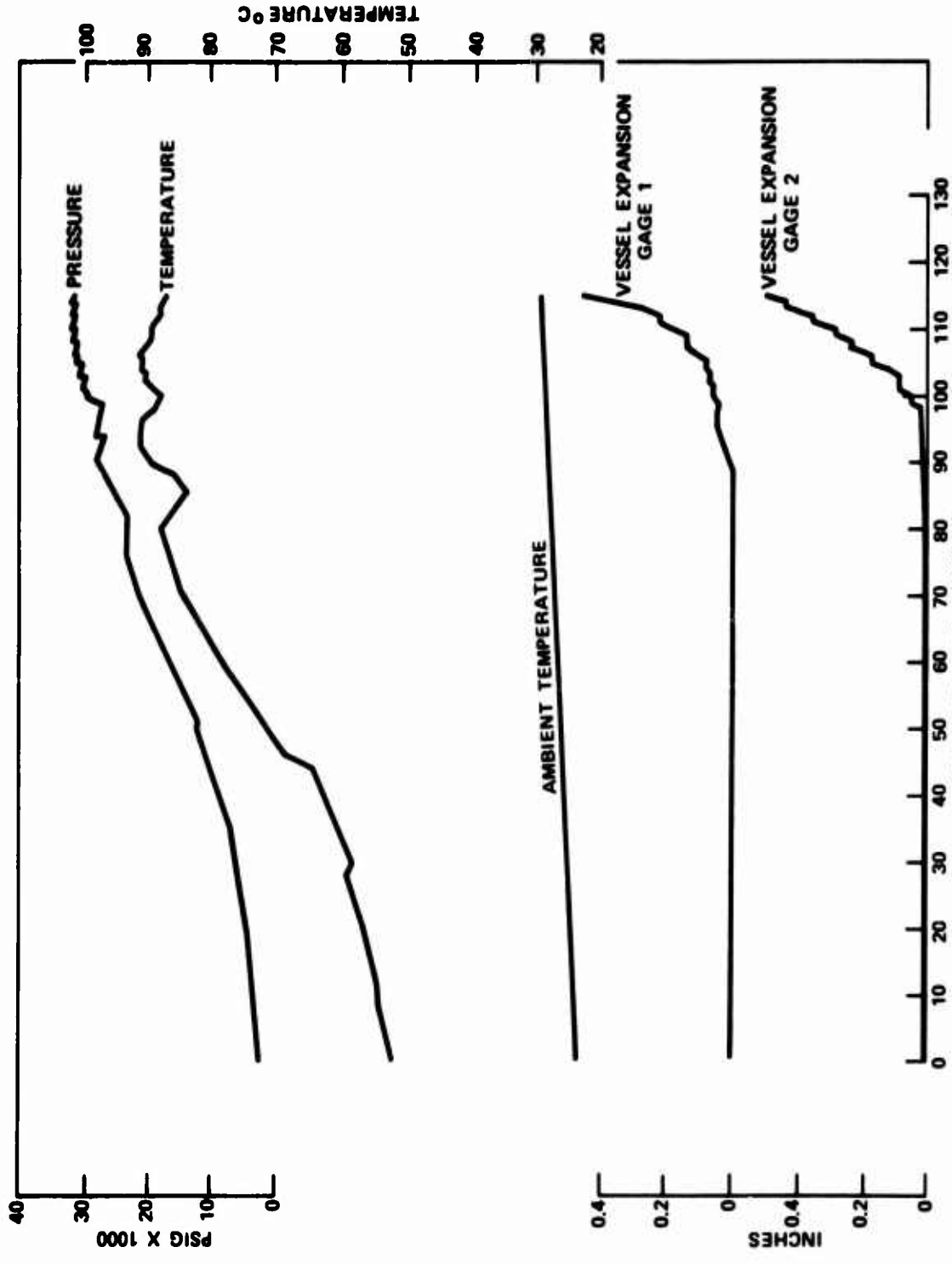

B–8 MEASURED VESSEL PARAMETERS; SHOT 7

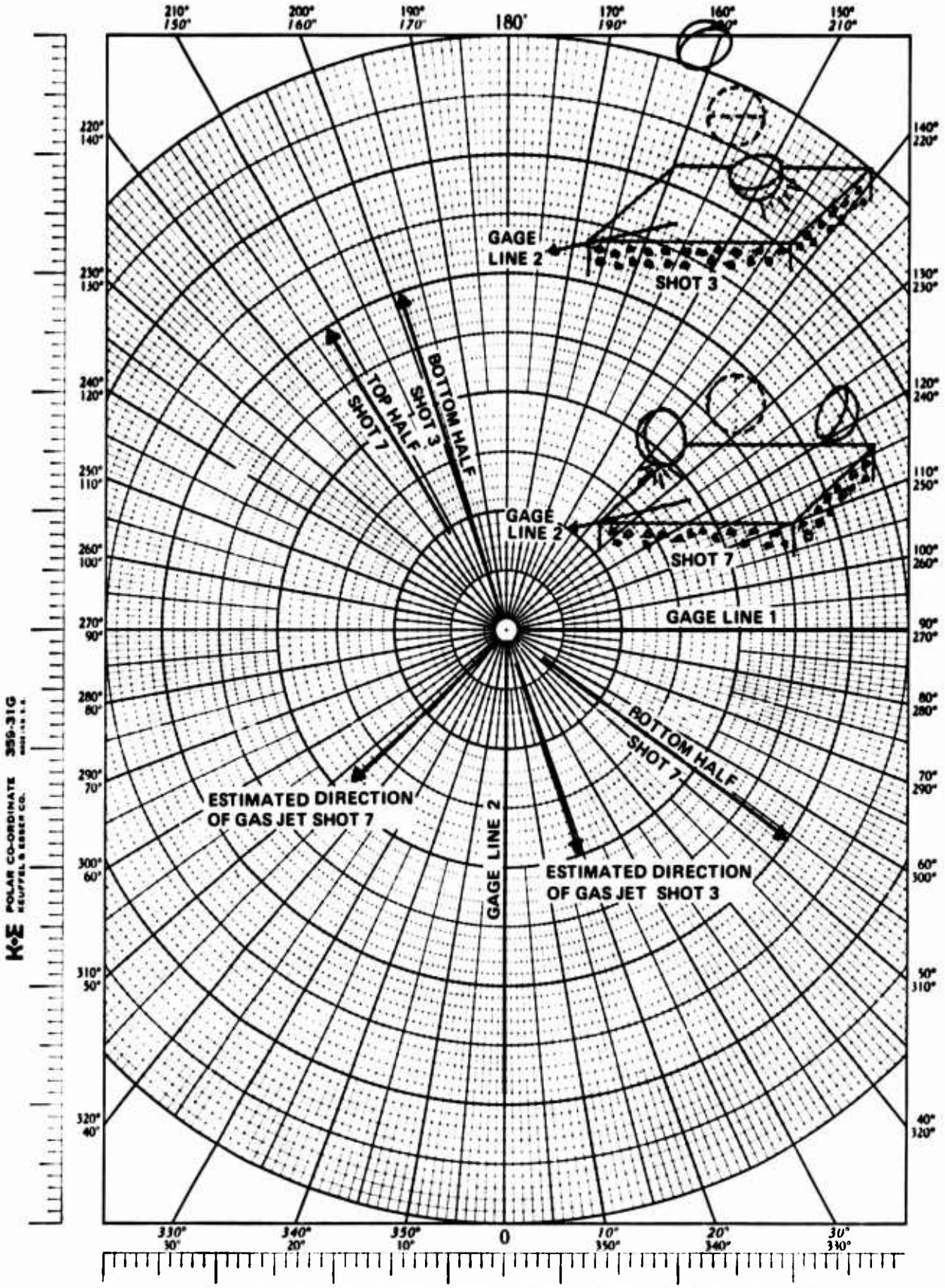

FIG. B.9 VESSEL RUPTURE GEOMETRY OF SHOT 3 AND SHOT 7; 30,000-PSI.

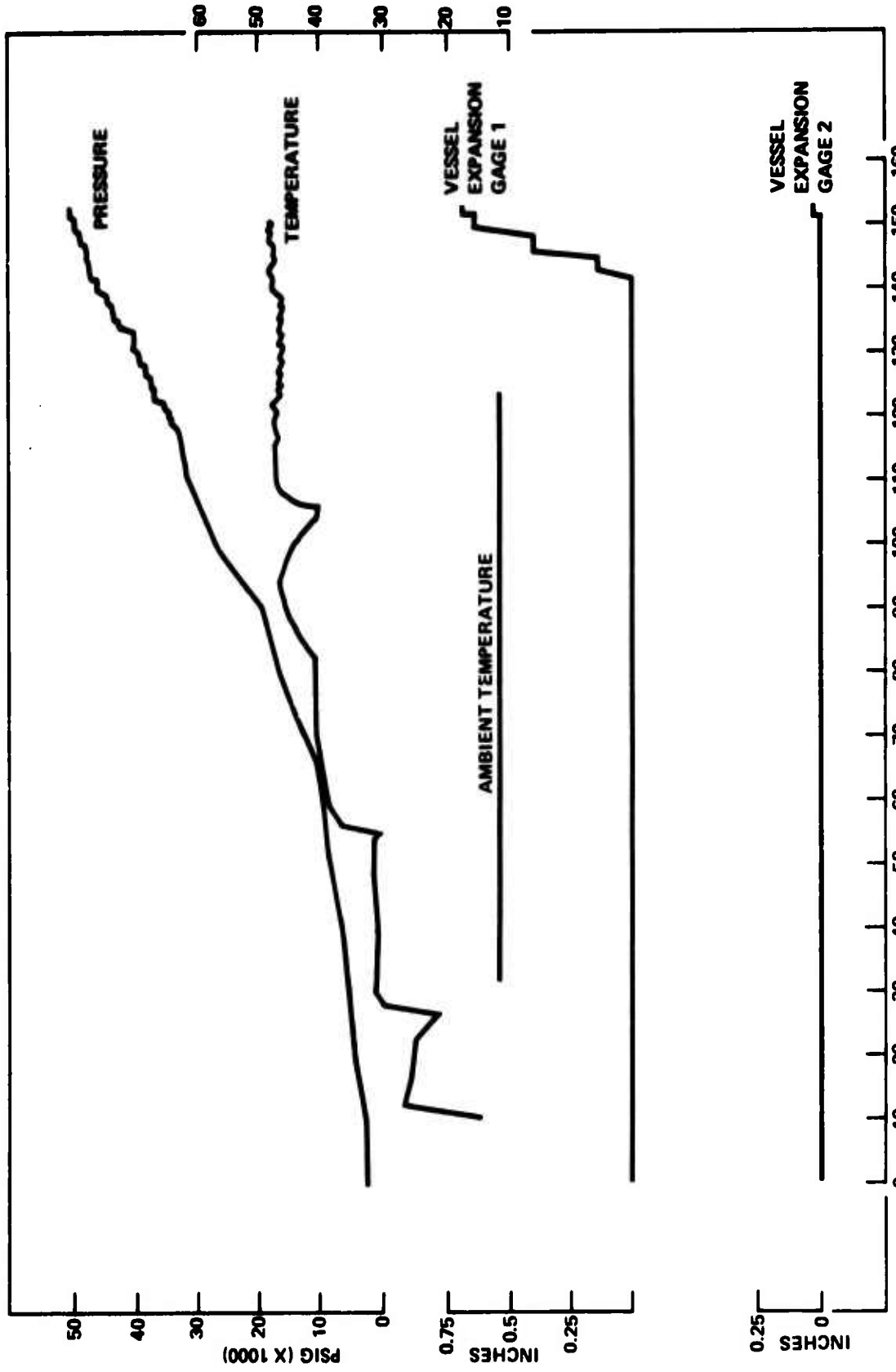

FIG. 8.10 MEASURED VESSEL PARAMETER; SHOT 4

FIG. B.11 MEASURED VESSEL PARAMETERS ; SHOT 5

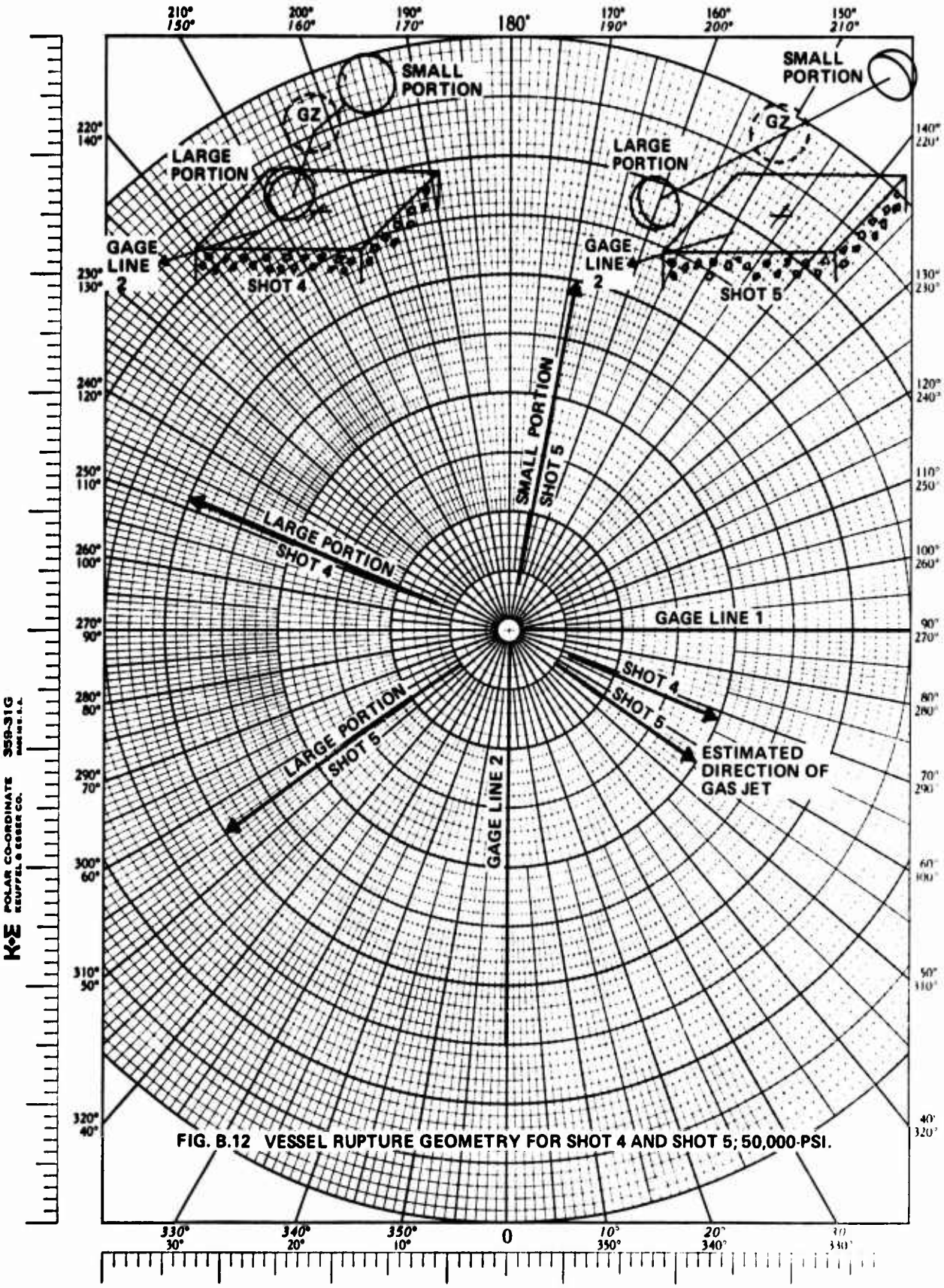

FIG. B.12 VESSEL RUPTURE GEOMETRY FOR SHOT 4 AND SHOT 5; 50,000-PSI.

ANNEX C AIRBLAST RESULTS

C.1 Airblast from Pentolite Spheres

The energy available from the pressure vessels used in this investigation was roughly equivalent to that available from 1 pound of TNT; but, the airblast generation by conventional explosions and tank rupture are not comparable. Since the blast performance of TNT and pentolite are reasonably well known (see reference C.1 for instance), it was felt prudent to obtain data under the conditions of this experiment to serve for rough comparisons and to check the blast instrumentation. Pentolite was used rather than TNT because of the difficulty in detonating 1-pound TNT spheres. Pentolite data is easily scaled to TNT data using the equivalent weight information in reference C.1.

Two 478-gm pentolite spheres were detonated at a height-of-burst (HOB) of 19.2 inches, the nominal HOB for the test vessels. The same blast instrumentation in the same arrangement was used for the pentolite tests and the unconfined vessel tests.

The pentolite data are tabulated in Table C.1. Blast overpressures are compared with the standard reference C.1 data in Figure C.1. Figures C.2 and C.3 show similar comparisons for positive shockwave durations and positive shockwave impulses.

A segment of the standard free air pentolite curve is included for comparison with our one-point measurements in Figure C.1. Agreement between measured and standard data is satisfactory. Pressure-time histories from the pentolite spheres are shown in Figure C.4.

C.2 Airblast from 15,000-psi Vessel Rupture

Measured airblast data from the two 15,000-psi vessel ruptures are tabulated in Table C.2. Airblast overpressures versus ground range have been plotted in Figure C.5.

The data displayed in Figure C.5 is typical of vessel-rupture data. At burst, an asymmetrical blast front develops as the fill gas jets out at vessel-wall openings. If the vessel bursts into many pieces, there are many jets which tend to coalesce into a spherically (or hemispherically) expanding shock front. The pressure in the shock front has a pronounced effect on the rate at which the front tends to coalesce. This comes about because at higher pressures the differences in shock velocities between that higher pressure shock and a slightly lower pressure shock are greater than they are at lower pressures. (In the lower limiting case, all shocks approach sonic velocity and never overtake.) For most tank ruptures, airblast pressures are comparatively low near the tank so that a shock front that

(C.1) Swisdak, M., "Explosion Effects and Properties; Part 1 - Explosion Effects in Air", Naval Surface Weapons Center NSWC/WOL/TR 75-116, to be published.

starts out non-spherical remains non-spherical.

This leads up to an explanation of the remarkable differences in airblast overpressures noted in Figure C.5. Both the 15,000-psi vessels ruptured along the equatorial weld, separating into two halves. By observing the direction in which the two haves were propelled, it is possible to tell which side of the vessel opened first since the two halves are pushed away from the opening in reaction to the first escaping jet. The airblast pressures will be higher in the vicinity of this jet.

In Figure C.5, jet directions are shown in relation to the gage lines in the upper right hand inset. Note that for shot 1 (the first vessel rupture) the jet is directed along the vicinity of line 2. Therefore, blast pressures along line 2 are higher than along line 1. (Line 3 was not in use on this test). For shot 2, the jet is directed almost directly away from line 1 where the lowest pressures were recorded. Similar shot-2 pressures are read along line 2 and the gage on line 3 since the jet was about equi-distance between the two lines. Note also that the shot-1 jet has about the same relation to line 1 as does the shot-2 jet to line 2. Thus shot-1, line-1 airblast pressures are similar to shot-2 line-2 airblast pressures in Figure C.5.

Pressure histories from the shot 1 vessel are shown in Figure C.6. Positive shock wave durations are shown in Figure C.7 and positive shockwave impulses are shown in Figure C.8. While impulse in a strong function of shockwave overpressure, shockwave durations are similar for all pressure levels at the same distance. Thus, positive shockwave durations in Figure C.7 are not as strongly related to jet direction as is the overpressure-related positive shockwave impulse in Figure C.8.

C.3 Airblast from 30,000-psi Vessel Rupture

Measured airblast data from the 30,000-psi vessel ruptures are tabulated in Table C.3. Airblast overpressures versus ground range are shown in Figure C.9.

The data displayed in Figure C.9 are again typical of pressure vessel-rupture data. Pressure amplitudes correlate with the estimated jet orientations shown in the Figure C.9 inset. The shot-3 jet was directed along line 2 where highest pressures were recorded. The lowest pressure was recorded directly away from the jet by the single gage on line 3.

On shot 7, the jetting occurred between lines 1 and 3 giving about equal pressures. Lowest pressures were again recorded away from the jet on line 1.

Note in Figure C.9 that the orientation of line 2 and the shot-7 jet is similar to the orientation between line 1 and the shot-3 jet. Again the airblast overpressures along these lines are similar.

Pressure-time histories for the shot-3 rupture are shown in Figure C.10. Positive shockwave durations and positive shockwave impulses are shown in Figures C.11 and C.12 respectively.

C.4 Airblast from 50,000-psi Vessel Rupture

Airblast data from the 50,000-psi vessel ruptures are tabulated in Table C.4. Airblast overpressures are given in Figure C.13. Again, the asymmetries displayed by the data in Figure C.13 are typical of vessel rupture data.

Both vessels seemed to jet between gage lines 1 and 2. However, as described in Section B.3, the shot-4 vessel ruptured with the fracture plane parallel to the ground; the shot-5 vessel's fracture plane was perpendicular to the ground. This may account for the relatively small difference between pressures on lines 1 and 2 for shot 4 and the correspondingly larger differences for shot 5. The reasoning here is that the shot-4 jet would have been wide in the plane parallel to the ground but narrower in the vertical plane; the reverse would be true of shot 5. This picture may be further illustrated for the gages at a 1-ft ground range and the free field gage at 1.75 feet. For shot 4 the 1-ft ground range gage shows higher pressure on line 1 than line 2. However the line-1/line-2 difference is not as great as for shot 5. Two things bring this about. The fact that the shot-4 vessel opened in a nearly horizontal plane would broaden the jet to decrease differences in pressure for the two lines. However, the rupture plane was tilted to favor gage line 1 where the highest pressure was measured. For shot 5, the rupture plane was nearly vertical and therefore narrowed the jet in this plane. This fact, plus the slight tilt of the jet toward gage line 2 accentuated the differences in pressures along lines 1 and 2 for shot 5.

The free field gages were up near the tanks center. Thus the line-1 and line-2 gages for shot 4 were both almost in the jet, and line 1 for shot 5 was also near the jet and registered only slightly lower pressure than the above two gages. Its companion gage on line 2 for shot 5 was well out of the narrow jet and registered the lowest pressure.

Pressure histories for shot 5 are shown in Figure C.14. Positive shockwave durations and positive shockwave impulses are shown in Figures C.15 and C.16 respectively. The large scatter in positive impulse in Figure C.16 reverses the trend of the 30,000-and 15,000-psi bursts where the overpressure scatter was greater than the scatter in impulse. In the case of the 50,000-psi rupture, the impulse scatter is greater than the overpressure scatter.

C.5 Airblast from the 15,000-psi Confined Vessel Test

As shown in Figure A.6, blast gages outside the confining structure walls were laid along three lines. Airblast pressures measured along these lines are shown in Figure C.17 and are given in Table C.5. Pressures measured along the line coming out of the box (line 2) are higher than along the other two lines but no higher than was predicted for a free field burst. Pressures behind the box are slightly lower than those measured at one side.

An attenuation factor relative to the pressure in front of the structure was calculated and is shown as a function of ground range and overpressure in Figure C.18.

Overpressure ratios for L_2/L_1 range from a high of 20 to 1 in Figure C.18 at 2.5 ft from ground zero to 2.2 to 1 at the 60-foot gage positions. This shows greater shielding at positions near the structure walls while the shockwave is less affected at greater distances.

Such behavior is expected from the behavior of similarly confined conventional explosions. Reference C.3 reports L_2/L_1 (front to side) ratios ranging from 3:1 at 20 psi down to about 2:1 at 1 psi. L_2/L_3 (front to back) ratios are slightly lower, 3.5:1 in the 20-psi region down to 2.2:1 in the 1-psi region. The front above refers to the structure's open side. Positive shockwave durations are given in Figure C.19. The uncertainties in measuring positive duration along line 3 ruled out their being included in the data. (See the pressure histories in Figure C.20.) Measured positive shock wave impulses are given in Figure C.21.

Pressure histories measured on the inside walls of the confining structure are shown in Figure C.22. (See Figure A.6 for the location of gage positions 1 through 6.) Based on the analysis in Annex B, the vessel first opened on the side next to gages 5 and 6. What is probably an airshock reaches gage 5 at 0.3 milliseconds. This is immediately followed by a rise which may be the argon front. Almost immediately, the gage goes off scale, probably from a parted cable. Gage 6 shows no air shock but does show a rise probably due to the argon front before it goes off scale; again, probably due to the cable parting.

Gages 3 and 4 show an airshock arrival at about 1 millisecond after burst. This is followed by a higher pressure at about 1.5 milliseconds, probably reflected from the vessel front which is by now in motion. The argon front arrives, driving position 4 off scale when the cable parts at about 1.8 milliseconds. The signal cable for gage 3 parts at about 3.2 milliseconds. Note that gage 4 is 6 inches further away from the side of the vessel that first opened than is gage 3.

Gages 1 and 2 see a nominal 4.6 psi shockwave at about 1 millisecond after burst. What we assume to be the argon gas front arrives at about 3 milliseconds. Since gages 1 and 2 are on the side opposite the side where first rupture occurred, the low air shock pressure and the late arrival of the argon may be expected.

Based on the above, wall load pressures are from two sources: the airshock ahead of the expanding argon gas and the momentum of the argon itself. In addition, the asymmetric situation within the confining structure results in multiple reflections at the structure walls. While some of the reflections are off the walls, others may be off the argon front. Therefore a qualitative analysis of the entire pressure-time history is speculative. The situation here is similar to that of a confined conventional explosion. That is, an airblast wave reaches the walls first and undergoes multiple reflections. This is followed by the static pressure due to the gaseous products. The static pressure reaches a peak and then decays at a rate determined by the venting time of the enclosure. This picture fits the overall pressure history measured in our case.

(C.3) Keenan, W. and Tancreto, J. "Blast Environment from Fully and Partially Vented Explosions in Cubicles", Minutes of the Sixteenth Explosives Safety Seminar, Page 1527 Volume II, 24-26 Sep 1974.

The gross pressure-time functions shown in Figure C.22 are probably adequate to determine confining structure wall response.

TABLE C.1 BLAST DATA FROM 478 - GRAM PENTOLITE SPHERE; HOB 1.6 FEET

GAGE POSITION	GROUND RANGE FT	OVER-PRESSURE PSI	ARRIVAL TIME MS	POSITIVE DURATION MS	IMPULSE PSI-MS
1-1	1.0	845	1.23	0.26	62.0
2-1	1.0	980	1.21	0.58	97.0
1-2	* 1.88	253	0.87	0.22	12.2
1-2	* 1.88	268	1.15	0.29	19.2
2-2	* 1.88	285	0.88	0.20	16.5
2-2	* 1.88	329	1.14	0.24	18.1
1-3	2.62	317	1.34	–	–
1-3	2.62	263	1.49	–	–
2-3	2.62	244	1.33	–	–
2-3	2.62	227	1.47	–	–
1-4	5.25	56.1	2.04	1.13	16.9
1-4	5.25	58.6	2.65	1.15	17.8
2-4	5.25	51.8	2.03	0.96	16.5
2-4	5.25	52.9	2.61	1.77	16.5
1-5	10.3	15.0	5.19	2.36	11.7
1-5	10.3	15.0	–	2.32	12.2
2-5	10.3	13.4	5.20	2.12	9.8
2-5	10.3	13.4	–	2.20	14.6
1-6	16.8	7.00	10.14	2.93	6.3
1-6	16.8	6.25	–	2.98	8.5
2-6	16.8	6.78	10.04	3.26	6.9
2-6	16.8	6.51	–	3.21	7.3
1-7	60.1	0.78	–	4.17	1.2
1-7	60.1	0.71	–	4.02	1.4
2-7	60.2	0.68	–	4.17	1.2
2-7	60.2	0.95	–	4.46	1.4
3-1	13.2	7.57	–	2.62	3.1
3-1	13.2	8.18	–	2.62	4.3

* SLANT RANGE

1

TABLE C.2 BLAST DATA FROM 15,000 PSI SPHERE, SHOT 1.

GAGE POSITION	GROUND RANGE FT	OVER – PRESSURE PSI	ARRIVAL TIME MS	POSITIVE DURATION MS	POSITIVE IMPULSE PSI – MS
1-1	1.0	14.8	0.69	0.88	10.7
1-2	1.70*	6.80	0.66	1.19	6.6
1-3	2.41	12.5	1.71	0.92	5.3
1-4	4.97	9.19	3.33	2.97	8.1
1-5	10.2	–	–	–	–
1-6	16.5	2.04	11.55	5.36	4.9
2-1	1.0	14.0	1.02	–	–
2-2	1.66*	24.2	0.11	1.13	28.6
2-3	2.41	31.6	1.06	1.32	27.1
2-4	4.96	23.2	2.46	2.01	–
2-5	10.2	7.84	5.93	5.06	14.5
2-6	16.4	4.88	11.16	4.75	12.2

* SLANT RANGE

2

TABLE C.2 (CONTINUED) BLAST DATA FROM 15,000 - PSI SPHERE; SHOT 2.

GAGE POSITION	GROUND RANGE FT	OVER – PRESSURE PSI	ARRIVAL TIME MS	POSITIVE DURATION MS	POSITIVE IMPULSE PSI – MS
1-1	1.0		–	–	–
1-2	1.70*	2.08	1.17	–	–
1-3	2.41	2.00	2.22	0.92	2.5
1-4	4.97	2.48	4.38	2.24	3.4
1-5	10.2	1.99	8.71	3.32	3.9
1-6	16.5	1.09	14.40	3.87	3.3
1-7	59.8	0.34	–	4.12	1.5
2-1	1.0	9.15	1.28	–	–
2-2	1.66*	7.64	0.65	–	–
2-3	2.41	12.1	1.88	1.16	9.6
2-4	4.96	9.20	3.54	2.16	4.6
2-5	10.2	2.04	7.47	4.16	3.6
2-6	16.4	2.98	12.87	3.79	3.9
2-7	60.1	0.41	–	5.45	0.97
3-1	13.2	3.89	–	4.39	12.3

* SLANT RANGE

TABLE C.3 BLAST DATA FROM 30,000 · PSI SPHERE, SHOT 3

GAGE POSITION	GROUND RANGE FT	OVER – PRESSURE PSI	ARRIVAL TIME MS	POSITIVE DURATION MS	POSITIVE IMPULSE PSI – MS
1-1	1.00	17.2	1.14	0.89	4.4
1-2*	1.71	11.3	0.65	0.75	5.7
1-3	2.42	16.1	1.16	2.47	12.3
1-4	4.93	11.8	3.18	4.12	14.6
1-5	10.2	6.04	6.53	5.16	5.1
1-6	16.6	3.17	12.09	4.96	2.8
1-7	59.8	0.54	–	5.95	1.1
2-1	1.0	22.7	0.80	0.65	4.7
2-2*	1.71	25.6	0.30	0.34	4.4
2-3	2.47	46.6	1.17	1.11	30.3
2-4	4.93	29.3	2.41	2.15	15.7
2-5	10.1	5.44	5.76	5.95	7.0
2-6	16.4	6.06	10.48	5.36	5.4
2-7	60.0	0.67	–	6.84	0.9
3-1	13.3	1.02	–	4.40	10.4

* SLANT RANGE

TABLE C.3 (CONTINUED) BLAST DATA FROM 30,000 · PSI SHERE; SHOT 7

GAGE POSITION	GROUND RANGE FT	OVER – PRESSURE PSI	ARRIVAL TIME MS	POSITIVE DURATION MS	POSITIVE IMPULSE PSI – MS
1-1	0.97	4.4	–	0.41	–
1-2	1.71*	4.16	–	–	–
1-3	2.60	3.54	2.58	–	–
1-4	4.97	2.75	4.24	3.55	6.0
1-5	10.1	2.69	8.12	3.75	5.3
1-6	16.5	1.94	13.50	4.52	3.6
1-7	60.0	0.46	–	5.24	0.8
2-1	0.97	8.70	1.27	0.71	–
2-2	1.71*	18.5	0.60	0.43	4.7
2-3	2.54	17.2	1.93	3.37	23.4
2-4	5.02	9.56	3.92	4.02	16.4
2-5	10.1	5.01	7.03	4.18	6.2
2-6	16.4	3.67	12.02	5.00	2.7
2-7	60.0	0.45	–	6.25	1.2
3-1	13.2	3.76	–	5.30	3.3

* SLANT RANGE

TABLE C.4 BLAST DATA FROM 50,000 PSI SPHERE, SHOT 4

GAGE POSITION	GROUND RANGE FT	OVER – PRESSURE PSI	ARRIVAL TIME MS	POSITIVE DURATION MS	POSITIVE IMPULSE PSI – MS
1-1	0.97	23.6	1.01	0.61	6.4
1-2	1.77	23.5	0.62	0.46	5.0
1-3	2.60	27.0	1.31	1.24	9.8
1-4	4.97	20.7	2.63	2.90	19.1
1-5	10.1	9.48	6.02	5.04	11.9
1-6	16.5	5.05	11.02	4.52	4.8
1-7	59.8	0.74	–	4.76	1.2
2-1	0.97	13.0	1.22	0.54	16.5
2-2	1.77	21.5	0.69	0.63	4.7
2-3	2.54	12.0	1.65	1.64	9.2
2-4	5.04	13.9	3.16	1.52	8.4
2-5	10.1	7.64	6.59	2.65	12.2
2-6	16.5	4.55	11.71	5.00	4.7
2-7	59.9	0.61	–	4.76	1.0
3-1	13.2	0.72	–	6.70	1.9

TABLE C.4 (CONTINUED) BLAST DATA FROM 50,000 - PSI SPHERE; SHOT 5

GAGE POSITION	GROUND RANGE FT	OVER - PRESSURE PSI	ARRIVAL TIME MS	POSITIVE DURATION MS	POSITIVE IMPULSE PSI - MS
1-1	0.97	56.9	–	0.48	15.5
1-2	1.77*	19.1	0.32	–	–
1-3	2.60	52.6	0.93	3.76	–
1-4	4.97	27.2	2.16	4.42	28.1
1-5	10.1	11.7	5.15	6.25	19.4
1-6	16.5	6.67	9.87	5.36	5.0
1-7	59.8	0.78	–	–	1.8
2-1	0.97	17.6	–	–	–
2-2	1.77*	8.1	0.35	–	–
2-3	2.54	19.9	1.35	1.27	5.5
2-4	5.04	8.54	3.01	1.62	2.2
2-5	10.1	4.57	6.56	3.87	3.9
2-6	16.5	3.59	11.59	4.17	2.4
2-7	59.9	0.41	–	4.46	0.4
3-1	13.2	1.70	–	5.36	1.8

* SLANT RANGE

TABLE C.5 BLAST DATA FROM 15,000 - PSI CONFINED SPHERE; SHOT 6

GAGE POSITION	GROUND RANGE FT	OVER – PRESSURE PSI	ARRIVAL TIME MS	POSITIVE DURATION MS	POSITIVE IMPULSE PSI – MS
1	1.0	4.48	0.89	–	–
2	1.0	4.8	0.96	–	–
3	1.0	8.6	1.16	–	–
4	1.0	8.97	1.02	–	–
5	1.0	80.0	0.29	–	–
6	0.96	52.6	–	–	–
1-3	2.50	1.20	3.47	0.89	1.8
1-4	5.04	1.41	–	1.31	
1-5	10.2	1.76	8.48	–	–
1-6	16.5	1.05	–	3.69	0.6
1-7	60.0	0.21	–	3.87	0.4
2-2	1.7 *	3.07	1.01	0.40	–
2-3	2.54	26.0	–	1.29	6.5
2-4	5.02	15.2	–	3.45	9.7
2-5	10.1	10.3	–	4.76	6.1
2-6	16.5	4.91	–	4.40	2.9
2-7	60.0	0.46	–	7.73	0.4
3-3	2.62	1.08	3.04	–	–
3-4	5.12	1.10	–	0.77	
3-5	10.2	0.92	11.08	–	–
3-6	16.6	0.18	–	–	–

* SLANT RANGE

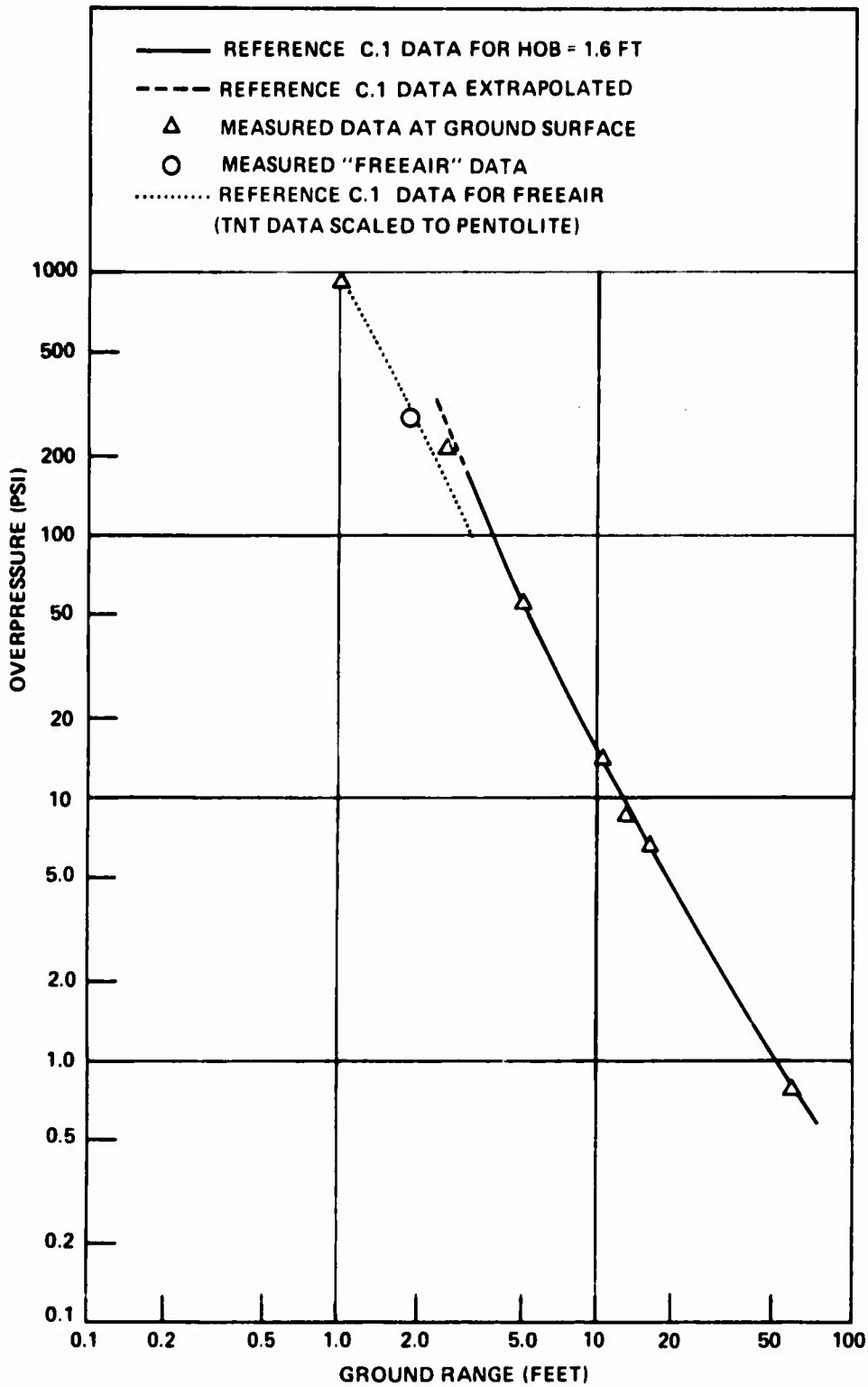

FIG. C.1 SIDE–ON AIRBLAST PRESSURES FOR 478–GRAM PENTOLITE SPHERES AT HOB = 1.6 FEET

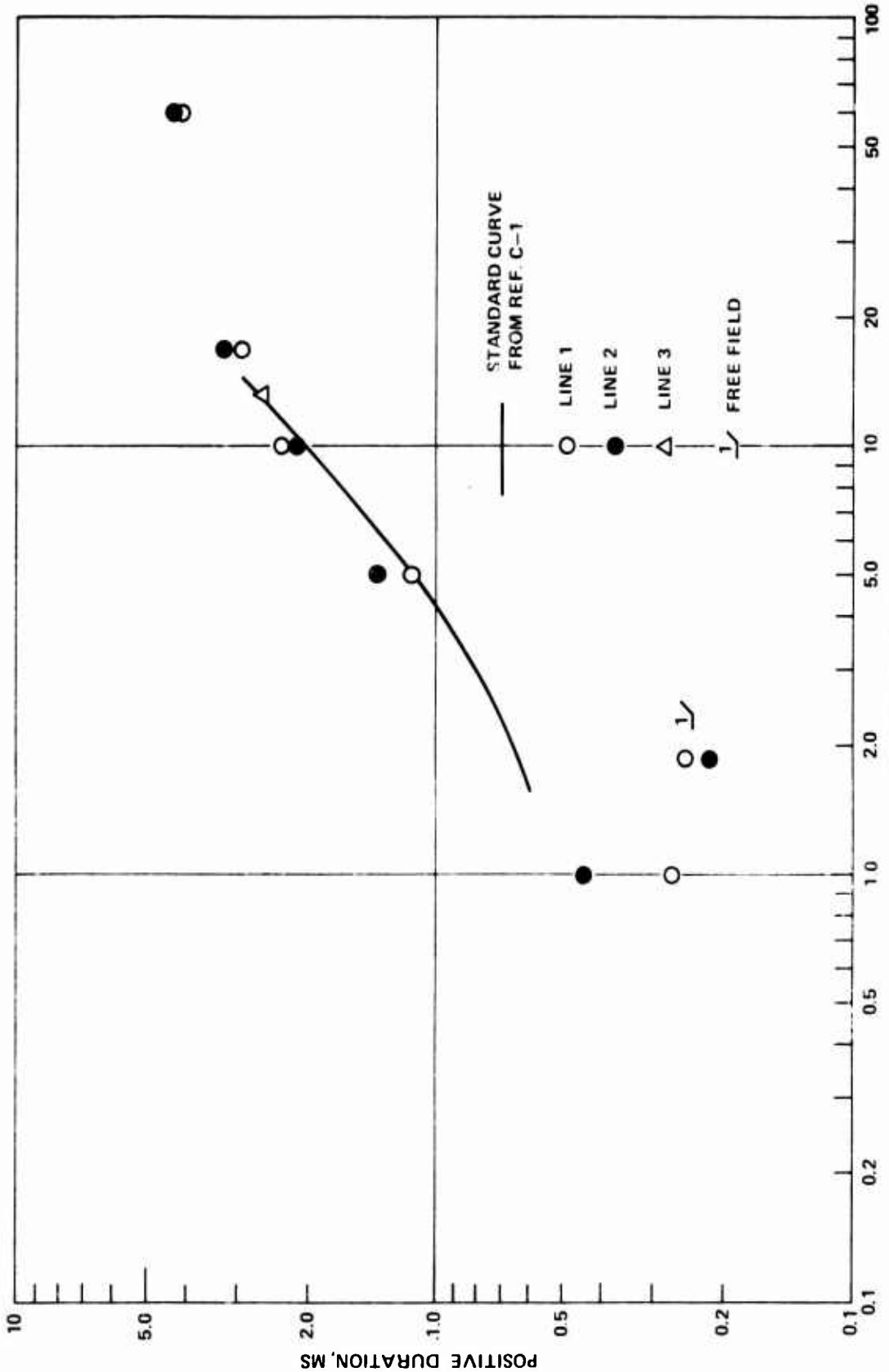

FIG. C.2 POSITIVE SHOCKWAVE DURATIONS FOR 478 - GRAM PENTOLITE SPHERES; HOB = 1.6 FEET

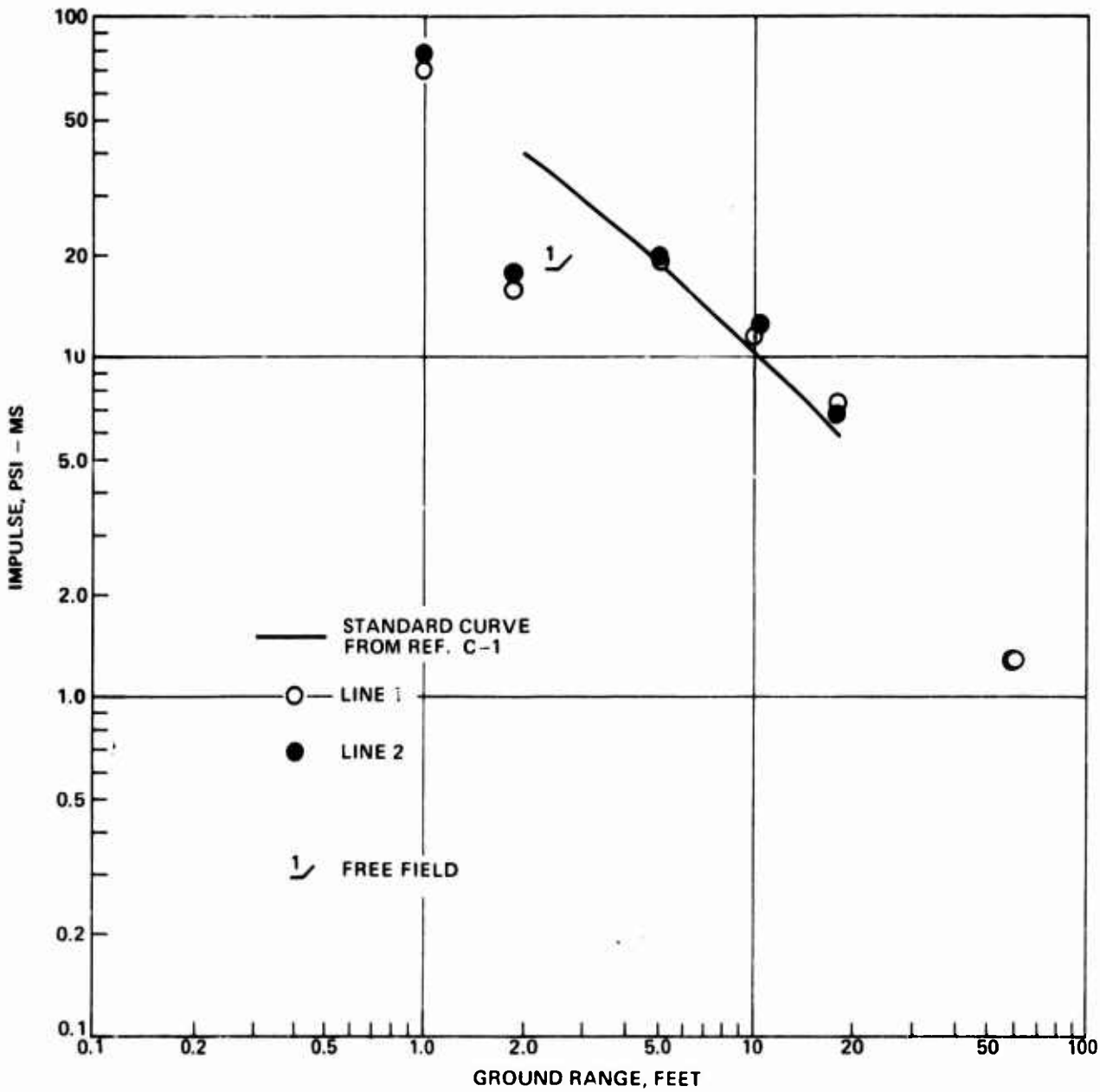

FIG. C.3 POSITIVE SHOCKWAVE IMPULSE FROM 478 · GRAM PENTOLITE SPHERES; HOB = 1.6 FEET

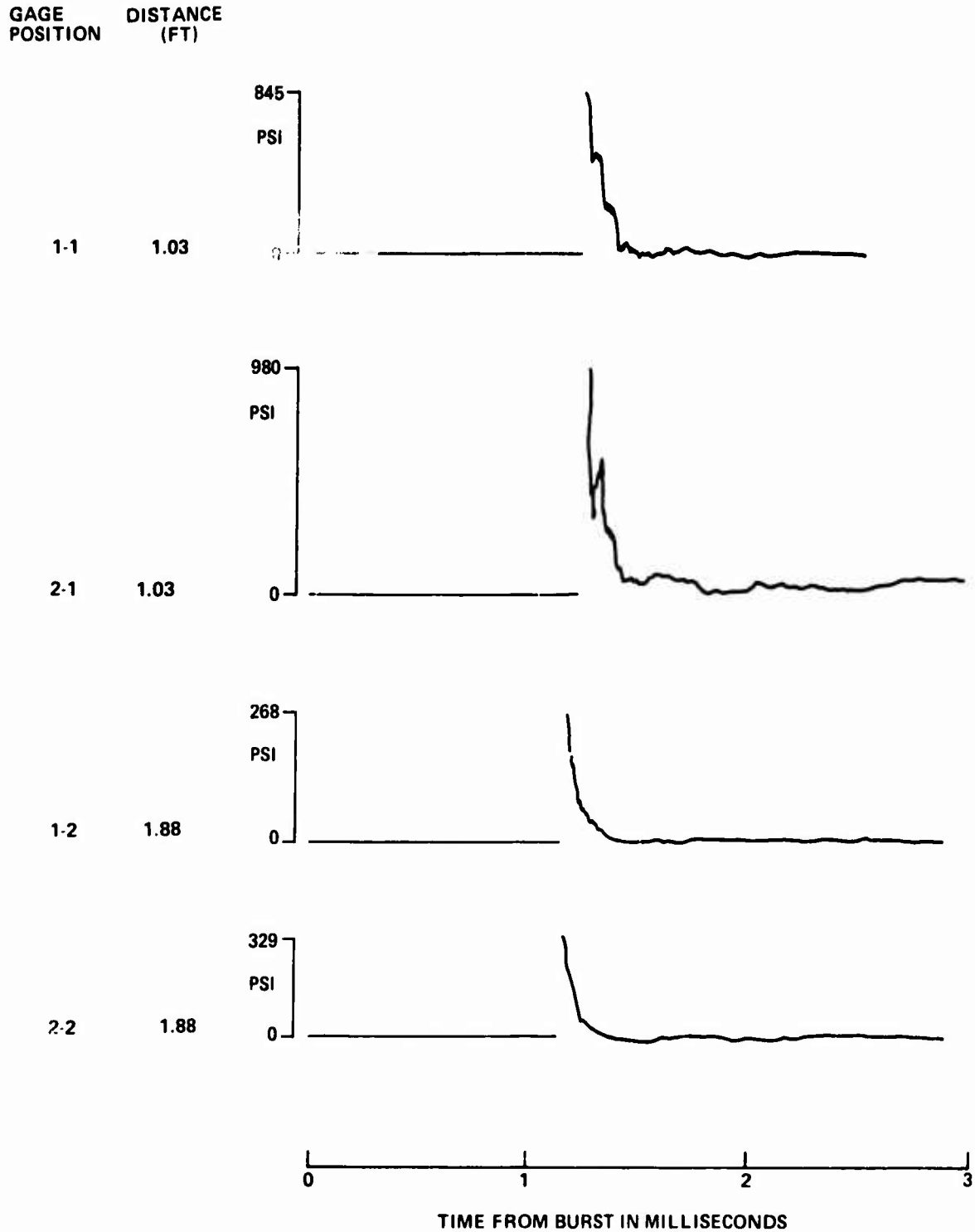

FIG. C.4 PRESSURE - TIME HISTORIES FROM 478 - GRAM PENTOLITE SPHERE; HOB = 1.6 FEET

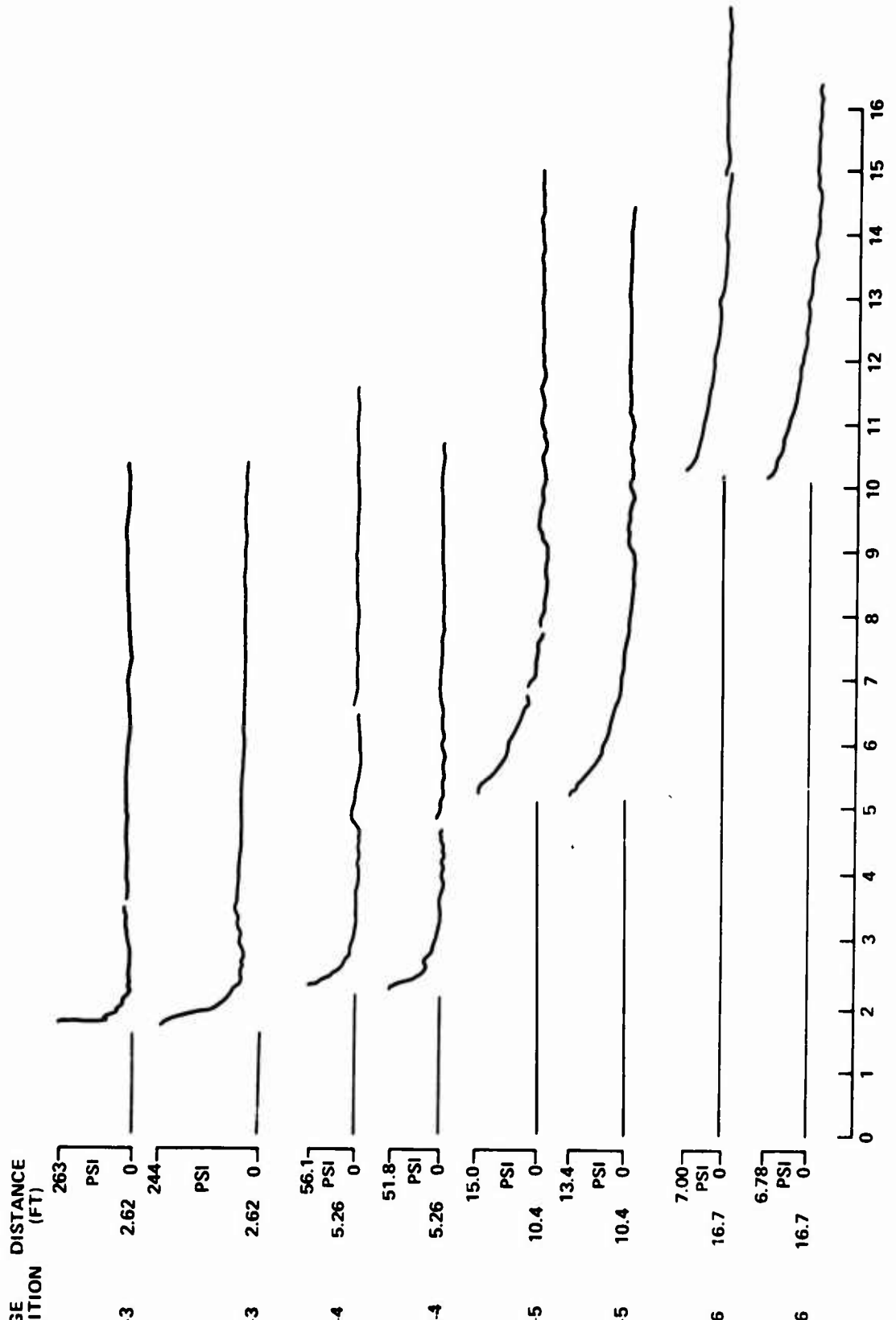

FIG. C.4 (CONTINUED)

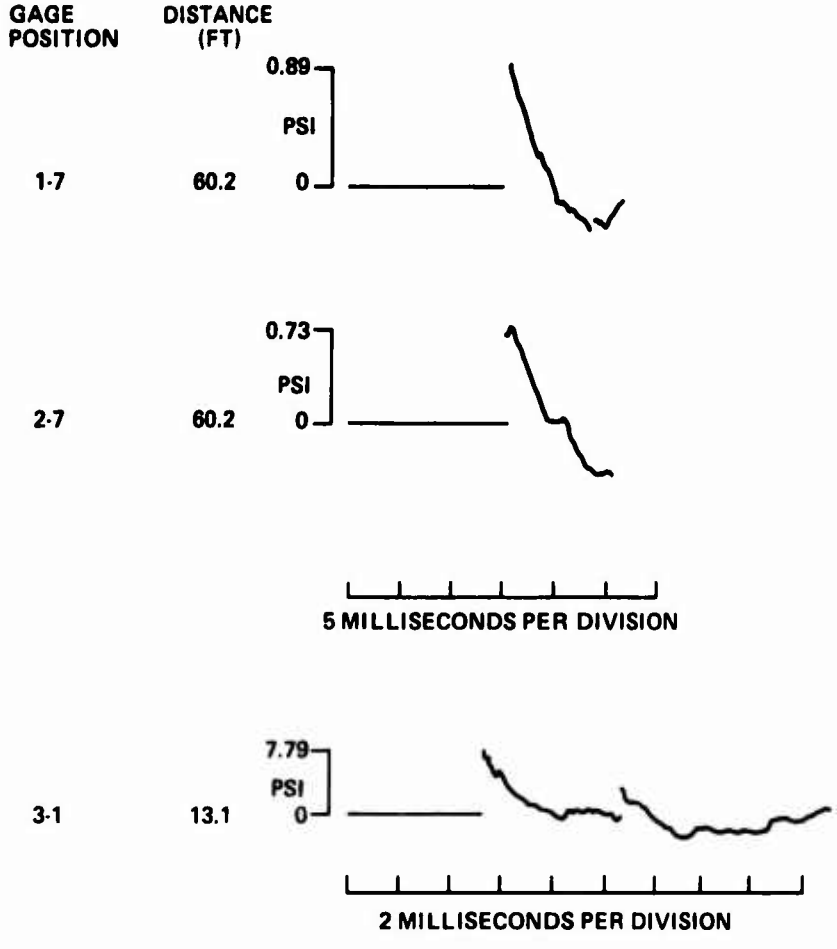

FIG. C.4 (CONTINUED)

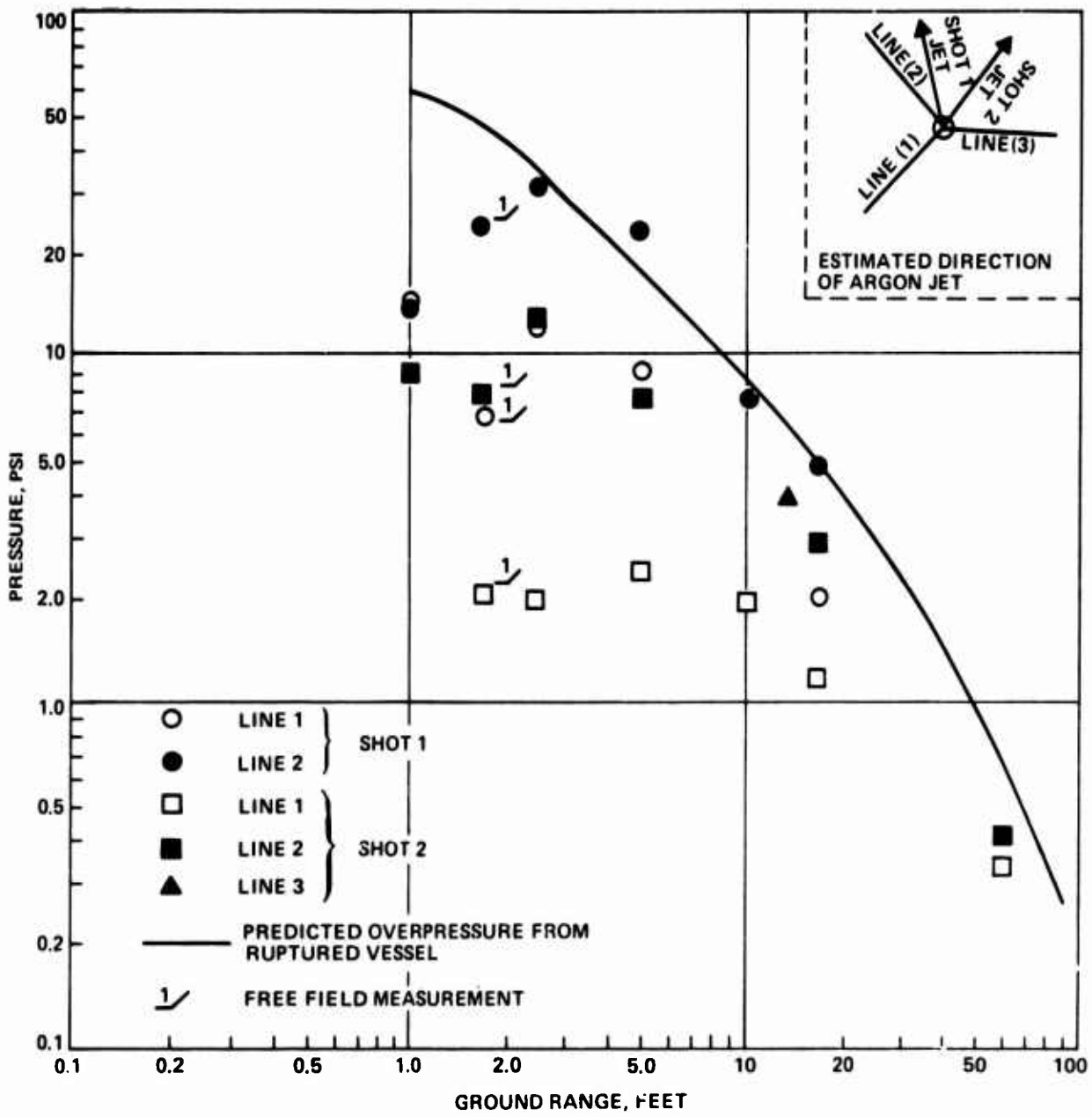

FIG. C.5 AIRBLAST OVERPRESSURE FROM 15,000-PSI VESSEL RUPTURE

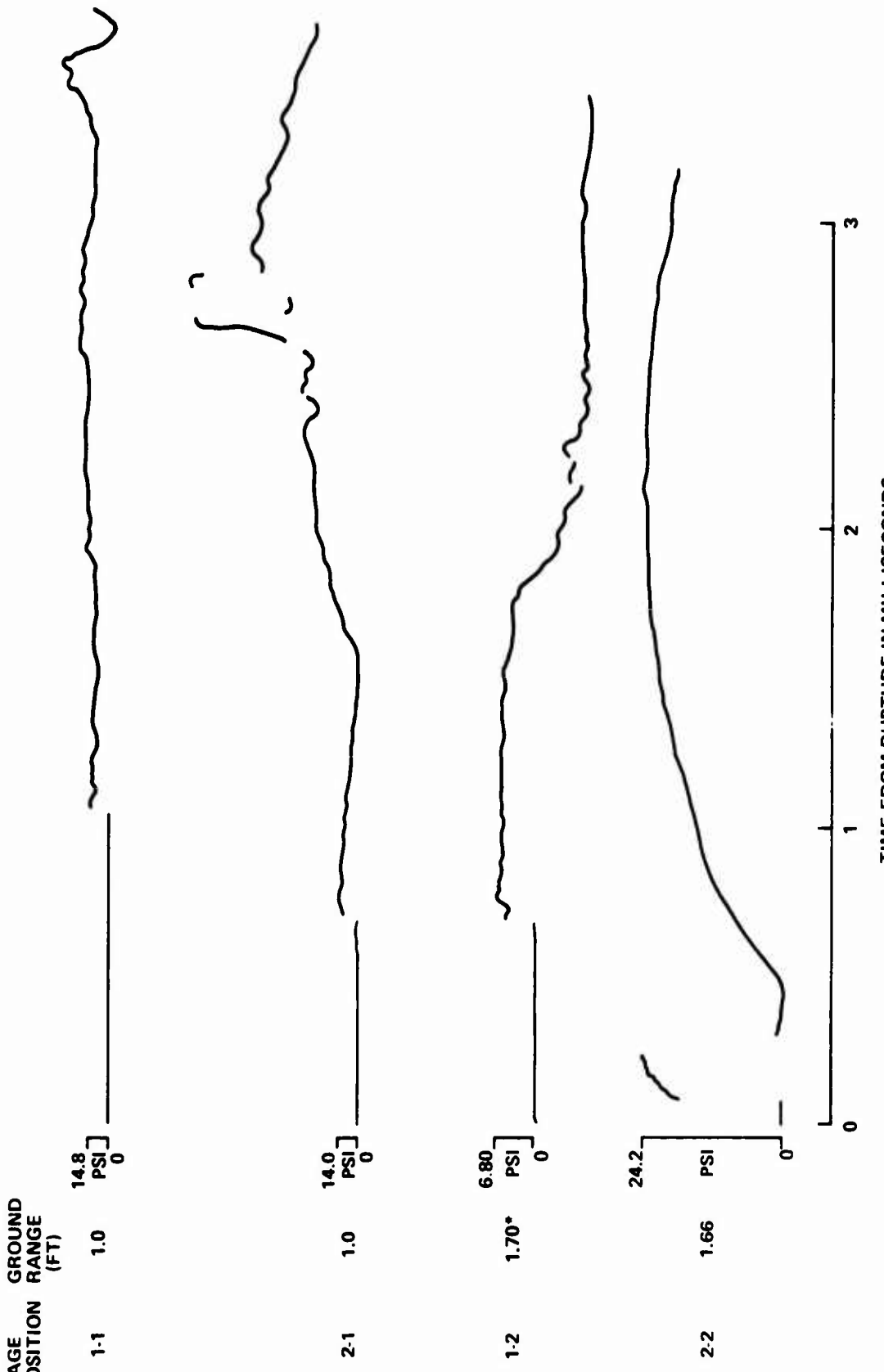

FIG. C.6 PRESSURE–TIME HISTORIES FROM 15,000-PSI SPHERE; SHOT 1

* SLANT RANGE

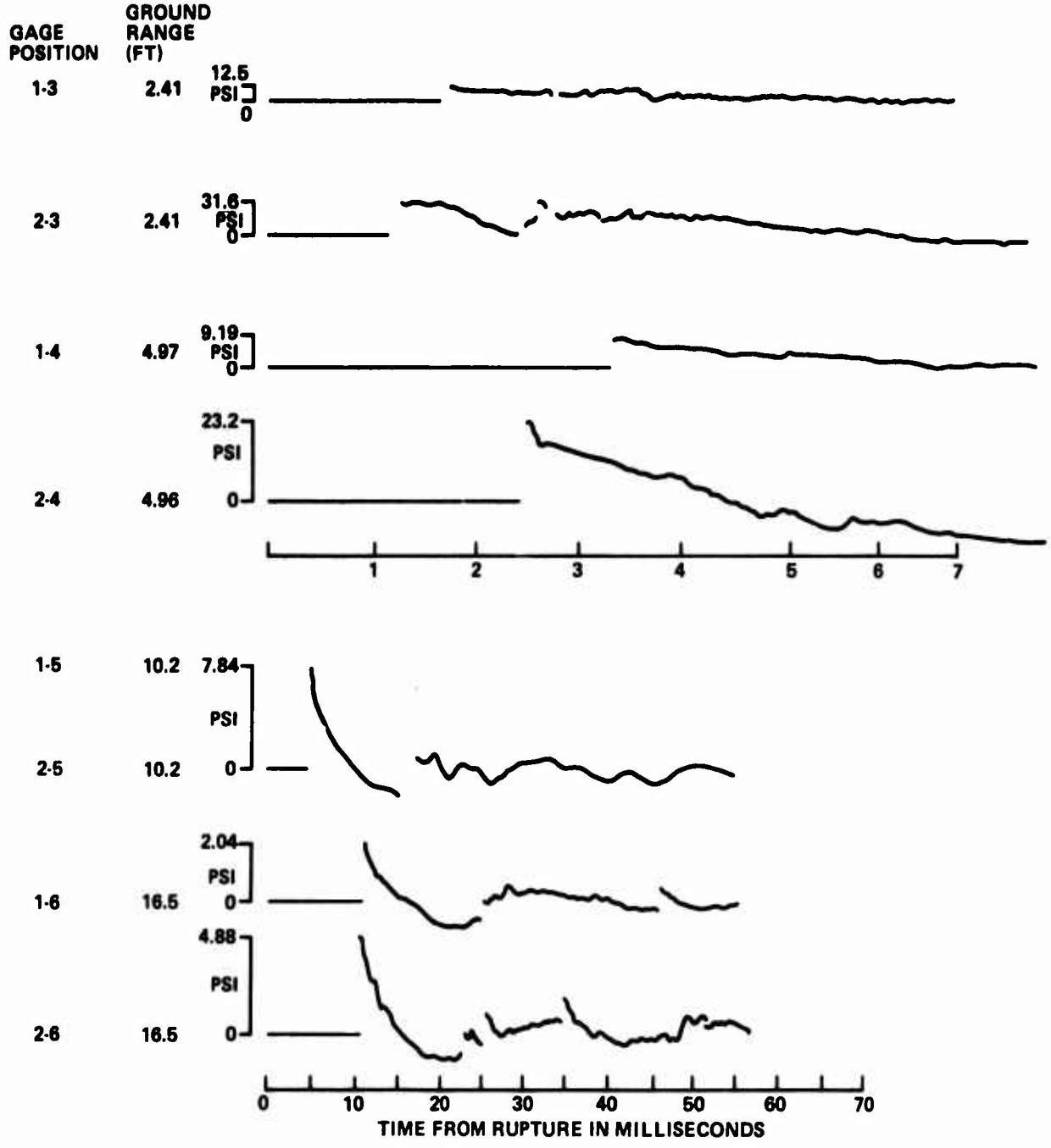

FIG. C.6 (CONTINUED)

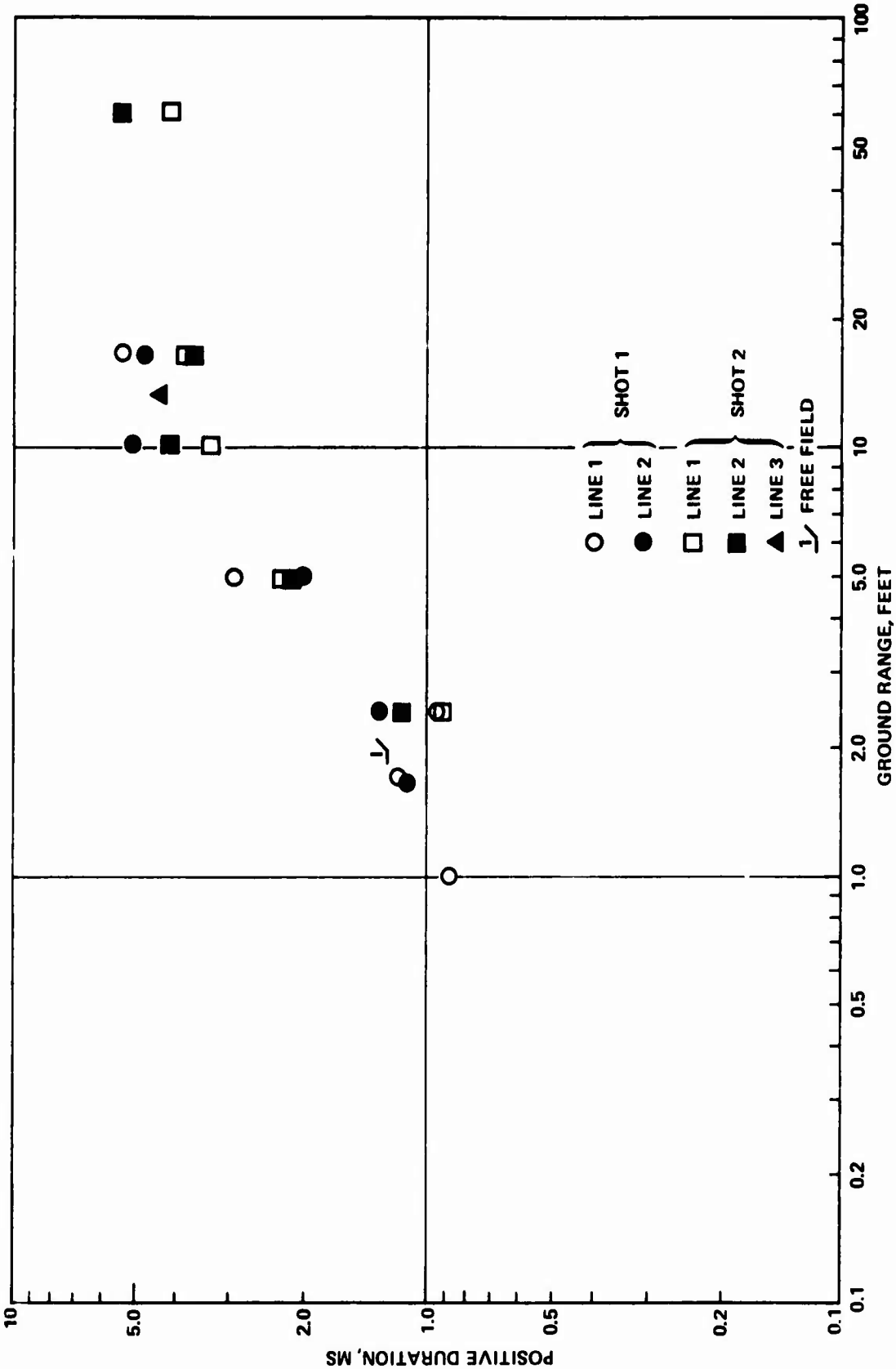

FIG. C.7 POSITIVE SHOCKWAVE DURATION FROM 15,000 - PSI VESSEL RUPTURE

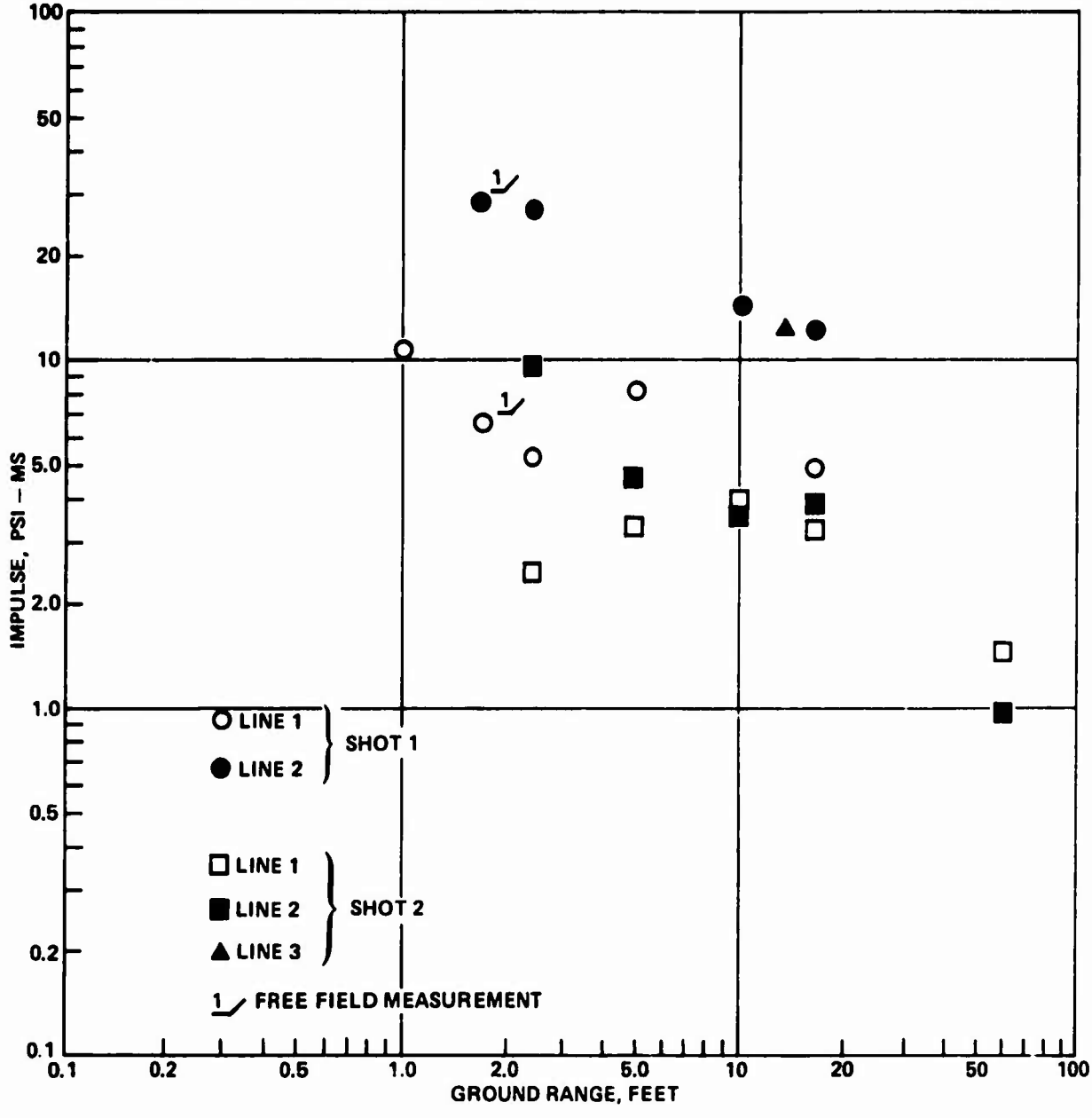

FIG. C.8 POSITIVE SHOCKWAVE IMPULSE FROM 15,000 - PSI VESSEL RUPTURE

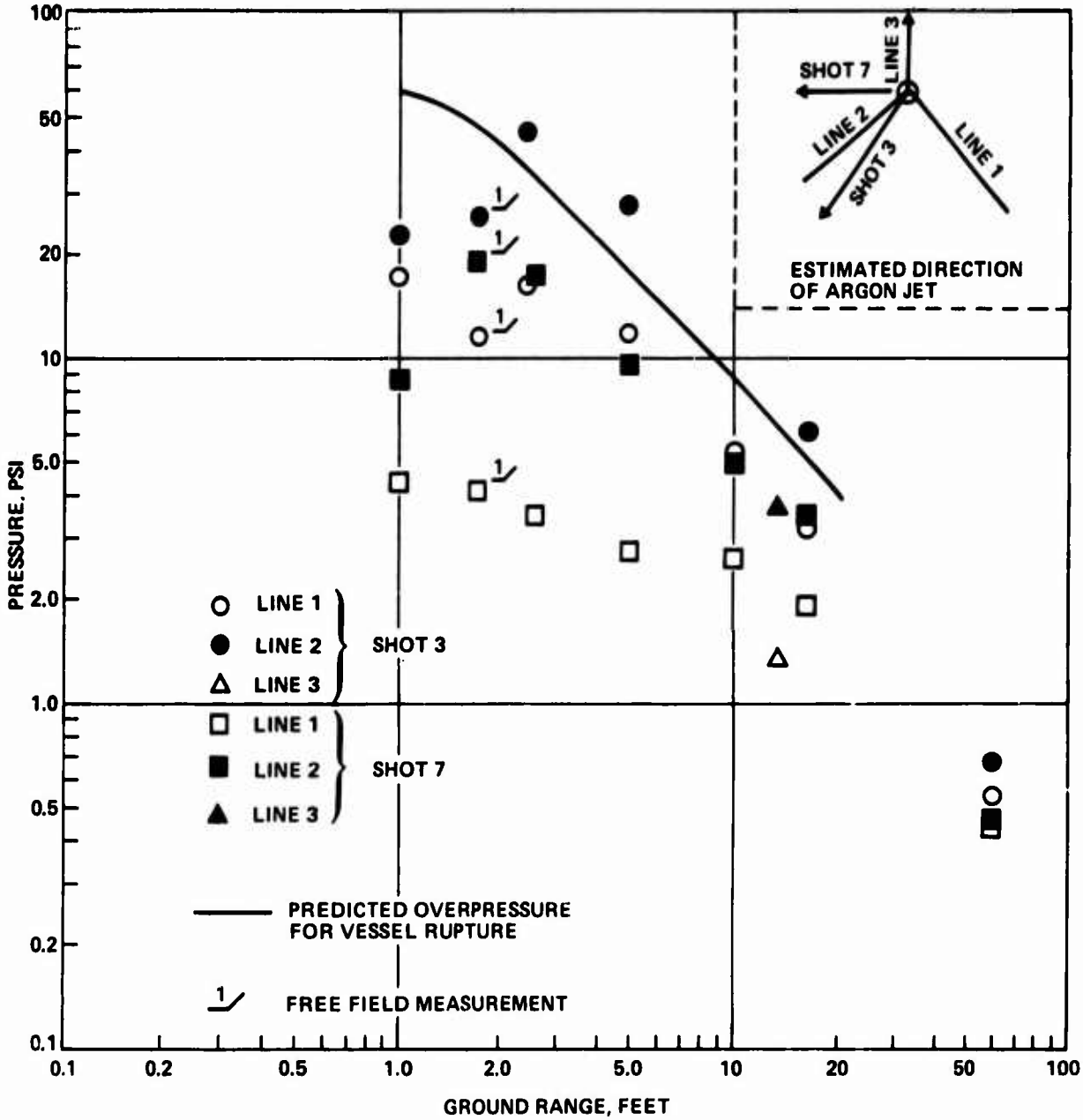

FIG. C.9 AIRBLAST OVERPRESSURE FROM 30,000 - PSI VESSEL RUPTURE

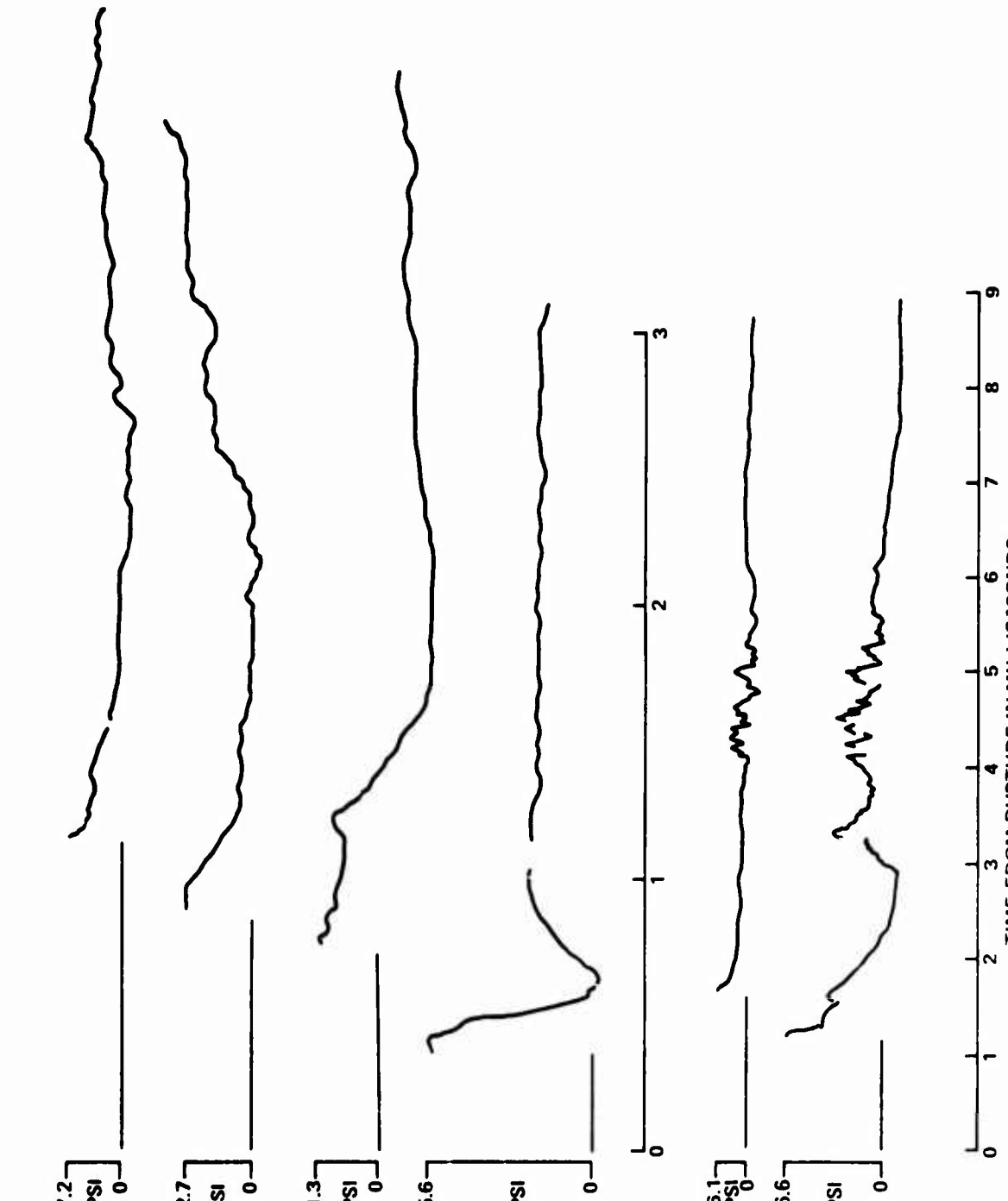

FIG. C.10 PRESSURE – TIME HISTORIES FROM 30,000-PSI SPHERE; SHOT 3

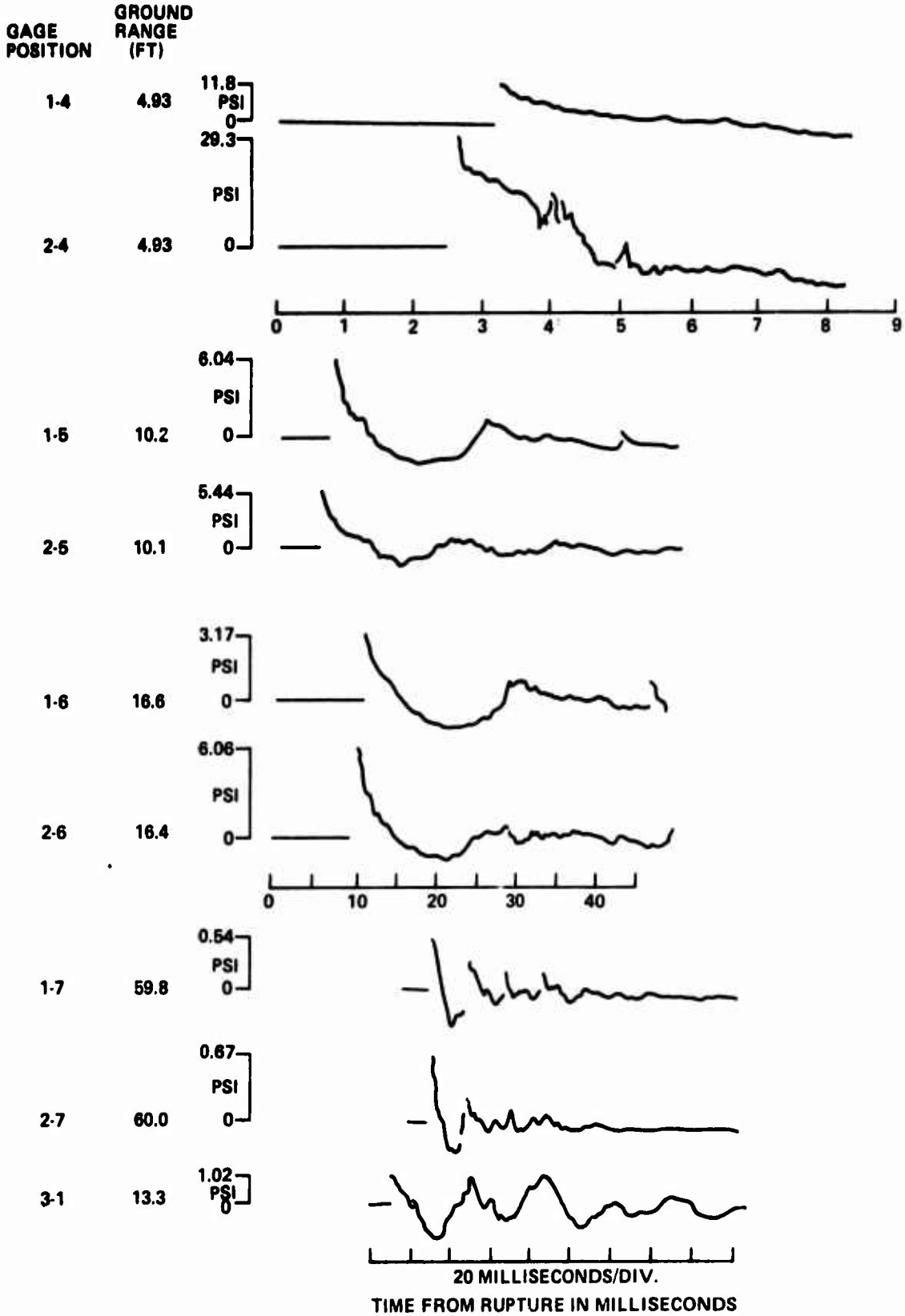

FIG. C.10 (CONTINUED)

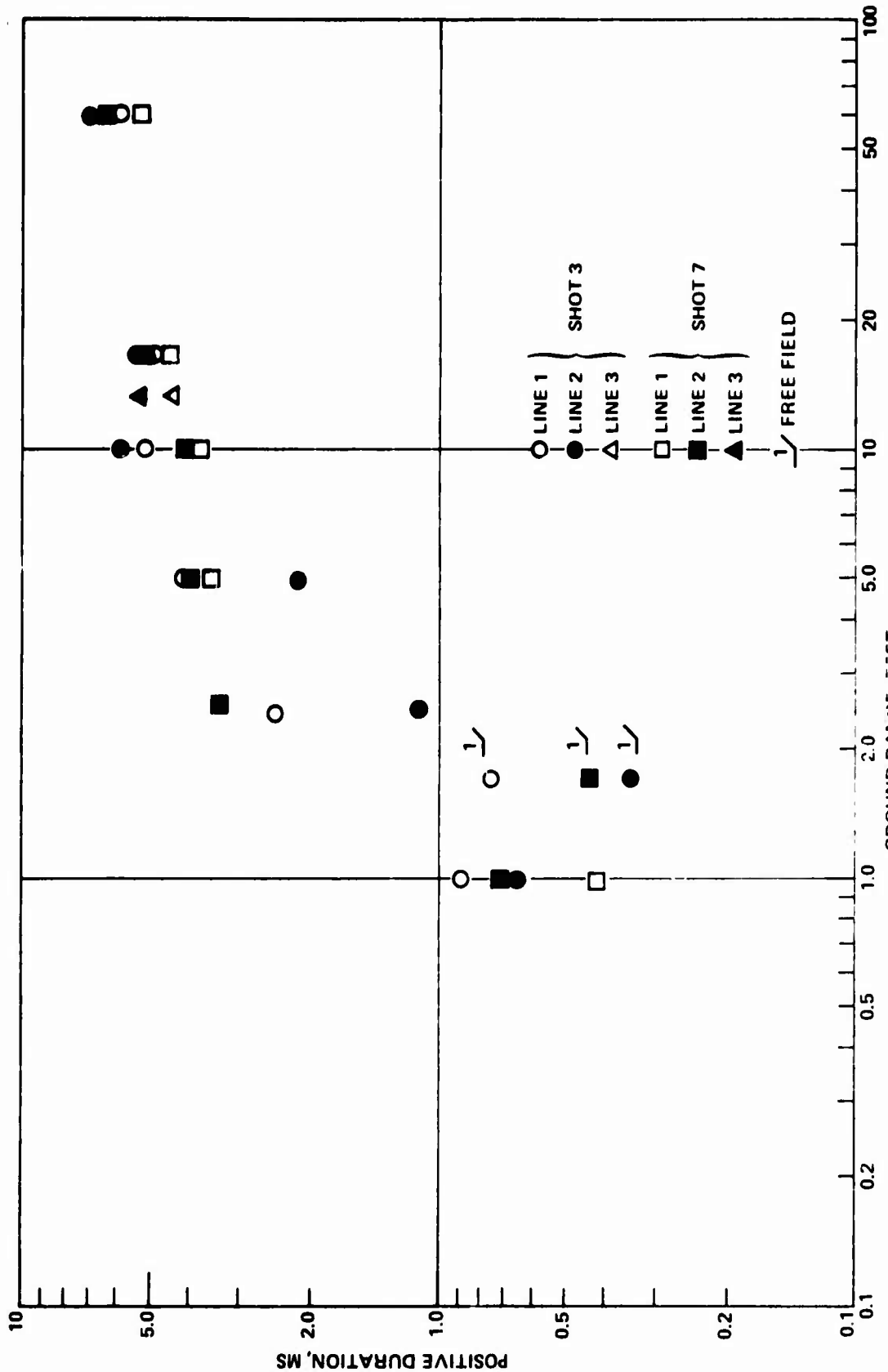

FIG. C.11 POSITIVE SHOCKWAVE DURATION FROM 30,000 - PSI VESSEL RUPTURE

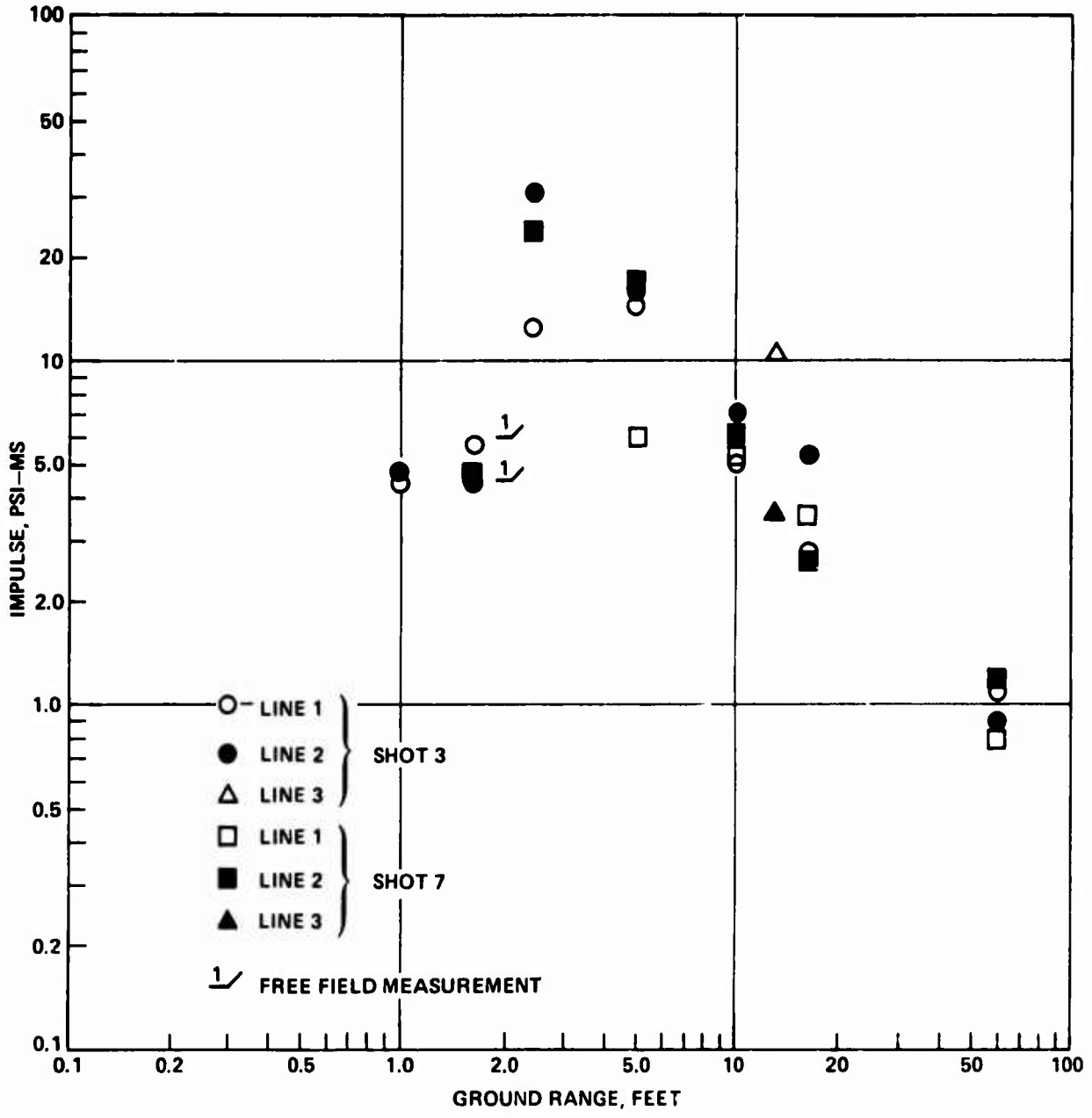

FIG. C.12 POSITIVE SHOCKWAVE IMPULSE FROM 30,000 - PSI VESSEL RUPTURE

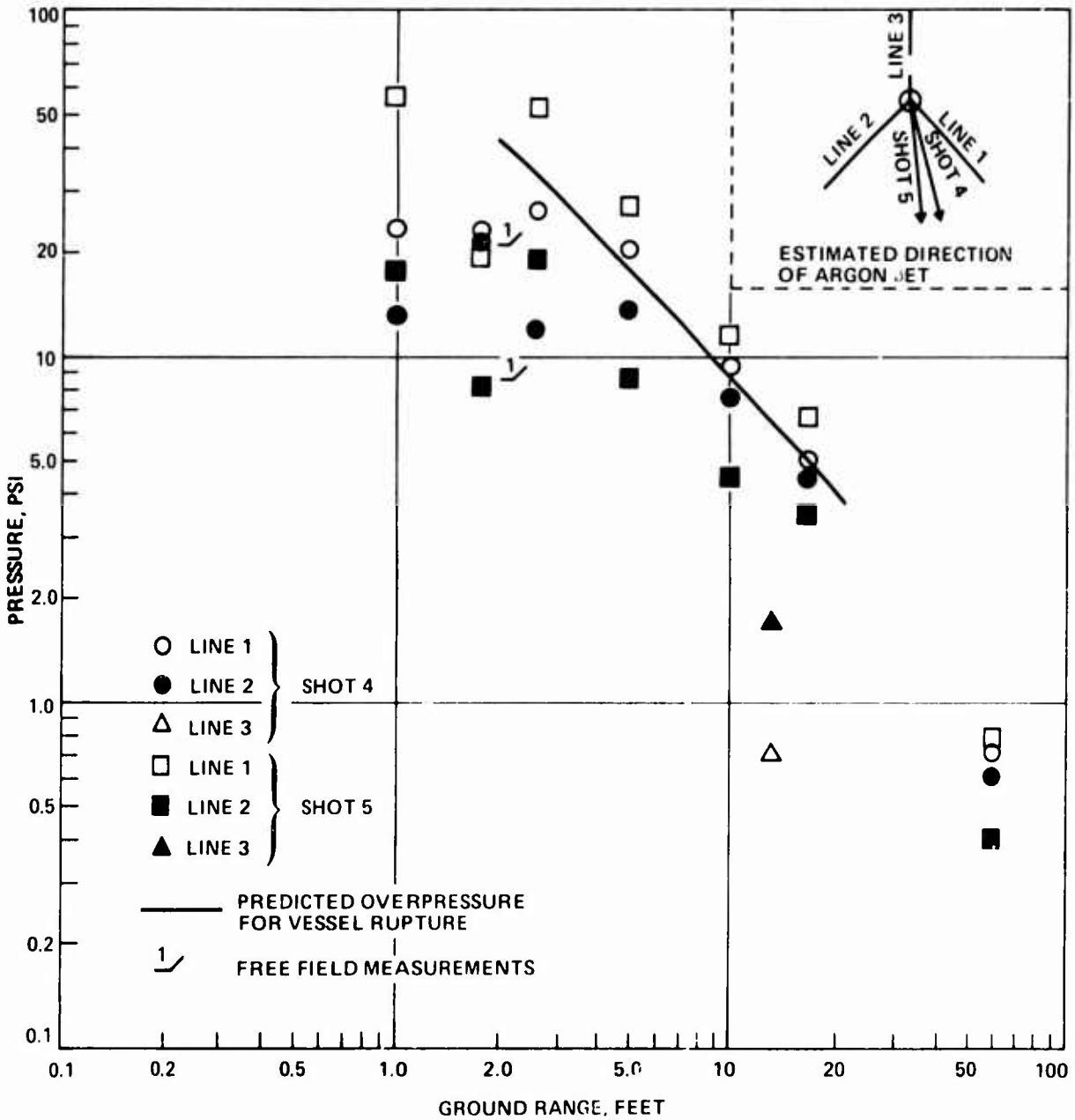

FIG. C.13 AIRBLAST OVERPRESSURE FROM 50,000 - PSI VESSEL RUPTURE

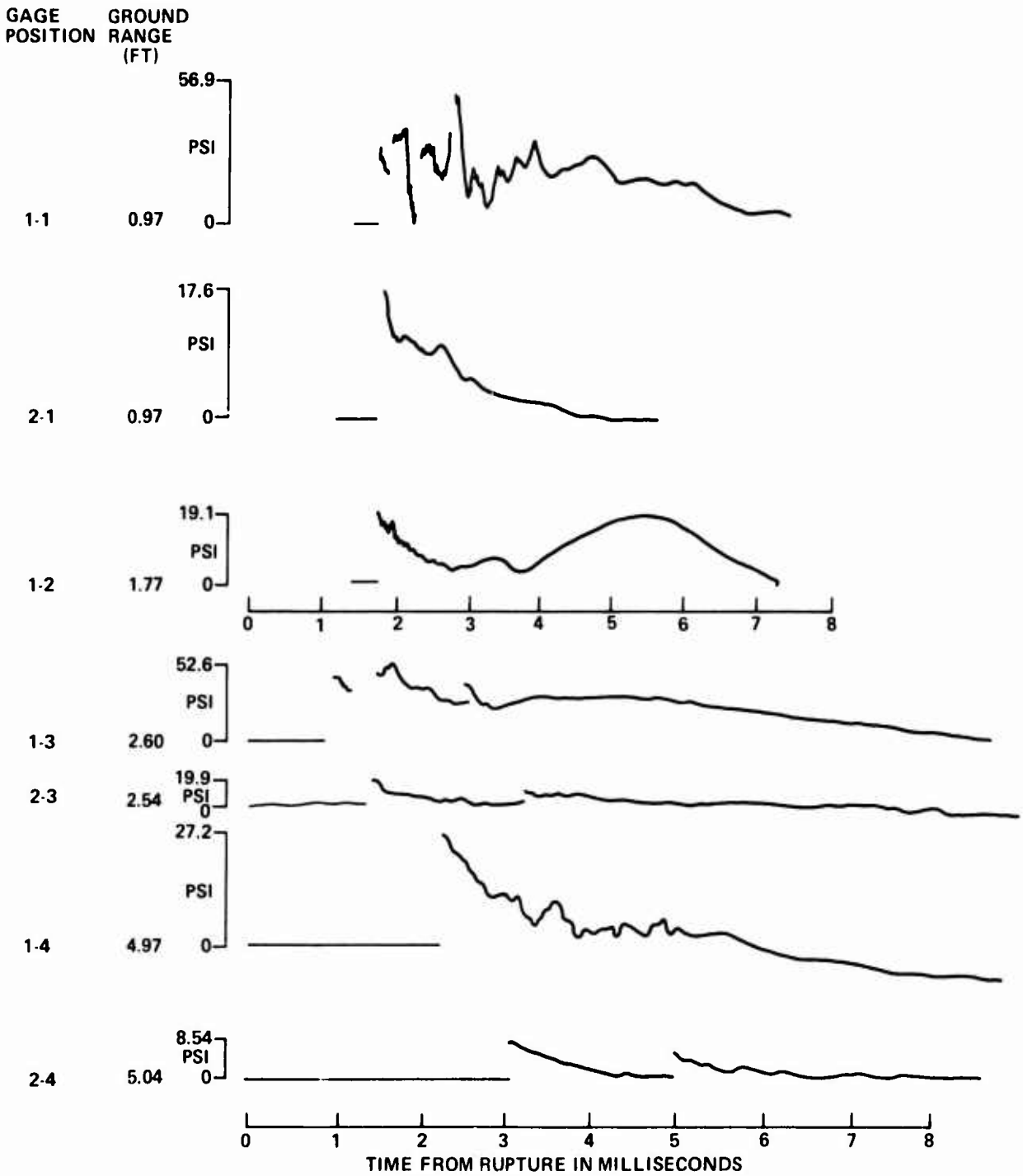

FIG. C.14 PRESSURE–TIME HISTORIES FROM 50,000 · PSI SPHERE; SHOT 5

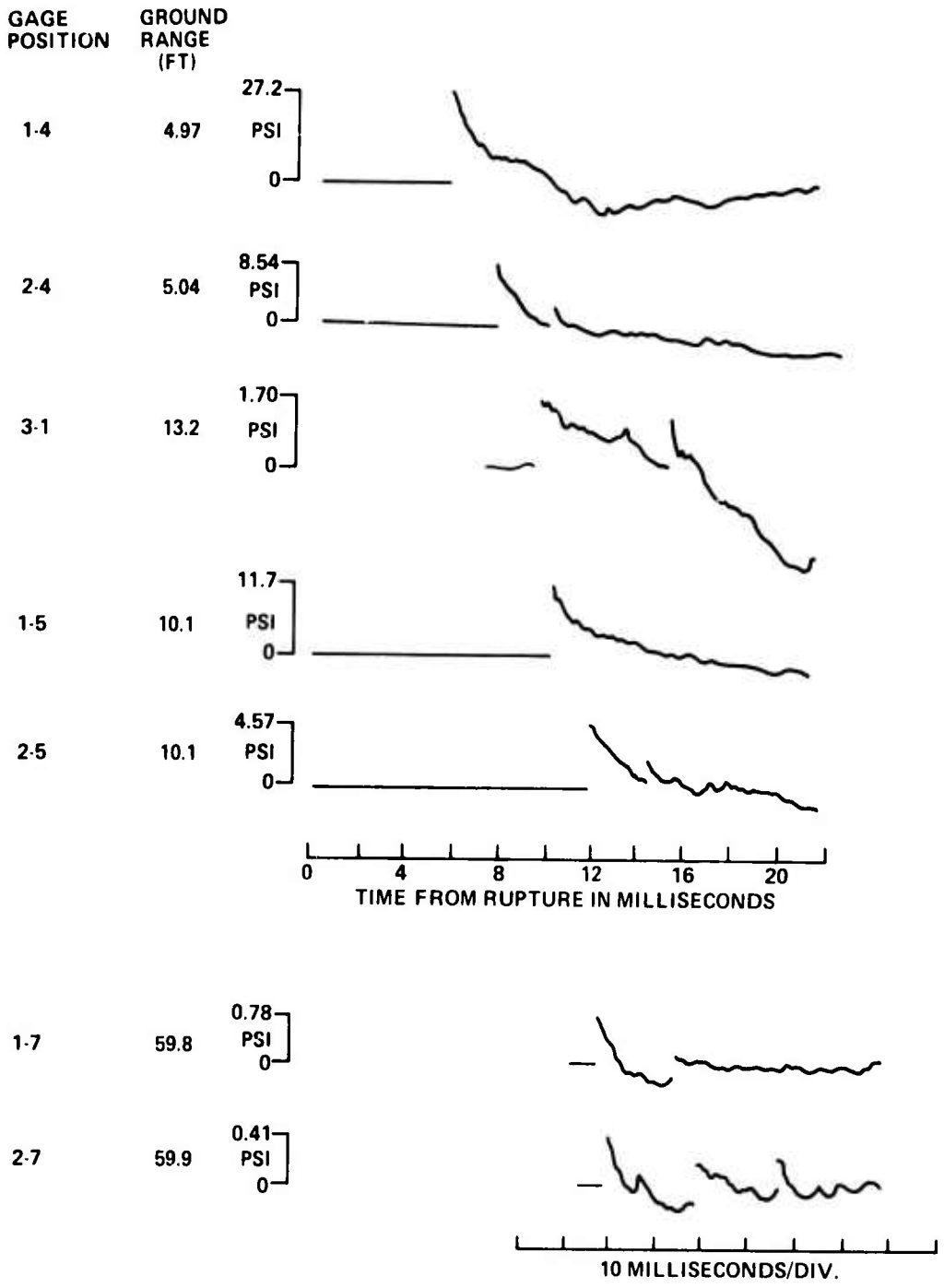

FIG. C.14 (CONTINUED)

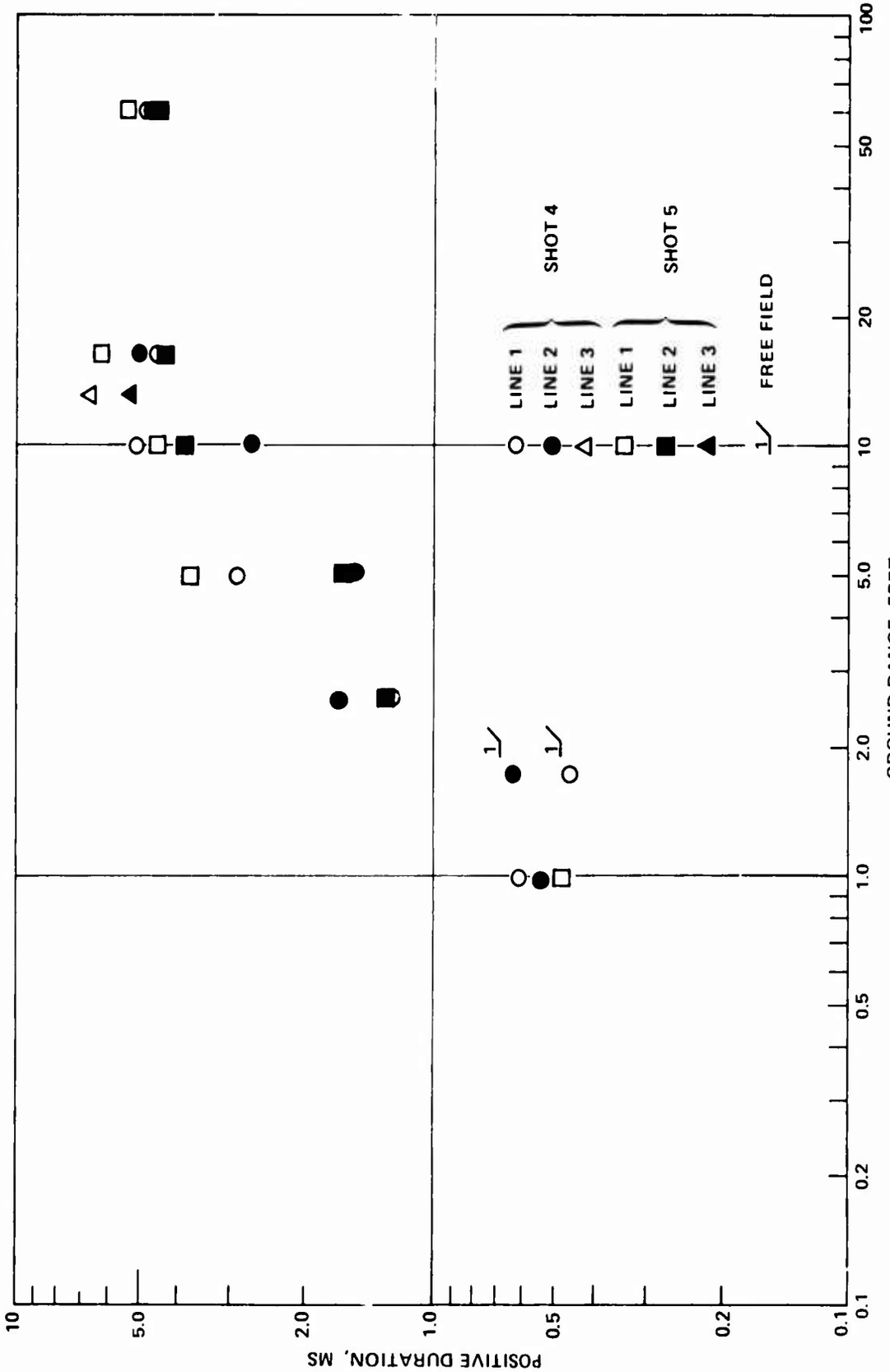

FIGURE C.15 POSITIVE SHOCKWAVE DURATION FROM 50,000 - PSI VESSEL RUPTURE

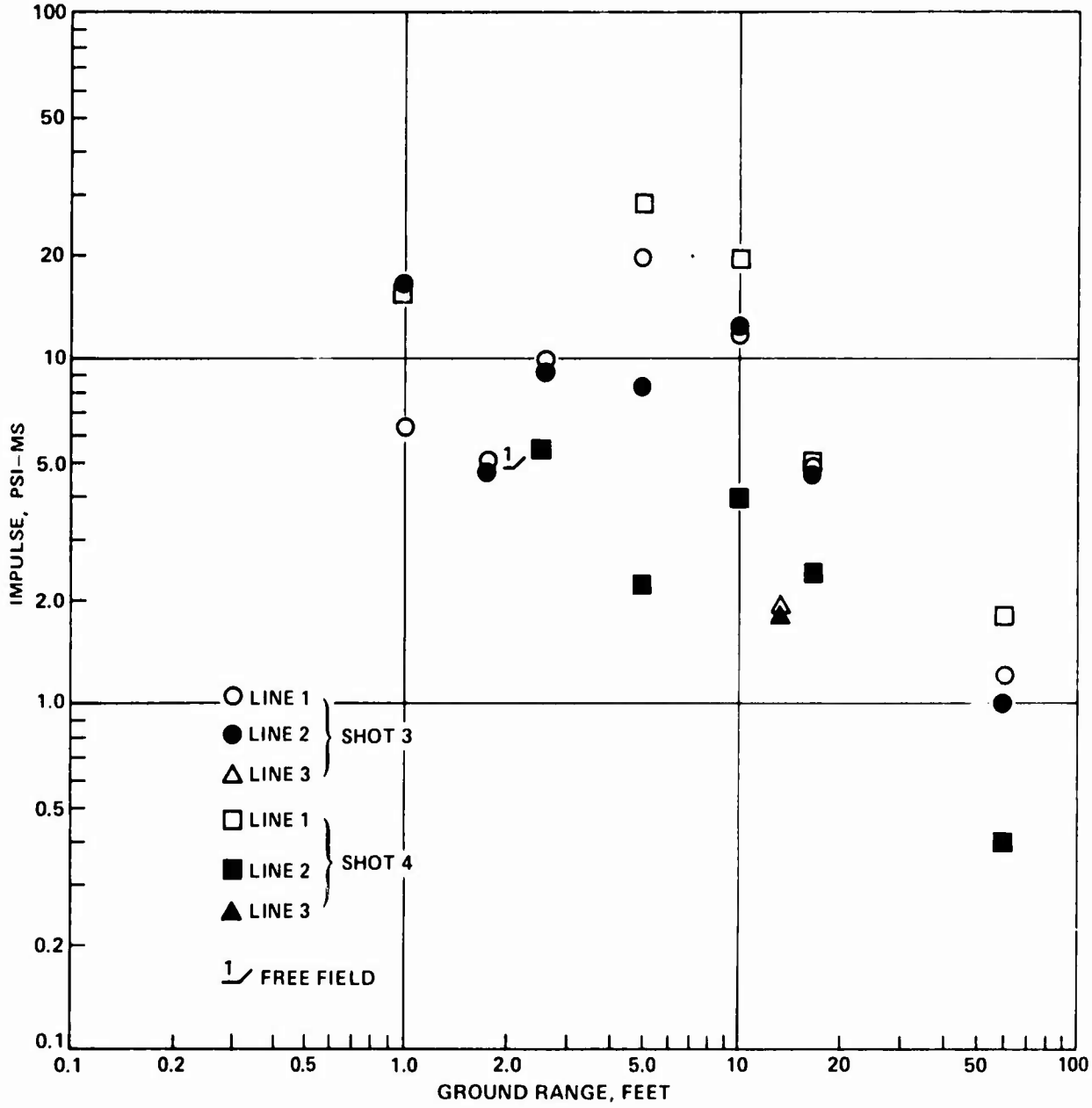

FIG. C.16 POSITIVE SHOCKWAVE IMPULSE FROM 50,000 - PSI VESSEL RUPTURE

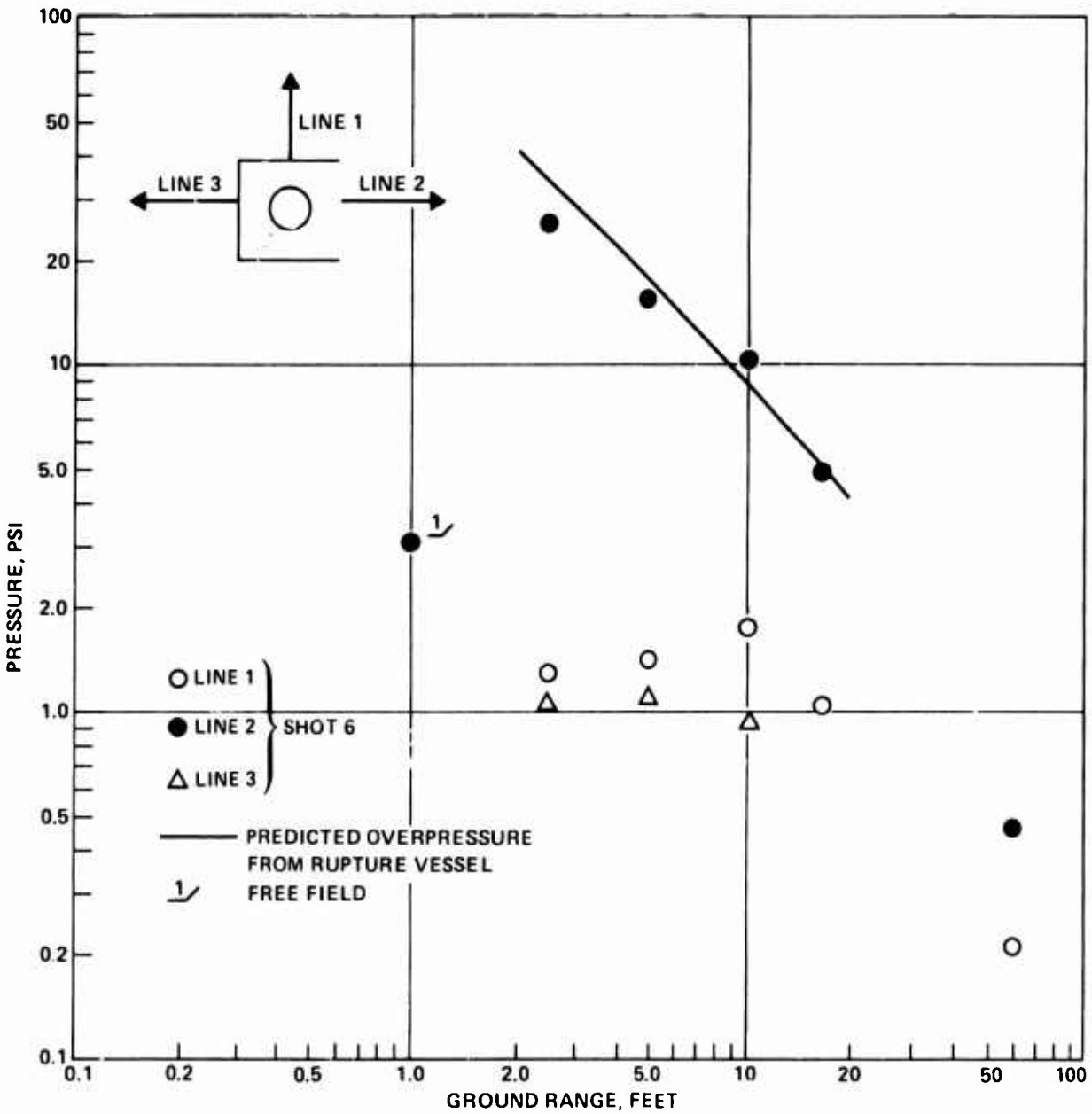

FIG. C.17 AIRBLAST OVERPRESSURES FROM THE CONFINED TEST

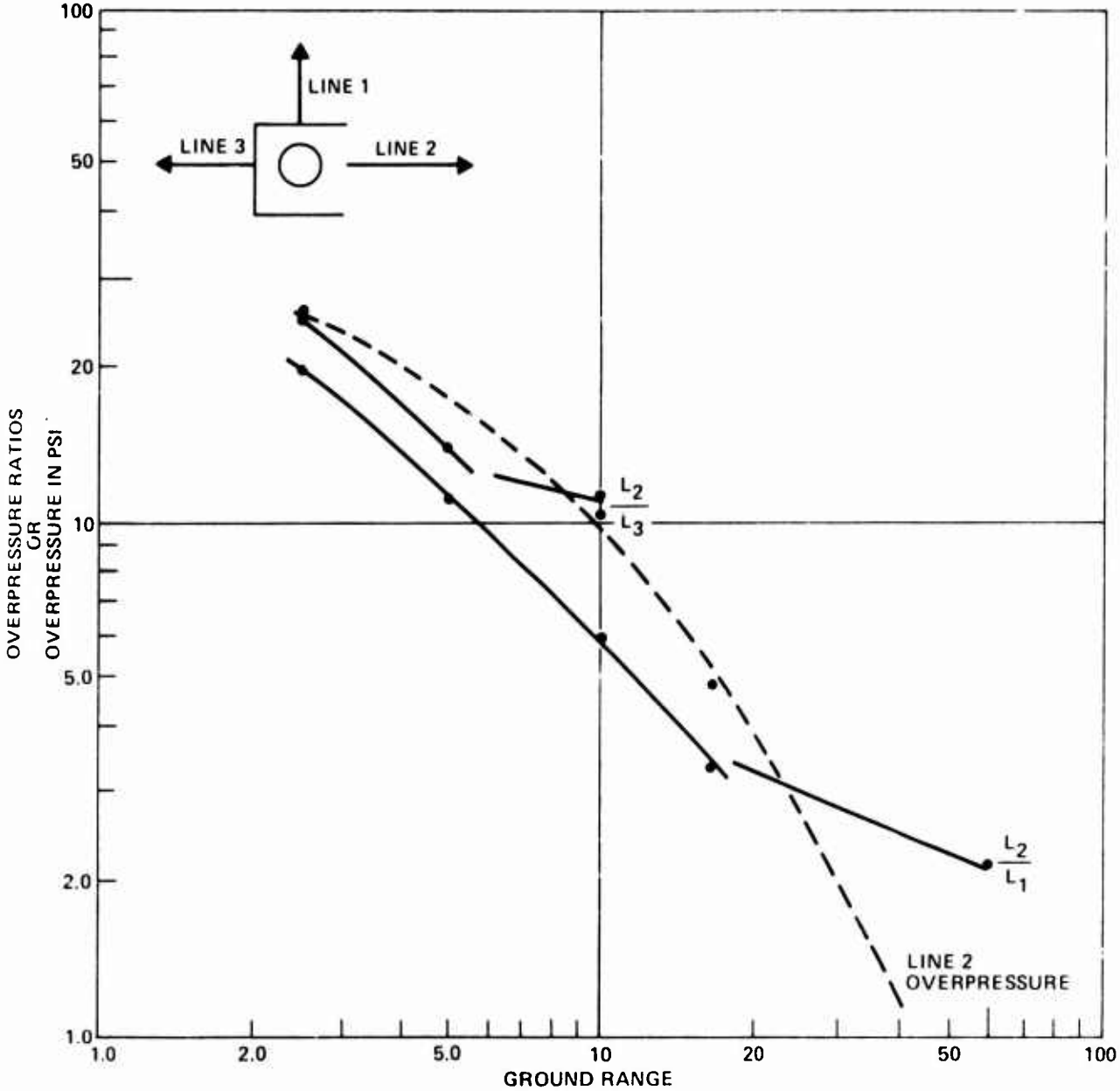

FIGURE C.18 OVERPRESSURE RATIOS VS GROUND RANGE

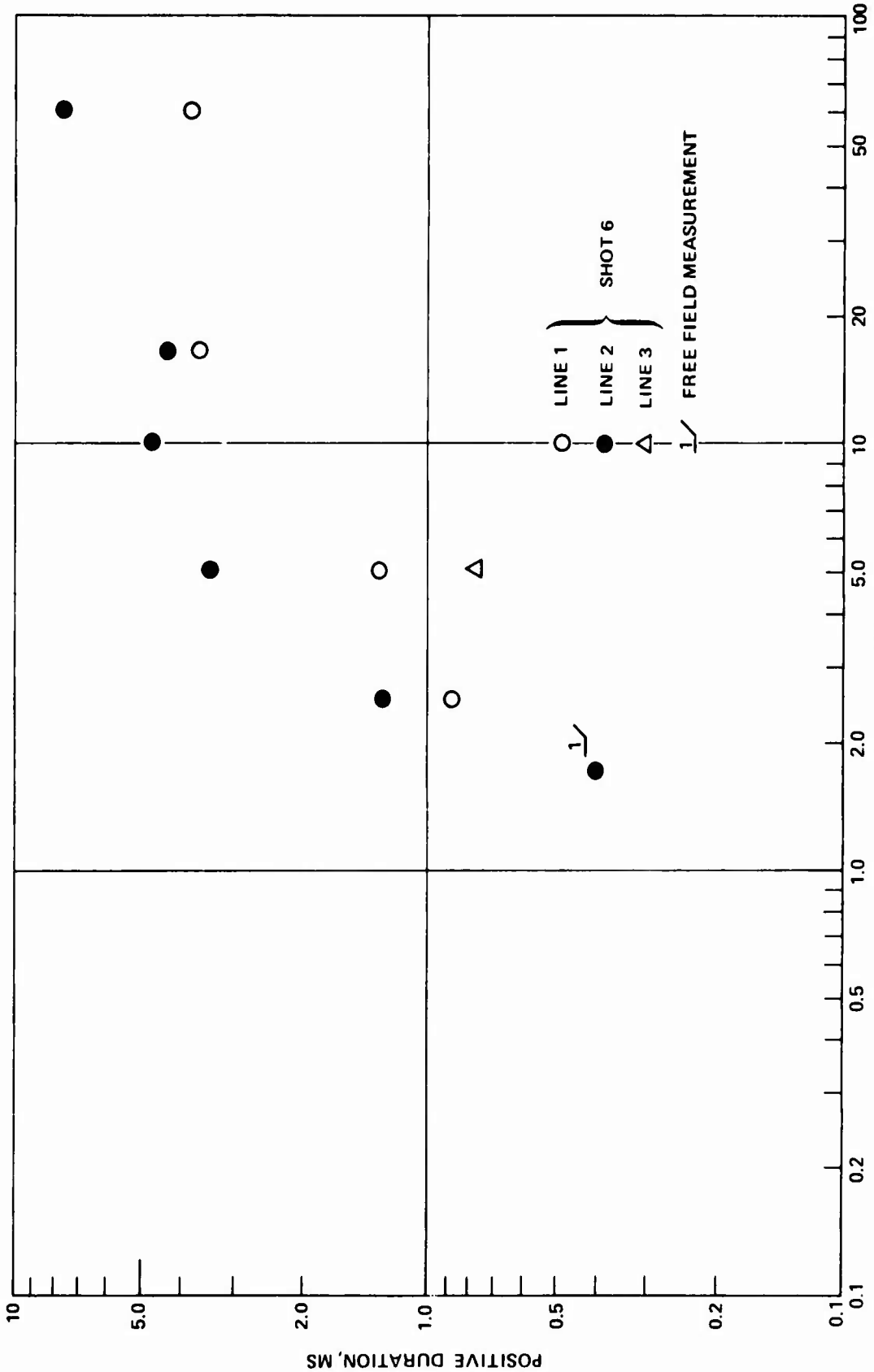

FIGURE C.19 POSITIVE SHOCKWAVE DURATION FROM 15,000-PSI CONFINED VESSEL RUPTURE

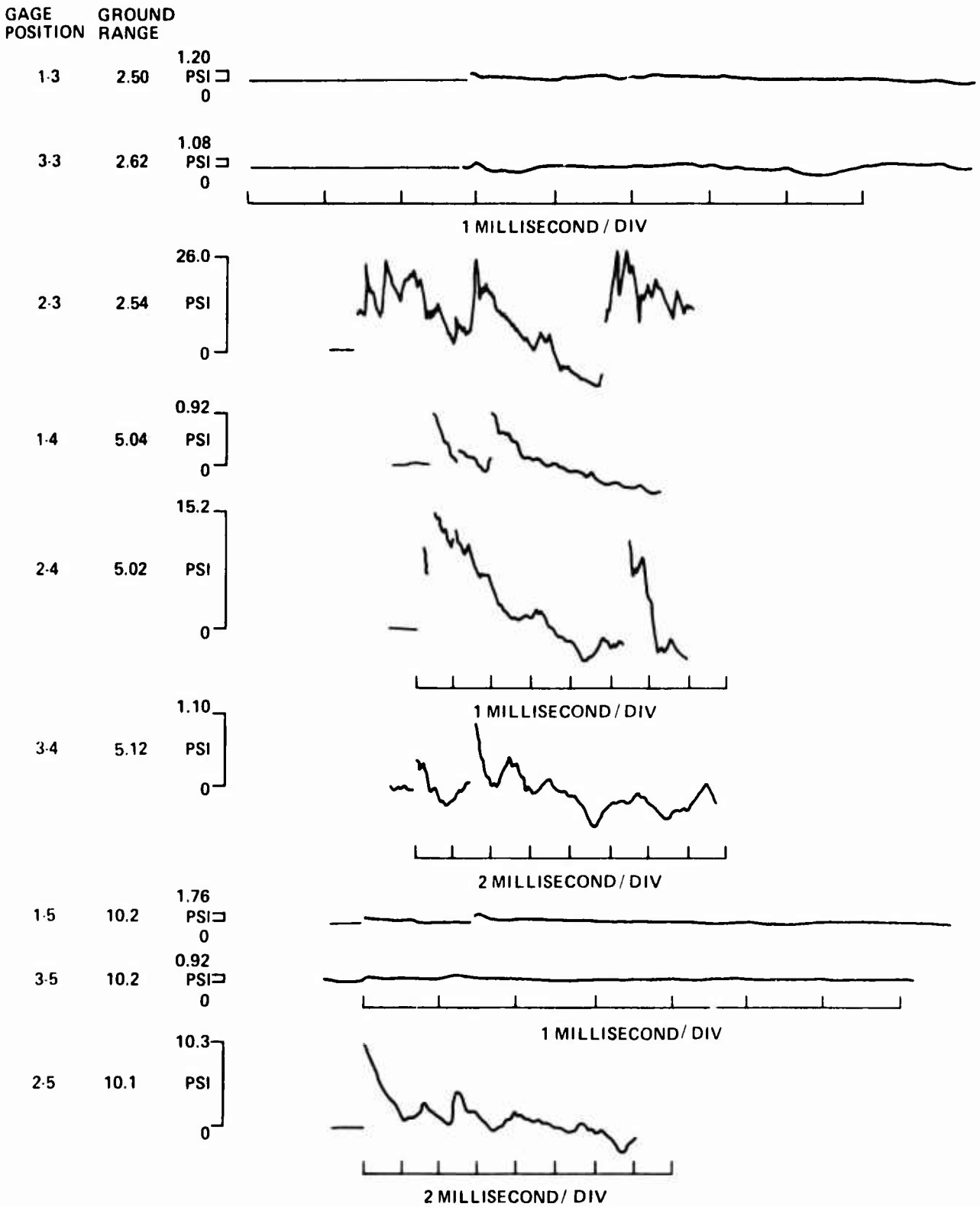

FIG. C.20 PRESSURE - TIME HISTORIES FROM CONFINED 15,000 - PSI SPHERE; SHOT 6

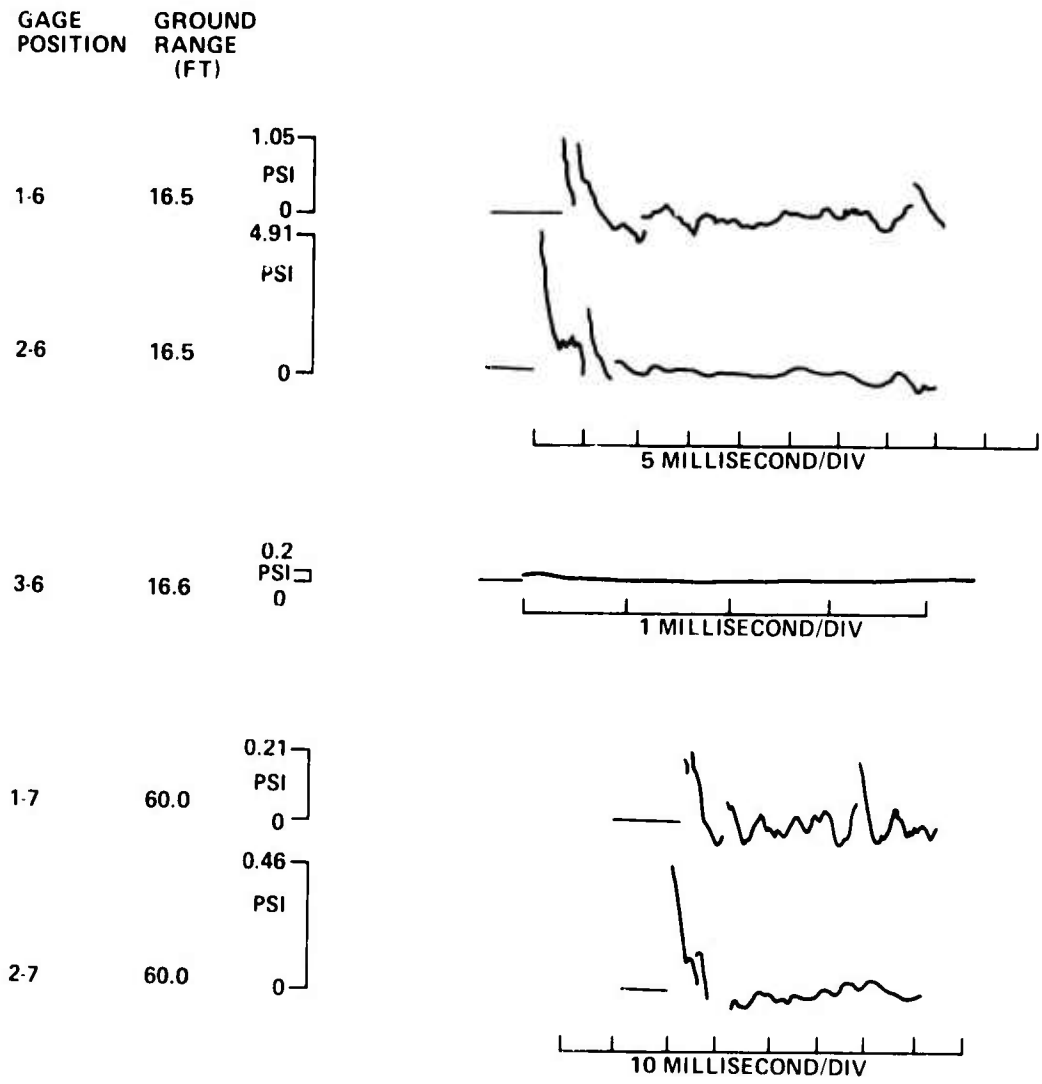

FIG. C.20 (CONTINUED)

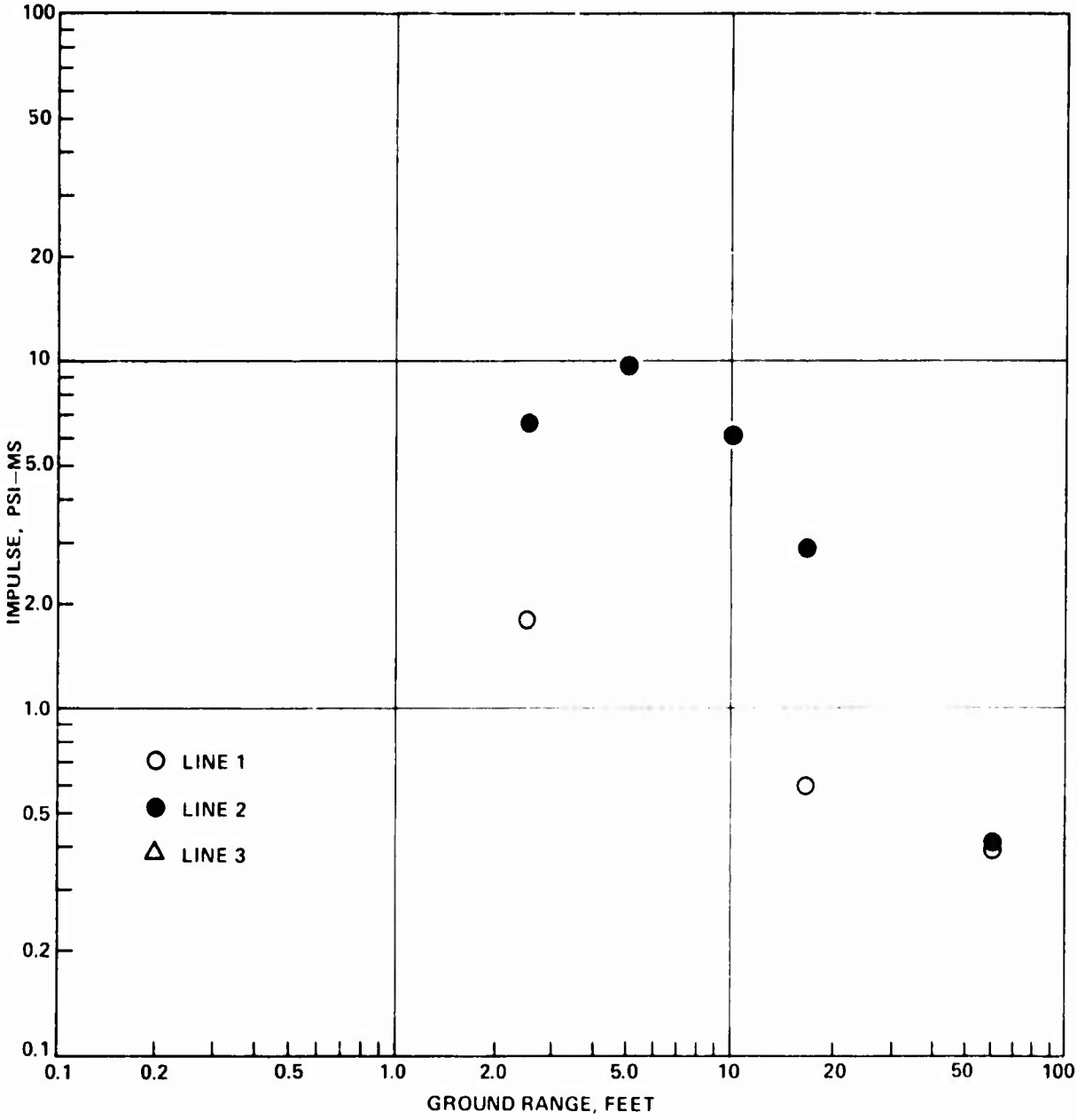

FIG. C.21 POSITIVE SHOCKWAVE IMPULSE FROM 15,000 - PSI CONFINED VESSEL RUPTURE

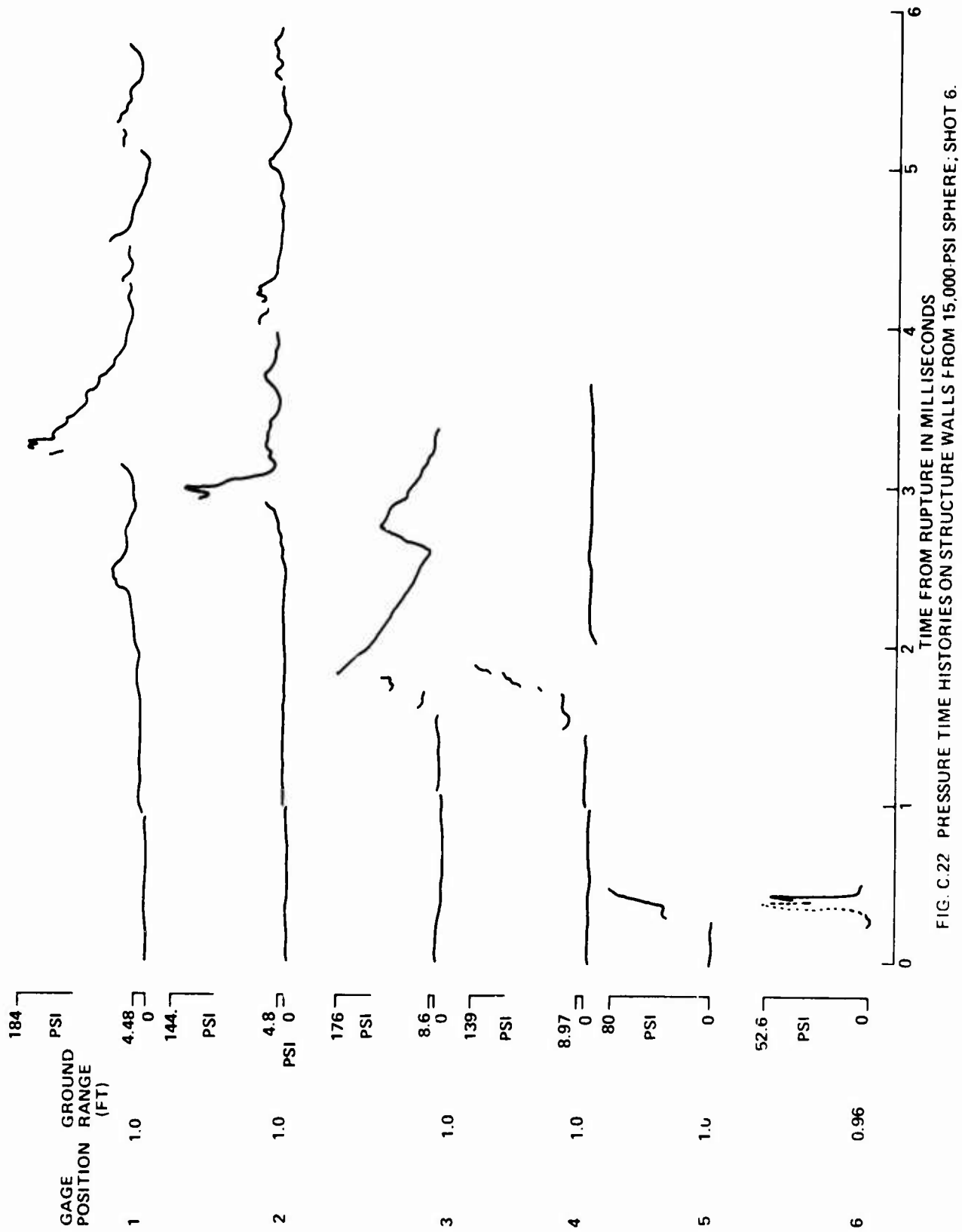

FIG. C.22 PRESSURE TIME HISTORIES ON STRUCTURE WALLS FROM 15,000-PSI SPHERE; SHOT 6.

ANNEX D FRAGMENT MEASUREMENTS

D.1 Fragment Instrumentation

The fragment instrumentation system is described in Annex A. The fragment velocity screens and their placement was an improved system based on the one described in reference 3. Unfortunately, all test vessels burst into two pieces. As a result, they seldom hit a breakwire system; and when they did, the counters failed to stop. Thus, almost no fragment velocities were measured with the screens.

However, in almost every case, one portion of the vessel impacted the concrete firing pad with considerable force. This produced an n-wave on the pressure-time (p-t) histories recorded at the airblast gage positions 1-1, 1-2, 1-3, and 2-3 (Figure A.5). The fragment velocity could then be determined from the arrival time of the n-wave and the distance the fragment traveled. Table D.1 presents the fragment velocity measurements. Figure D.1 shows positions of recovered fragments.

D.2 Fragments from 15,000-psi Vessels

Figure D.2 shows the recovered sections of shots 1, 2 and 6. Figure D.2a is the bottom portion of the shot-1 vessel found 665 feet from GZ. The flatter part is where the fragment impacted the concrete pad. The recovered section weighed 52.4 pounds. The averaged measured fragment velocity for this half (before impact with the concrete pad) was 318 feet/second. Figure D.2b is the bottom half of the shot-2 vessel found 552 feet from GZ. Again the flattened portion of the fragment is that part that struck the concrete pad. This half weighed 52.7 pounds. The average fragment velocity before impact with the pad was 324 feet/second. Figure D.2c and D.2d are the fragment halves from the confined vessel, shot 6. Figure D.2c is the bottom portion. Figure D.2d is the top portion of the vessel. The top portion impacted the rear wall of the steel confining structure. Both halves weighed 51.1 pounds. No fragment velocities were measured for this test.

For the 15,000 psi vessels there were 2 unrecovered halves - one each from shots 1 and 2. Figure D.1 shows the estimated direction these halves traveled. A search for the unrecovered fragments out to 1600 feet for shot 1 and 2500 feet for shot 2 was carried out. Since the search area for the shot-1 fragment was clear plowed ground, the lost fragment should have been found. That it was not, suggests that it traveled further than this distance. The shot-2 fragment path was over an area covered with 2-to 3-foot high grass. Even our extended search for this fragment may have overlooked its position. The estimated elevation angles of the trajectory was 54° for shot 1 and 64° for shot 2. Calculation using a drag coefficient of 0.165 and an initial velocity of 325 ft/sec show a maximum height and distance for such fragments would be 610 feet and 1680 feet respectively for shot 1. For shot 2 the maximum height and distance for the unrecovered vessel fragment was 750 feet and 1389 feet respectively.

D.3 Fragments from 30,000-psi Vessels

Figure D.3 shows the recovered portions of shots 3 and 7. Figure D.3a is the bottom half of the shot-3 vessel found inside the arena. This section weighed 147.5 pounds. The mean fragment velocity for this half was 353 feet/second. Figures D.3b and c are the top and bottom halves of the shot-7 vessel respectively. The average fragment velocity was 274 feet/second for the bottom portion of the vessel. (The top portion did not impact the concrete pad). These pieces weighed 93.5 and 108 pounds for the top and bottom sections respectively.

The unrecovered fragment from shot 3 had an estimated elevation angle of 70°. Figure D.1 shows the azimuth direction of this half of the vessel. A search of this area out to 600 feet was carried out. Using an initial velocity of 353 feet/second for this fragment the calculated maximum height and distance is 818 feet and 1136 feet respectively. Therefore, the fragment probably landed in a wooded area where we were unable to find it.

D.4 Fragments from 50,000-psi Vessels

Figure D.4 shows the recovered fragments from Shots 4 and 5. Figure D.4a is the large portion of the shot-4 vessel found inside the arena. This section of fragment weighed 258 pounds or 65% of total tank weight. The average velocity from this fragment was 216 feet/second before impact with the concrete firing pad. Figure D.4b and c are the large and small portions of the shot-5 vessel. Both pieces hit the arena wall. The large piece, Figure D.3b, weighed 271 pounds, 66% of the total weight. The small portion weighed 142 pounds. The larger portion went through two velocity screens. One at 6.5 feet indicated a velocity of 270 feet/second. The other screen was 17.5 feet away and was tripped at 64.6 milliseconds for an average velocity of 270 feet/second also. No measurements were made on the smaller portion.

The unrecovered small portion of the shot-4 vessel had an estimated elevation angle of 78°. Figure D.1 shows the direction in which the fragment is thought to have traveled. A search in this area out to 600 feet was carried out. Using a drag coefficient of 0.165, we calculated maximum height and distance of 886 feet and 722 feet respectively.

TABLE D.1 FRAGMENT DATA

SHOT #	VESSEL TYPE	FRAGMENT WEIGHT POUNDS	FRAGMENT VELOCITY FEET/SEC		DISTANCE FRAGMENT TRAVELED (FEET)
1	15,000	52.4	310(1)	BOTTOM HALF	
1		52.4	321(1)		665(3)
		TOP HALF NOT FOUND			1680(4)
2	15,000	52.75	324(1)		
2		52.75	330(1)	BOTTOM HALF	
2			317(1)		(552)(3)
		TOP HALF NOT FOUND			1380(4)
3	30,000	147.5	354(1)		
3		147.5	373(1)	BOTTOM HALF	INSIDE THE
3		147.5	348(1)		ARENA
3		147.5	338(1)		
		TOP HALF NOT FOUND			1136(4)
4	50,000	258	215(1)		
4		258	216(1)	LARGE PORTION	INSIDE THE
4		258	210(1)		ARENA
4		258	221(1)		
		SMALL PORTION NOT FOUND			722(4)
5	50,000	271	270(2)		INSIDE THE
5		142			ARENA
6	15,000	51.1	none		
6		51.1	none		
7	30,000	108	290(1)		INSIDE THE
7		108	250(1)		ARENA
7		93.5	none		

1. VELOCITY MEASUREMENTS MADE FROM P - T HISTORIES
2. VELOCITY MEASUREMENTS MADE FROM BREAK WIRE SYSTEM .
3. MEASURED DISTANCE TRAVELED
4. ESTIMATED DISTANCE TRAVELED

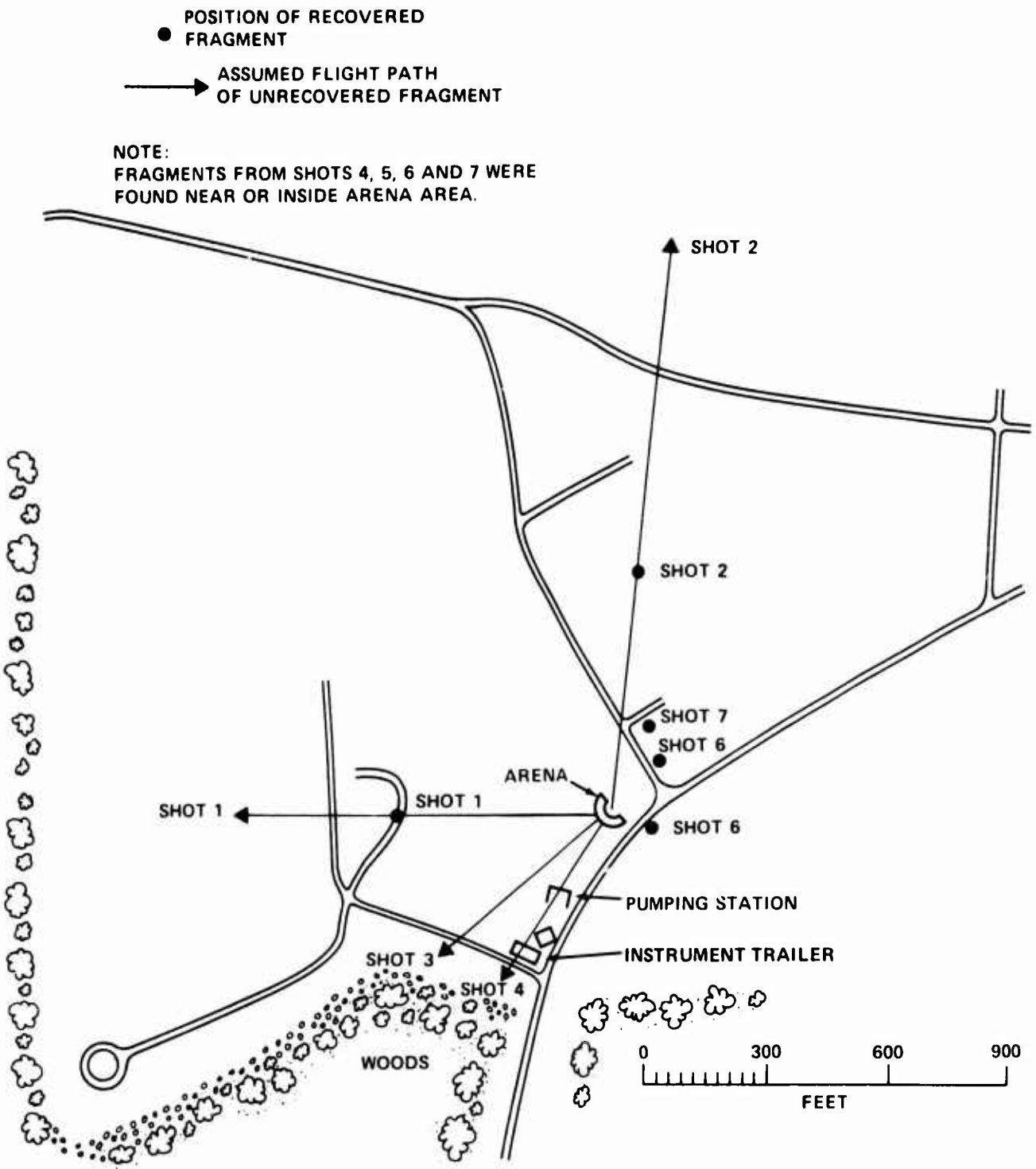

FIG. D.1 FIRING SITE AT NSWC, DAHLGREN, VA.

a. SHOT 1

b. SHOT 2

c. SHOT 6

d. SHOT 6

FIG. D.2 FRAGMENTS FROM 15,000-PSI VESSEL

a. SHOT 3

b. SHOT 7

c. SHOT 7

FIG. D.3 FRAGMENTS FROM 30,000-PSI VESSEL

a. SHOT 4

b. SHOT 5

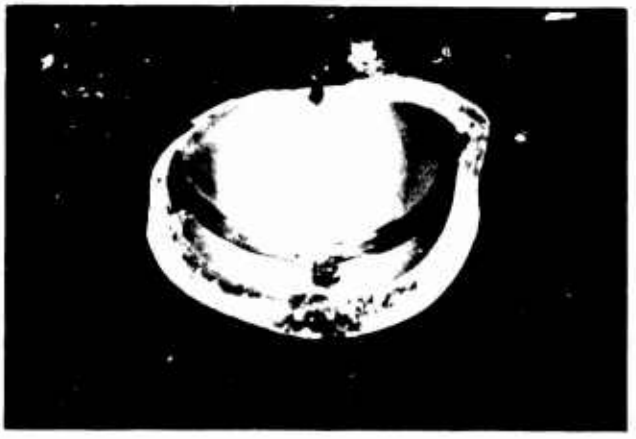

c. SHOT 5

FIG. D.4 FRAGMENTS FROM 50,000-PSI VESSEL

ANNEX E CALCULATIONS OF AIRBLAST FROM PRESSURIZED ARGON SPHERES

(By D. Lehto)

E.1 Equation of State of Argon

Both of the hydrocodes used here (WUNDY and TUTTI) require an equation of state either in the general form $P = P(\rho,E)$ or as $P(\rho,S)$ isentropes that pass through the desired initial points. The Redlich-Kwong equation of state (reference E.1) is apparently accurate for argon (reference E.2) but it is in the $P(\rho,T)$ form and is not usable in our hydrocodes without further work. If a large number of calculations involving argon were to be done, it would be worth while to develop a $P(\rho,E)$ equation of state. Since only a few initial conditions are of interest here, we take the simpler course and use individual isentropes. The expansion isentrope from each initial condition is fitted with some convenient function. The fits used here are given in Table E.1.

The use of an isentropic argon equation of state (EOS) is not quite correct because two entropic processes occur in the argon: the second shock, characteristic of spherical explosions, that moves inward from the expanding gas/ambient air interface, and any reflected shocks from nearby walls.

We obtain our argon EOS data from the tables of Din (reference E.3) and of Brahinsky and Neel (reference E.4). The Din tables are given in more detail in Little (reference E.5).

Figure E.1 shows the T-S diagram for argon with lines drawn in to show isothermal compression to 15,000, 30,000 and 50,000 psi and the isentropic expansion paths when the tank is ruptured. When the argon has expanded to about 40 atm pressure, the saturation line is reached and the argon will become opaque due to partial condensation.

Figure E.2 shows the same compression and expansion paths, this time on a P-V plot. Note that the isothermal compression curve becomes quite steep above about 15,000 psi , indicating that little energy is involved in further compression to 50,000 psi . This means that a 50,000-psi, 17°C tank will give about the same airblast as a 15,000-psi , 17°C tank. The expansion isentropes turn sharply at the saturation line.

(E.1) O. Redlich and J. N. S. Kwong, "On the Thermodynamics of Solutions. V. An Equation of State. Fugacities of Gaseous Solutions," Physical Review 44: 233-244 (1949).
(E.2) J. P. Kois, personal communication.
(E.3) F. Din, Thermodynamic Functions of Gases, Volume 2: Air, Acetylene, Ethylene, Propane and Argon (Butterworth, London, 1956).
(E.4) H. S. Brahinsky and C. A. Neel, Tables of Equilibrium Thermodynamic Properties of Argon. Volume III. Constant Entropy, Arnold Engineering Development Center AEDC-TR-69-19, AD684532, Mar 1969.
(E.5) W. J. Little, Tables of Thermodynamic Properties of Argon from 100 to 3000K, Arnold Engineering Development Center AEDC-TDR-64-68, AD434368, Apr 1964.

One of the main purposes of these calculations was to provide predictions of blast overpressures for the experiments to be done with 15,000 and 50,000 psi tanks at ambient temperature. Consequently, these intial conditions are stressed here.

Figure E.3 shows the P-V isentropes for tanks heated to 1000°C and 1750°C. These curves are much closer to ideal-gas behavior (straight lines of slope -5/3) than are those for the cold tanks of Figure E.2. The point for 50,000 psi , 1750°C lies in a region where we find no EOS data. Isentropes in this region were obtained by extrapolating the Brahinsky and Neel (reference E.4) tables. This extrapolation is not very accurate because of the strong real-gas effects in this region. A Redlich-Kwong EOS adapted to $P(\rho,E)$ or $P(\rho,S)$ would be useful here.

E.2 One-Dimensional Flow Calculations

Figure E.4 gives the calculated peak air shock overpressure versus distance from the tank center for several argon pressures and temperatures. The solid parts of the curves are "extrapolated" pressures from the WUNDY (reference E.6) calculations. (An artificial-viscosity calculation rounds off the peak of a shock front. The true peak can be found by extrapolating the pressure versus radius profile at a fixed time to the radius of maximum artificial viscosity. The size of the extrapolation is usually about ten percent for a WUNDY calculation and may be as large as a factor of two for a TUTTI calculation.)

Within about one tank radius from the tank surface, the pressure in the expanding argon following the air shock can have a higher pressure than the air shock. The peak argon pressure is shown by dotted lines in Figure E.4.

The dashed low-pressure portions of the curves of Figure E.4 are obtained by matching the TNT free-air curve to the ends of the solid curves.

The points at a radius of 0.62 feet (the initial argon sphere radius) are calculated from the shock tube equation as shown on page 81 in reference E.7. These points are joined to the ends of the solid curves with smooth dashed curves, using WUNDY unextrapolated pressures (not shown) as a guide.

The procedure for getting the shock-tube initial pressures in the air shock is now described because the results give a useful guide in interpolating the curves of Figure E.4 to pressures and temperatures that are not shown. The procedure is as follows:

(1) An isentrope is prepared for the desired initial argon conditions.

(2) An integration is carried out to get particle velocity versus pressure in the isentropic expansion.

(E.6) D. Lehto and M. Lutzky, One-Dimensional Hydrodynamic Code for Nuclear-Explosion Calculations, Naval Ordnance Laboratory NOLTR 62-168, AD615801, Mar 1965. (The WUNDY Fortran Listings in this report are obsolete. This report is being rewritten.)
(E.7) W. Liepmann and A. Roshko, Elements of Gas Dynamics, John Wiley and Sons, Inc., London, 1958.

(3) The particle velocity versus pressure results are plotted on a graph along with the shock particle velocity versus pressure relation for the desired ambient gas (here, ideal air), as shown in Figure E.5. The intersection of these curves gives the desired air shock pressure to be plotted at a radius of 0.62 feet on Figure E.4. (If both the argon and ambient air are regarded as ideal gases, the air shock pressure may be obtained directly by solving the shock tube equation by iteration.)

Figure E.6 shows this initial air shock pressure varies with argon pressure and temperature. At high temperatures, the argon behaves as an ideal gas.

Figure E.7 shows calculated pressure versus time calculations at distances of 3, 4, 5 and 6 feet from a one cubic foot 15,000 psia, 17°C argon tank. The notation "CS" indicates arrival of the argon/air contact surface at the gage location. The calculated curves are somewhat ragged and can be improved by using finer zoning in the WUNDY calculation.

E.3 Two-Dimensional Flow Calculations

The results described so far are for a free-air explosion with strictly radial flow. When a reflecting surface is present, the flow is no longer one-dimensional and a two-dimensional calculation must be done. A two-dimensional flow Eulerian hydrocode, TUTTI, was written for this purpose. It is based on the FLIC (Fluid-In-Cell) method of Gentry, et al (reference E.8). FLIC as described in reference E.8 is for only one material. Air and argon in the range of interest here have quite different properties where they adjoin at the contact surface. The argon has undergone expansion and is quite cold (for argon initially at 17°C in the tank), while the air has undergone compression and is warm. Continual computational diffusion of these two materials into each other causes error. For this reason, TUTTI was written as a two-material hydrocode in which the argon and air do not mix.

We now consider the problem of a 15,000 psi , one cubic foot sphere of argon centered 50 cm above a rigid plane surface. The argon is the real gas of Figures E.1, E.2 and E.3; the air is an ideal gas with a gamma of 1.4 (the air does not get compressed enough to require a real-gas equation of state). We consider initial argon temperatures of 17°C and 1750°C.

Figure E.8 shows TUTTI results for the shapes of the contact surface and shocks for the 15,000-psi , 17°C tank. The reflected shock transmitted into the argon is not shown; it lies very near the reflecting surface and has trouble moving into the argon because of the strong outward argon flow and because of the low sound speed in the cold mixed-phase argon (about 100 m/s). The reflected shock tends to diffract around the argon rather than try to go through it. This is contrary to our experience with HE and nuclear explosions, in which the reflected shock travels more rapidly in the fireball than in the adjacent air.

(E.8) R. A. Gentry, R. E. Martin and B. J. Daly, "An Eulerian Differencing Method for Unsteady Compressible Flow Problems," J. Comput. Phys. 1: 87-118 (1960).

Figures E.9 and E.10 show the TUTTI pressure-time calculations along the reflecting surface. The large rounded peak following the air shock for the 17°C tank in Figure E.9 is due to the pressure in the expanding argon. This peak is represented by the dotted lines in Figure E.4. The peak air shock pressures for the 17°C tank have been corrected (dashed curves) by applying the shock reflection factors of reference E.9 to the WUNDY free-air pressure-distance curve of Figure E.4. Figure E.11 shows the peak air shock pressure versus distance along the surface. The rounding off of the TUTTI air shock peak is considerable but lessens as the distance from the tank increases, because the shock grows in length and thus contains more of the calculational zones. Figures E.12 and E.13 show the distribution of pressure along the reflecting surface at fixed times.

These calculations all neglect the kinetic energy of the tank fragments and are thus expected to overestimate the shock pressures for a spherical tank rupture. However, the actual tanks were found to burst open like clam shells rather than break up into small fragments. This would cause the pressures to be enhanced in the direction of the argon jet from the splitting tank and to be reduced in the opposited direction. The jet is expected to be a broad plume in the tank. A rough calculation with TUTTI of such a plume suggests that the shock overpressures in the direction of this plume will be about a factor of two greater than in a direction 90 degrees from the plume axis.

These TUTTI calculations can be made arbitrarily accurate by spending an arbitrarily large amount of money on them, but the cost is proportional to the cube of the spatial resolution. The TUTTI runs described here cost about $100 each and occupied 130K of storage on a CDC 6500. A 25 by 50 computational grid was used. Because the reflecting surface was a simple plane, it was possible to sharpen up the rounded peaks of the shocks with reflection factors applied to the free-air results. For more complicated shock interactions in which accurate peak pressures are important, more accurate TUTTI calculations are needed. If it is impulse that is important rather than peak pressure, the rounding of the shock does little harm.

(E.9) S. Glasstone, The Effects of Nuclear Weapons, U. S. Atomic Energy Commission, U. S. Government Printing Office, 1962, page 147.

TABLE E.1 APPROXIMATE ANALYTIC FITS TO THE ARGON ISENTROPES

The equations are: $P = C_0 \rho^{\gamma}$

where P = absolute pressure ($dyne/cm^2$)
ρ = density (g/cm^3);

$$\log P = C_1 + C_2(\log V) + C_3(\log V)^2$$

where P = absolute pressure (psia)
V = specific volume (cm^3/mole)
log = $\log_{10}$.

P(psia)	T(C)	ρ Range (g/cm^3)	C_0	γ	C_1	C_2	C_3
15000	17	$\rho > 0.587$	1.053E9	5.77	—	—	—
		$\rho \leq 0.587$	8.059E7	0.95	—	—	—
50000	17	$\rho > 0.8322$	1.663E8	9.250	--	—	—
		$\rho \leq 0.8322$	3.540E7	0.8293	—	—	—
15000	1000	(same as 50000 psia, 1750 C)					
15000	1750	$\rho > 0.05911$	—	—	8.816	-3.1499	0.2620
		$\rho \leq 0.05911$	11.291E9	5/3	—	--	—
30000	1750	$\rho > 0.07474$	—	—	8.6356	-3.226	0.2857
		$\rho \leq 0.07474$	6.980E9	5/3	—	--	—
50000	1750	$\rho > 0.10005$	—	—	8.152	-3.0552	0.2668
		$\rho \leq 0.10005$	4.802E9	5/3	—	—	—

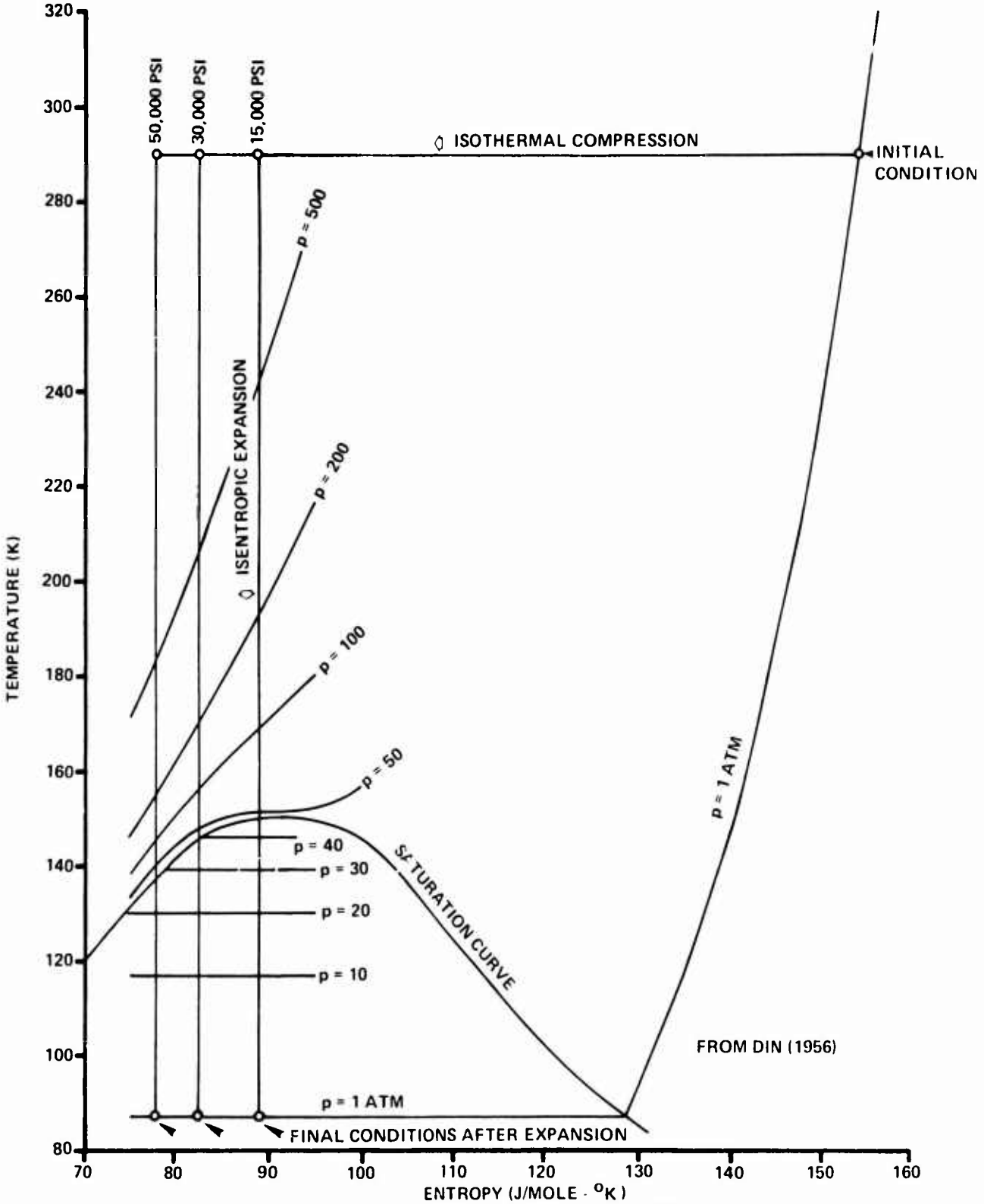

FIG. E.1 T VS S DIAGRAM FOR ARGON

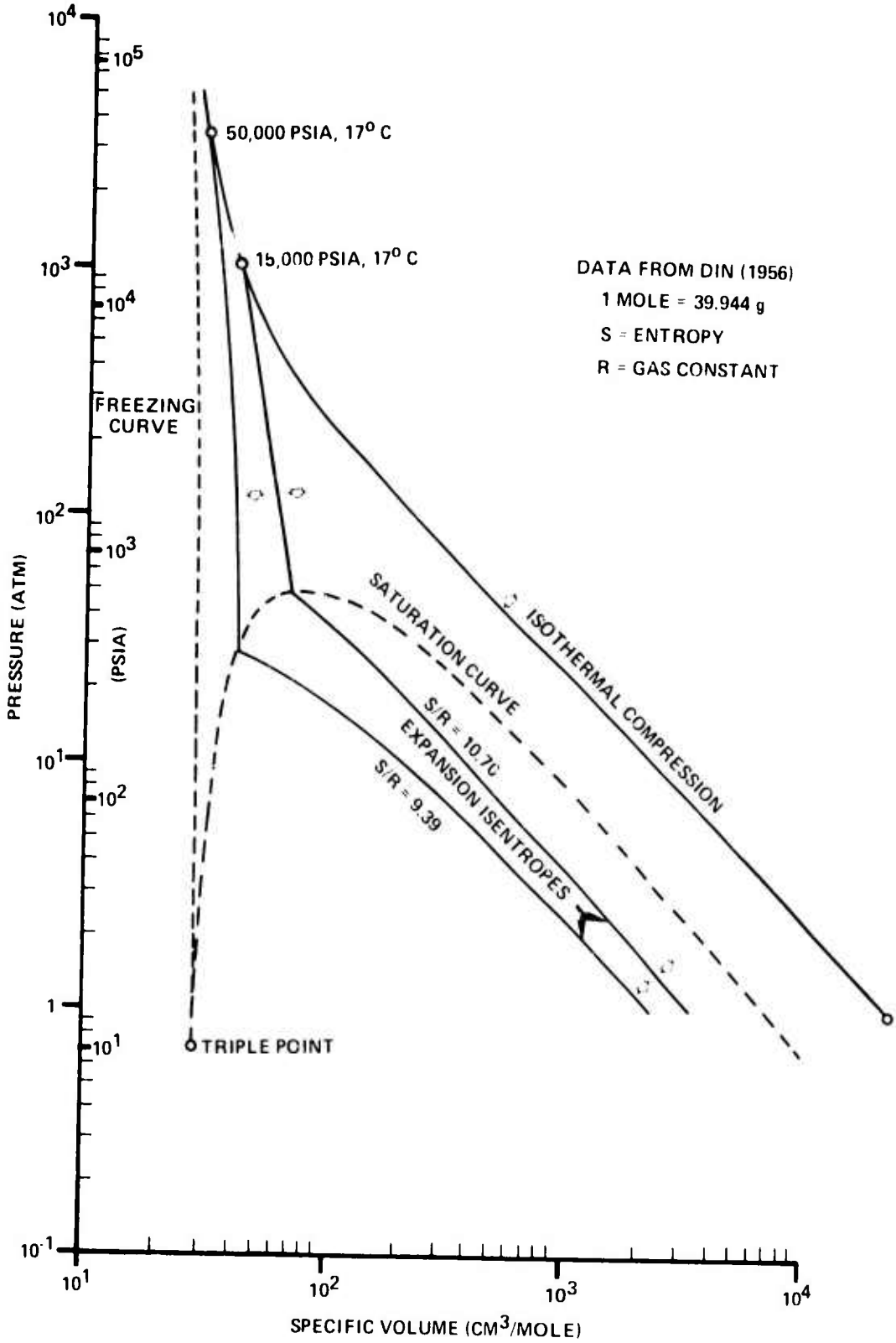

FIG. E.2 ARGON P - V COMPRESSION AND EXPANSION PATHS FOR COLD TANKS

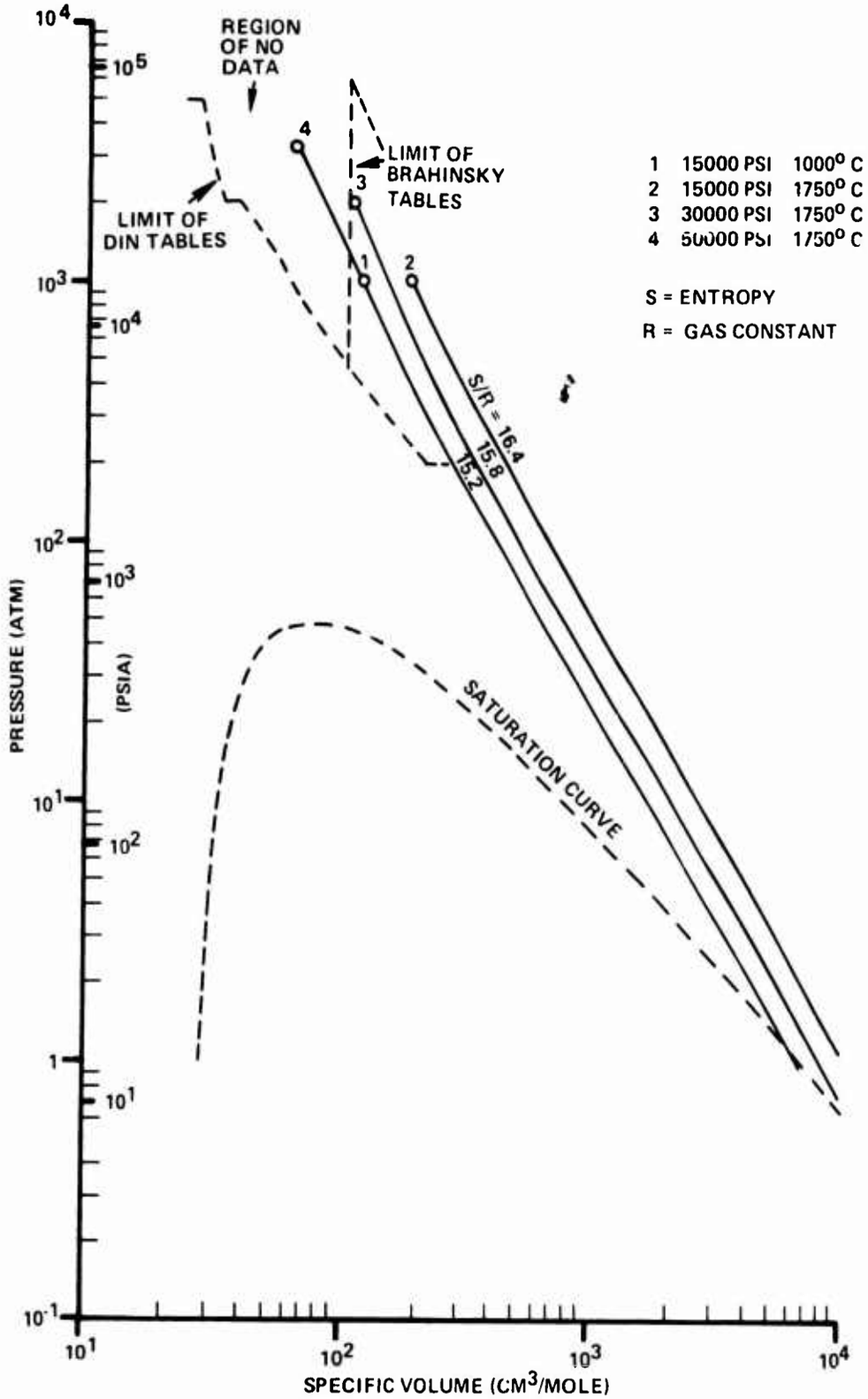

FIG. E.3 ARGON P - V ISENTROPES FOR HOT TANKS

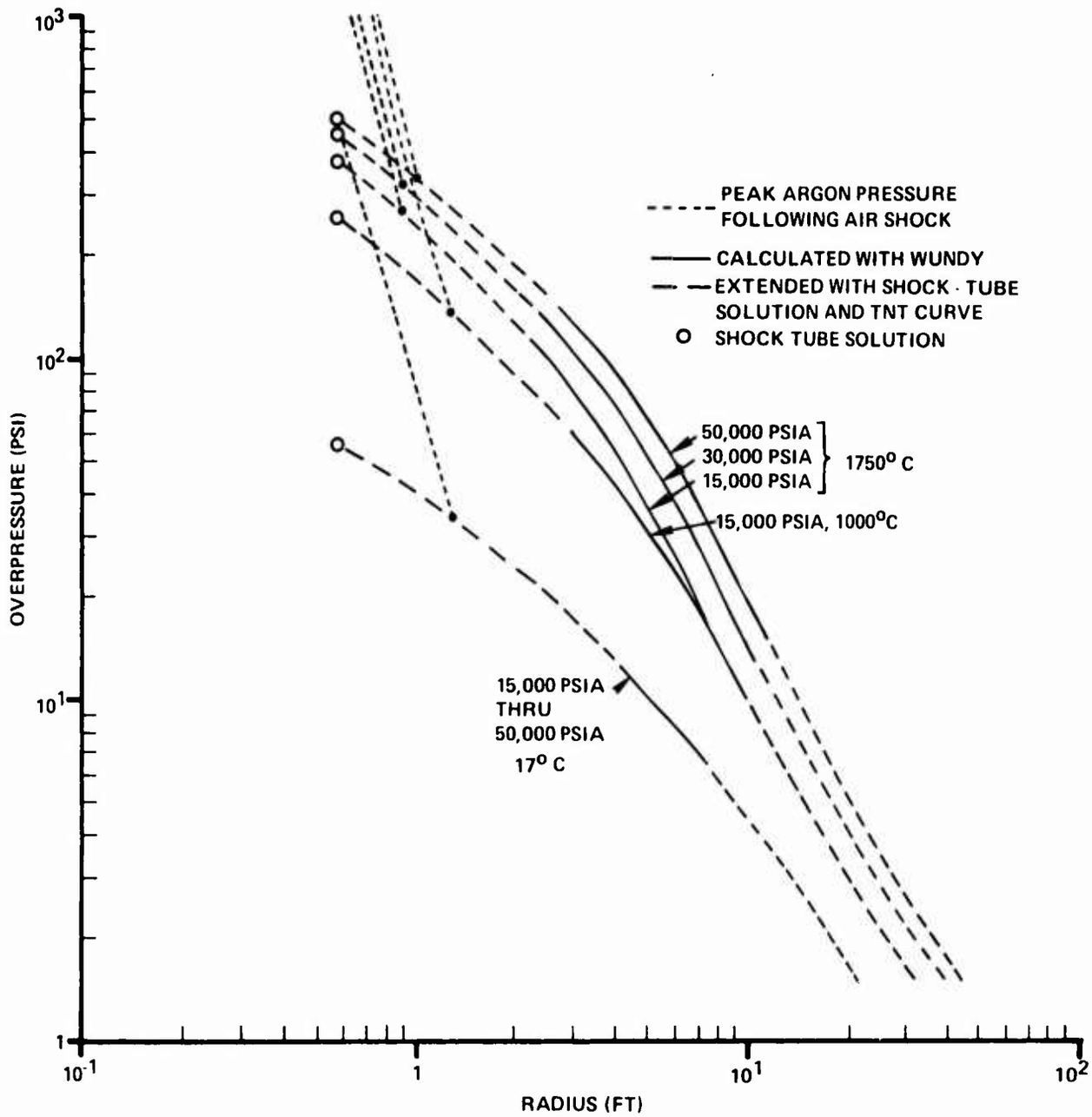

FIG. E.4 PEAK FREE · AIR SHOCK OVERPRESSURE VS DISTANCE FOR 1 FT^3 ARGON TANKS

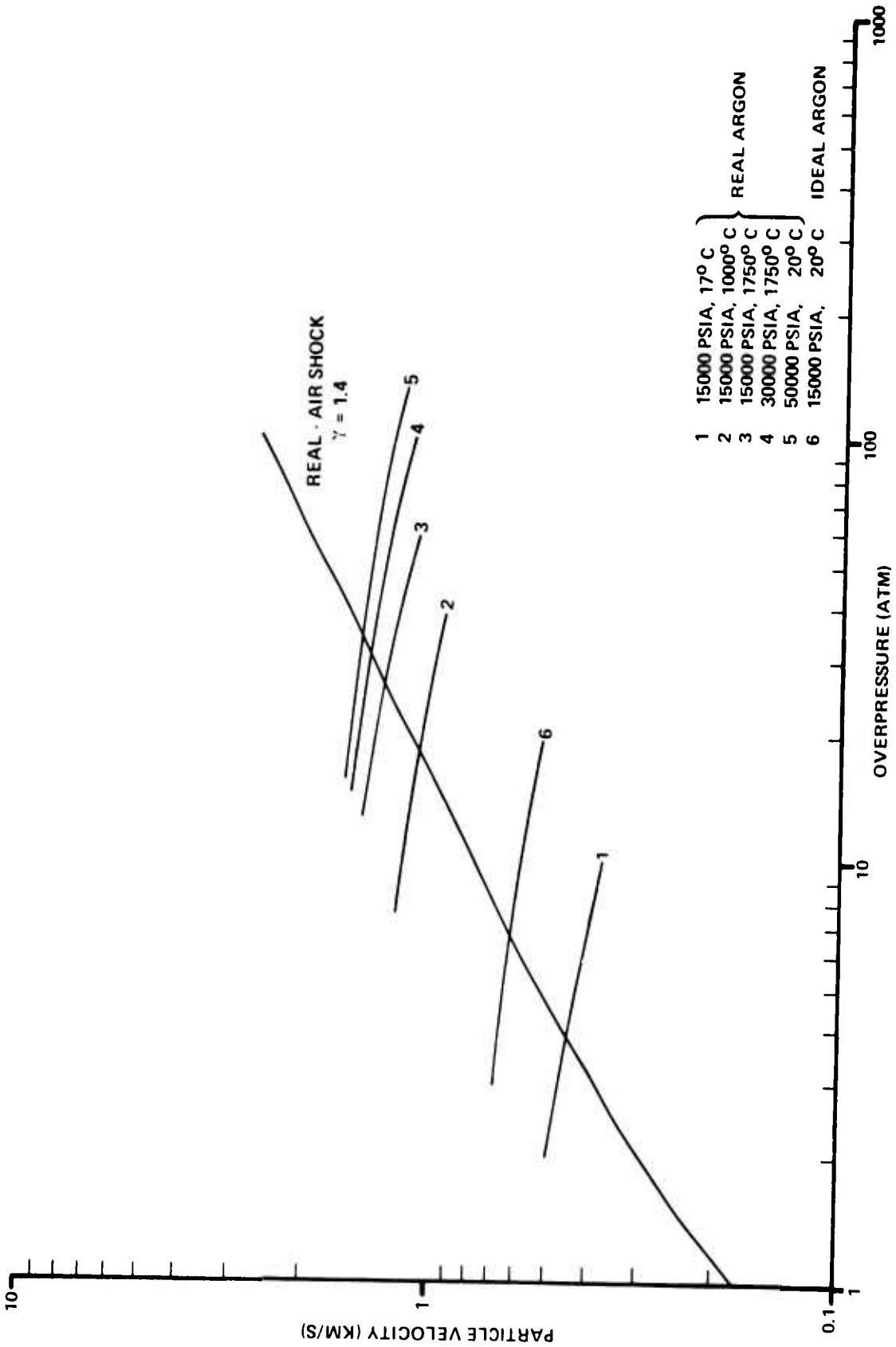

FIG. E.5 GRAPHICAL SOLUTION OF SHOCK - TUBE EQUATION

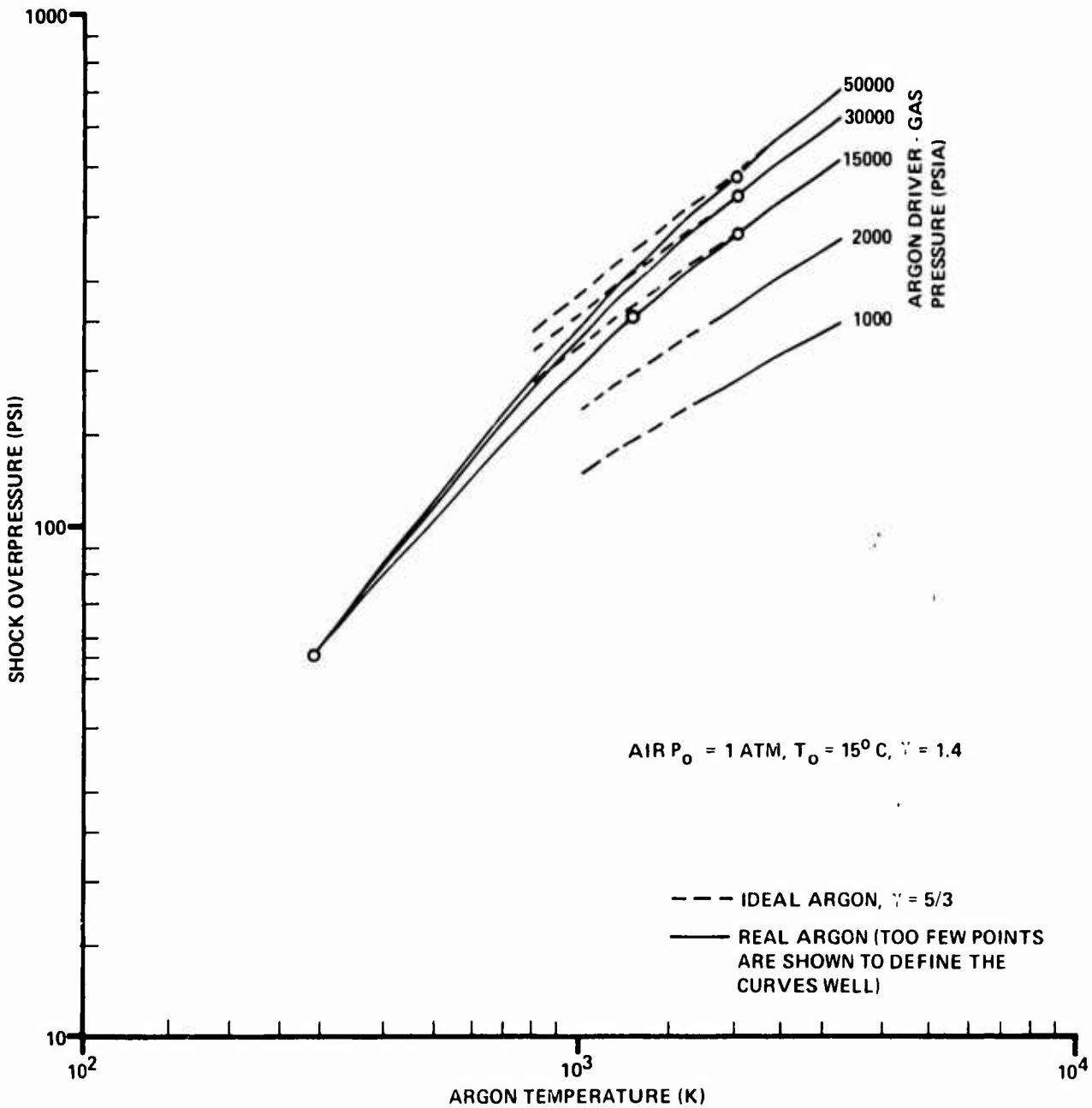

FIG. E.6 INITIAL AIR SHOCK PRESSURE IN ARGON/AIR SHOCK TUBE

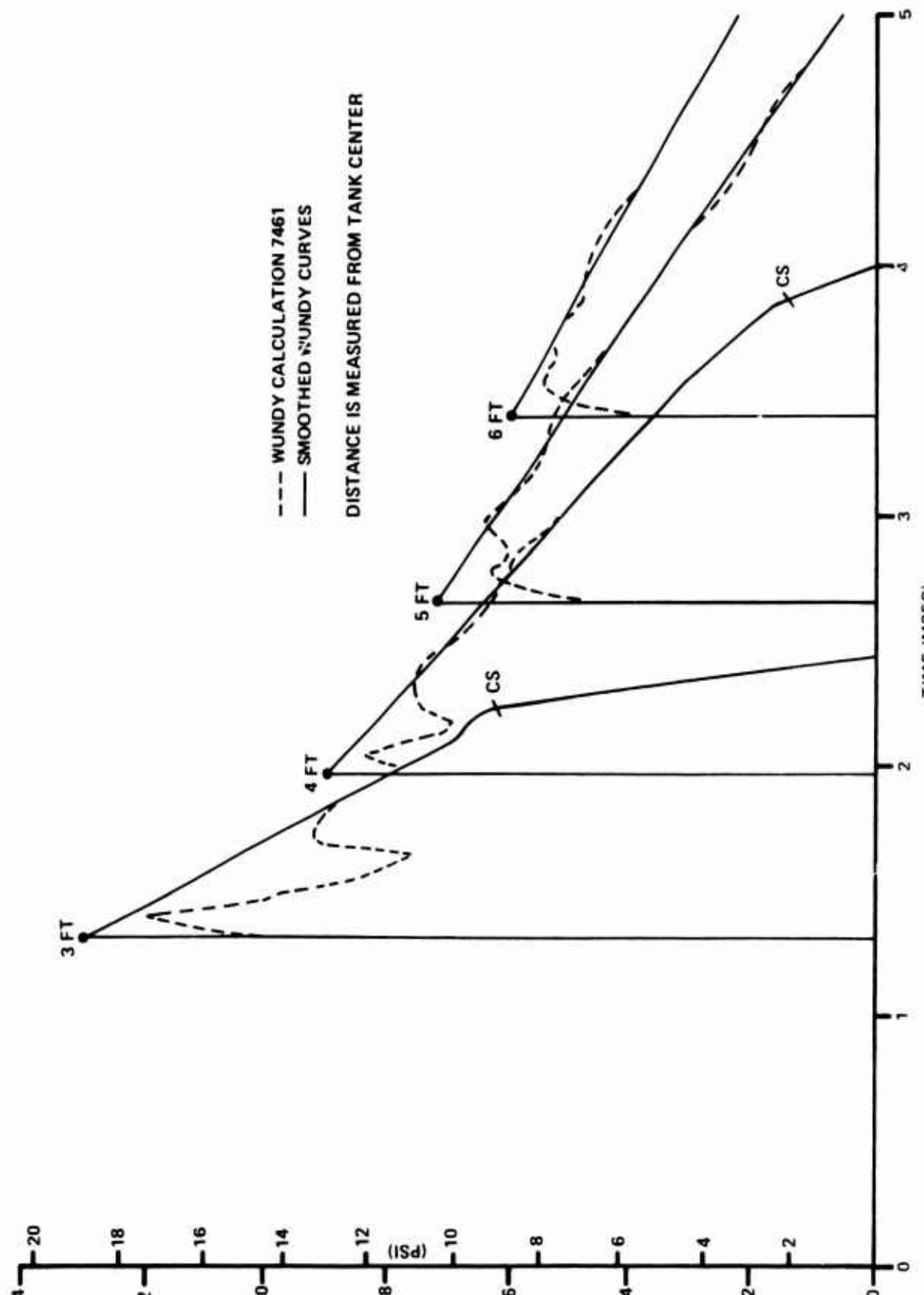

FIG. E.7 FREE - AIR PRESSURE VS TIME AT VARIOUS DISTANCES FROM SPHERICAL 1 FT^3 15,000 PSI, 17° C ARGON TANK

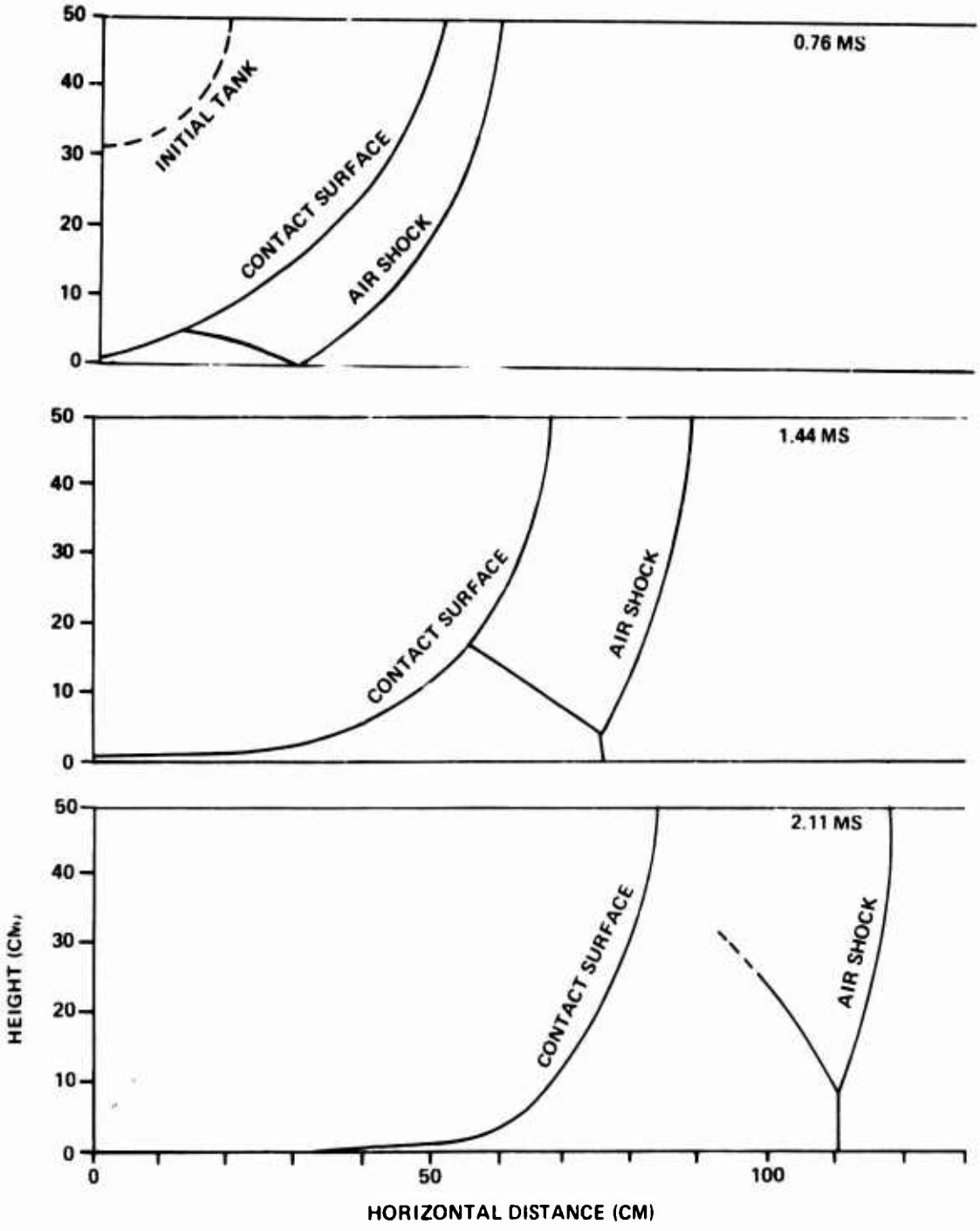

FIG. E.8 CONTACT SURFACE AND AIR SHOCK CONFIGURATIONS FOR SPHERE OF 15,000 - PSI, 17° C ARGON

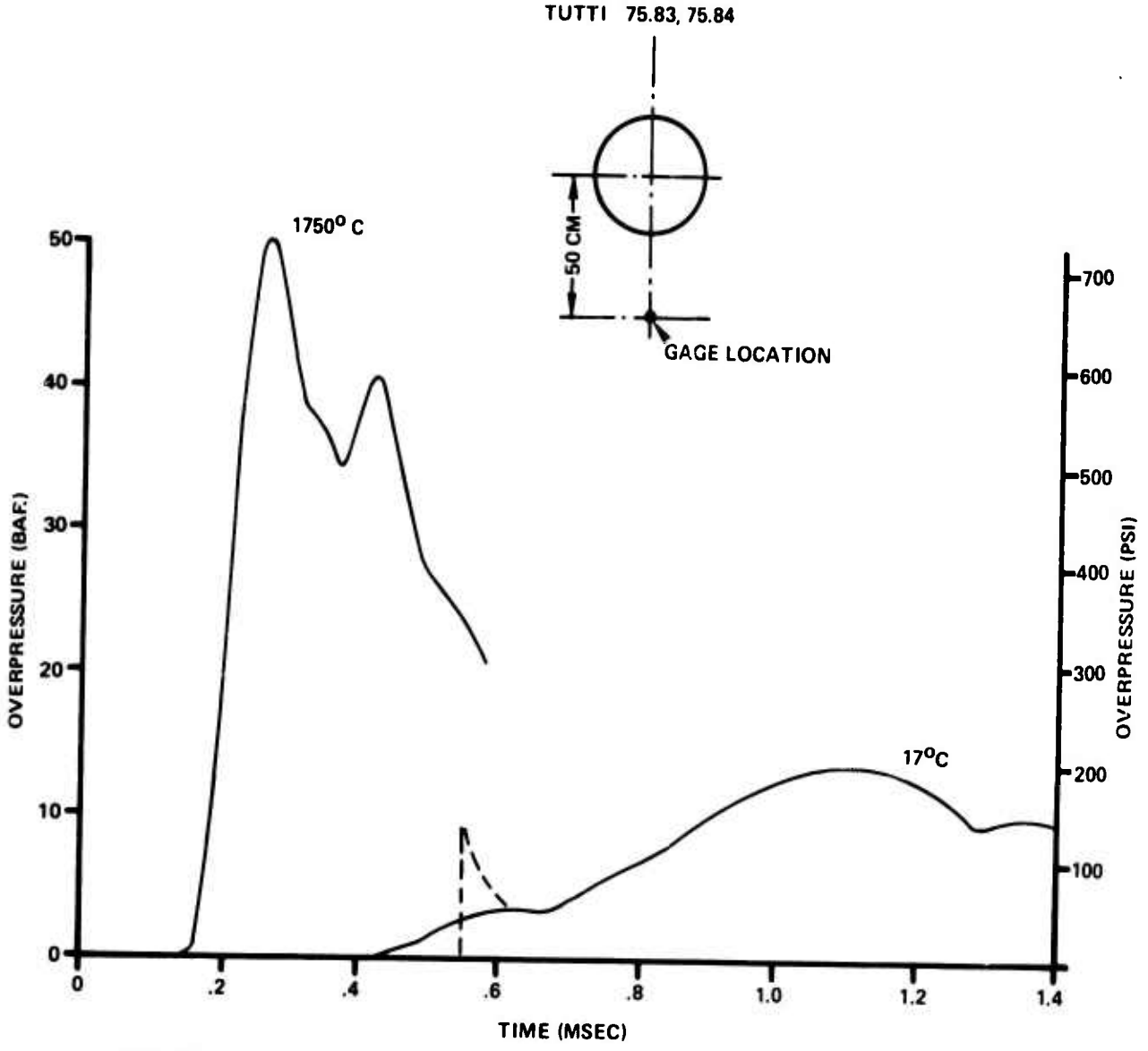

FIG. E.9 PRESSURE VS TIME ON SURFACE DIRECTLY BELOW 1 FT^3 15,000 - PSI ARGON TANK AT 17° C AND AT 1750° C

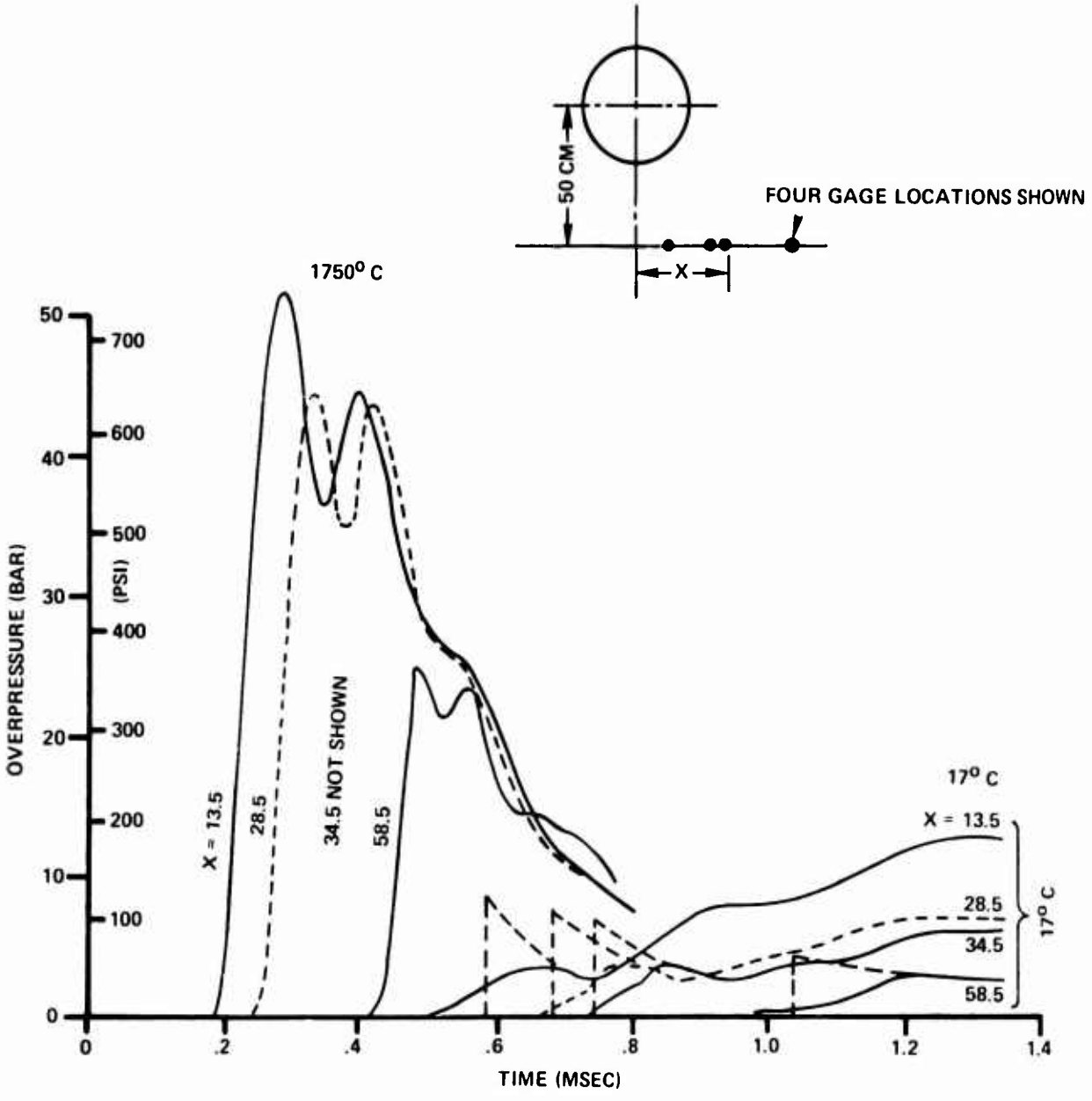

FIG. E.10 PRESSURE VS TIME ALONG THE SURFACE FROM A 1 FT^3 TANK OF ARGON BURST AT 15,000 PSI.

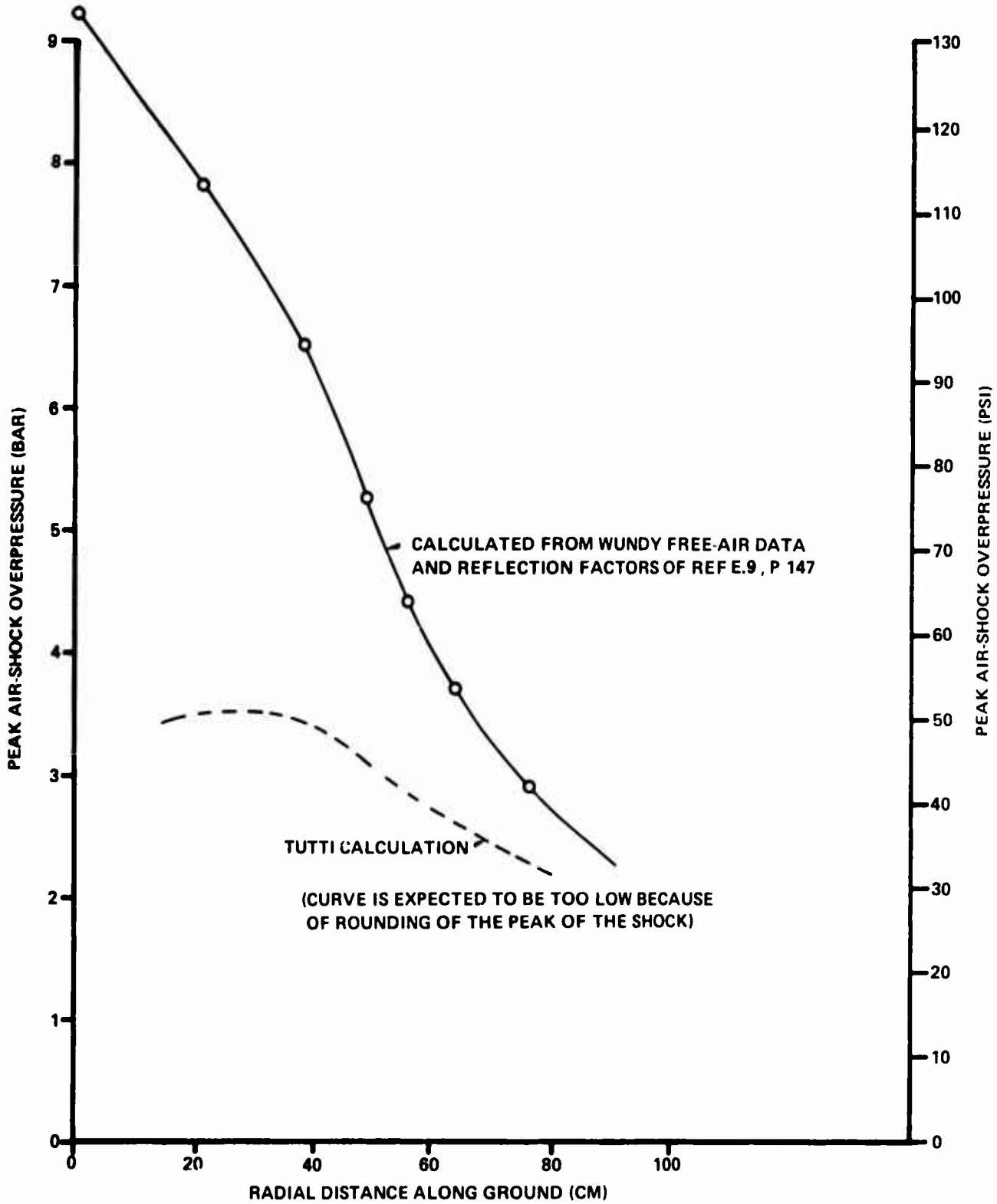

FIG. E-11 PEAK AIR-SHOCK OVERPRESSURE VS GROUND RANGE FOR 1 FT^3 15,000 - PSI, 17° C ARGON TANK WITH CENTER 50 CM FROM SURFACE

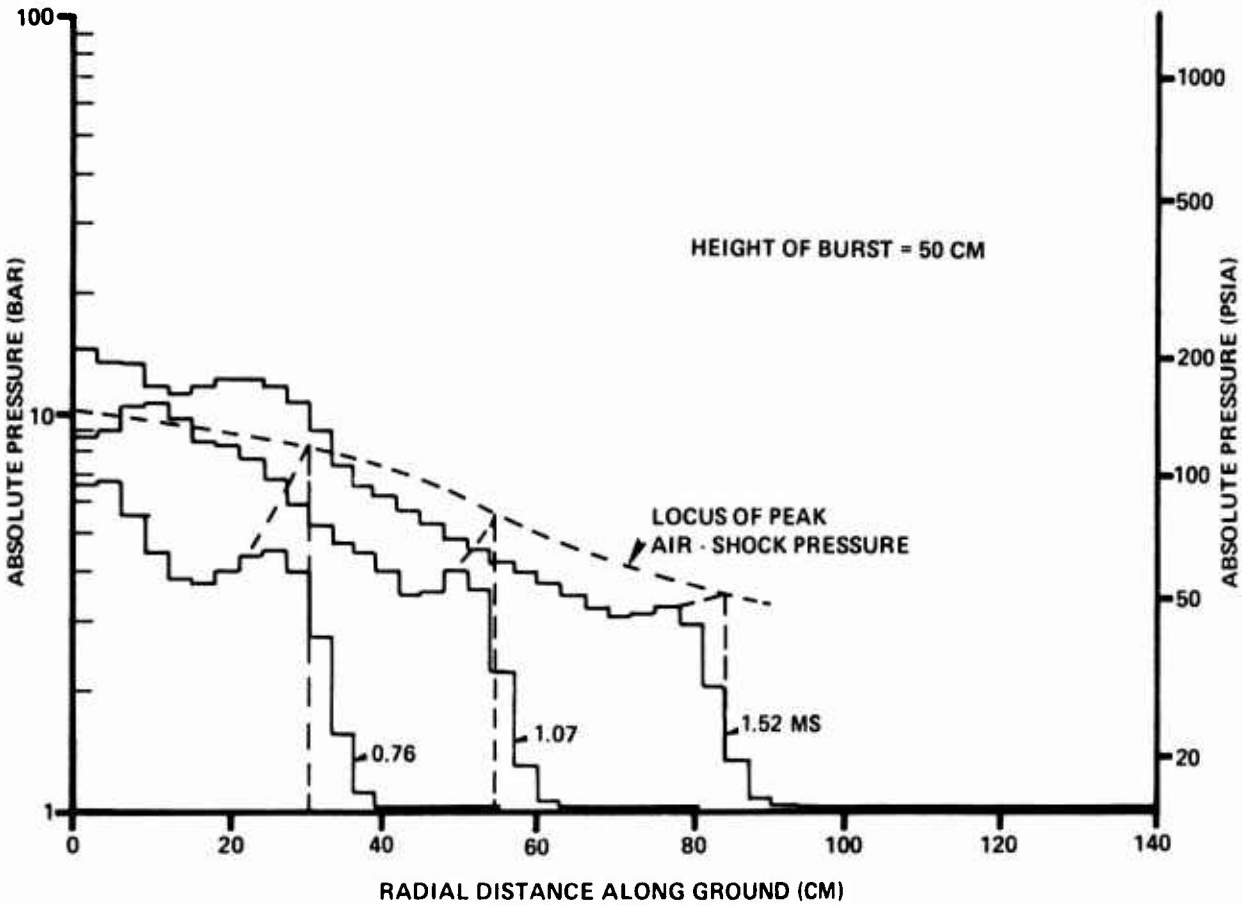

FIG. E.12 PRESSURE DISTRIBUTION ALONG SURFACE FROM SPHERICAL 1 FT^3 15,000 - PSI ARGON TANK AT 17° C

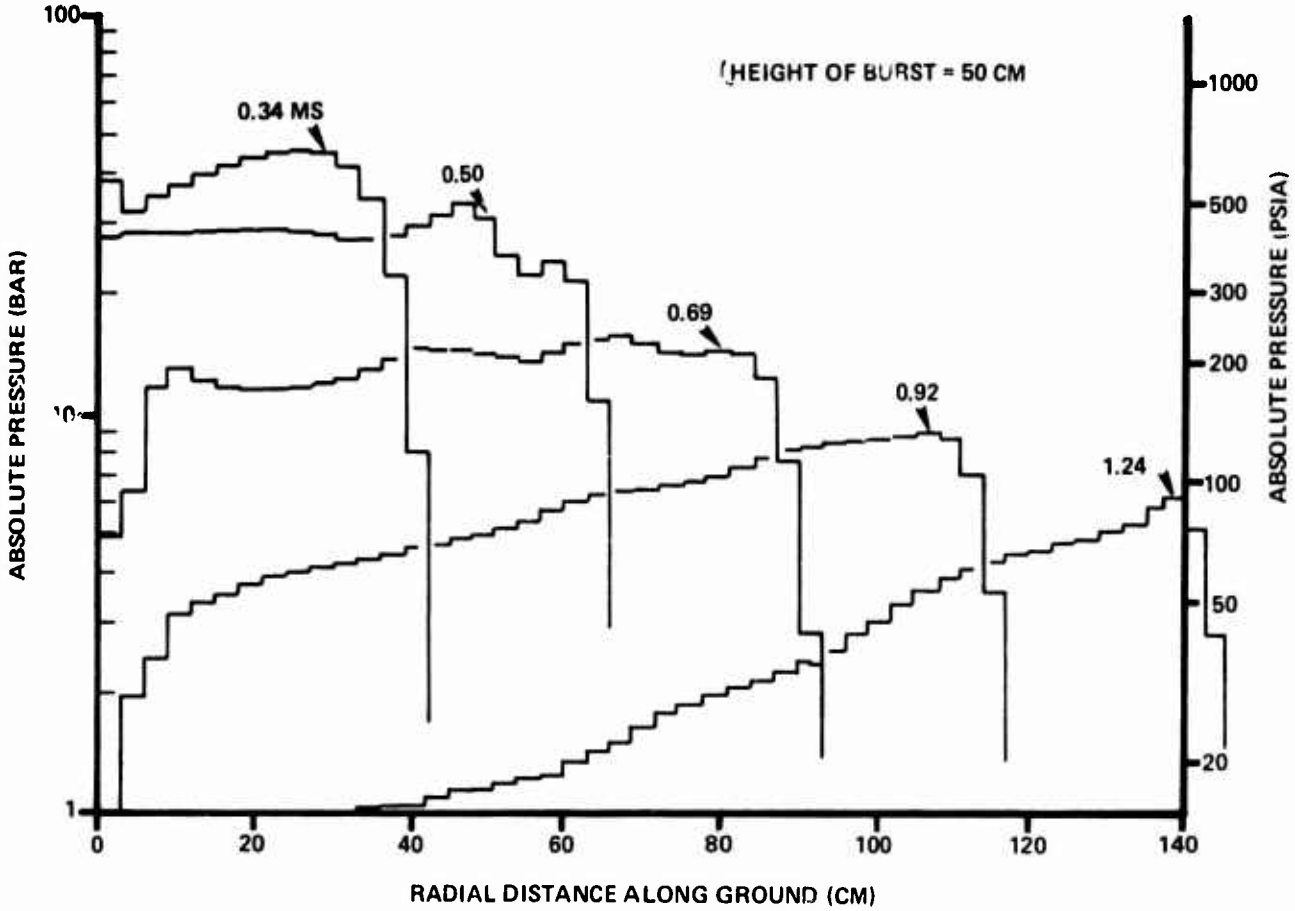

FIG. E.13 PRESSURE DISTRIBUTION ALONG SURFACE FROM SPHERICAL 1 FT^3 15,000 - PSIA ARGON TANK AT 1750° C